Medizinische Hochschule Hannover

Abteilung Molekular- und Zellphysiologie

AG Vegetative Physiologie 4220

Adaptation of the CO_2 permeability of various cells and organelles to their specific metabolic needs

INAGURALDISSERTATION

zur Erlangung des Grades einer Doktorin der Naturwissenschaften

- Doctor rerum naturalium - (Dr. rer. nat.)

vorgelegt von

Mariela Eugenia Arias Hidalgo

(San José, Costa Rica)

Hannover, 2017

Angenommen durch den Senat: 07.11.2017

Präsident: Prof. Dr. med. Christopher Baum

Wissenschaftliche Betreuung: Prof. Dr. med. Gerolf Gros

Wissenschaftliche Zweitbetreuung: Prof. Dr. rer. nat. Anaclet Ngezahayo

1. Referent :   Prof. Dr. med. Gerolf Gros
2. Referent: Prof. Dr. rer. nat. Anaclet Ngezahayo
3. Referent: Prof. Dr. rer. nat. Matthias Gaestel

Tag der mündlichen Prüfung: 07.11.2017

Prüfungsausschuss

Vorsitz: Prof. Dr. rer. nat. Matthias Gaestel

4. Prüfer: Prof. Dr. med. Gerolf Gros
5. Prüfer: Prof. Dr. rer. nat. Anaclet Ngezahayo
6. Prüfer: Dr. rer. nat. Matthias Gaestel

Wissenschaftliche Betreuung:

Prof. Dr. med. Gerolf Gros, PD Dr. med. Volker Endeward

Wissenschaftliche Zweitbetreuung:

Prof. Dr. Anaclet Ngezahayo

1. Erst-Gutachterin / Gutachter:

2. Gutachterliche Stellungnahme durch:

3. Gutachterin / Gutachter:

Tag der mündlichen Prüfung:

Erklärung zur Dissertation

Hiermit erkläre ich, dass ich die Dissertation **"Adaptation of the CO_2 Permeability of various cells and organelles to their specific metabolic needs"** selbstständig verfasst habe. Im der unter Betreuung von Herr Prof. Dr. med. Gerolf Gros und Privat-Dozent Dr. med. Volker Endeward ohne sonstige Hilfe durchgeführt und bei der Abfassung und der Anfertigung der Dissertation keine anderen als die dort aufgeführten Hilfsmittel benutz habe. Ich habe keine entgeltliche Hilfe von Vermittlungs- bzw. Beratungsdiensten (Promotionsberater oder anderer Personen) in Anspruch genommen. Niemand hat von mir unmittelbar oder mittelbar entgeltliche Leistungen für Arbeiten erhalten, die im Zusammenhang mit dem Inhalt der vorgelegten Dissertation stehen. Ich habe die Dissertation an folgenden Institutionen angefertigt: Abteilung Molekular und Zellphysiologie AG Vegetative Physiologie, MHH.

Die Dissertation wurde bisher nicht für eine Prüfung oder Promotion oder für einen ähnlichen Zweck zur Beurteilung eingereicht. Ich versichere, dass ich die vorstehenden Angaben nach bestem Wissen vollständig und der Wahrheit entsprechend gemacht habe.

Hannover, den 5 Juni, 2017

Mariela Eugenia Arias Hidalgo

Acknowledgements

First of all, I will like to thank my family for their support and help, especially my husband who has been always there for me "for better and for worse".

Thanks to Prof. Dr. med. Gros for accepting me as his student and for being the best "Doktorvater" that a student could ever have. I have no words to express my gratitude for being always concerned about me and for making this experience so enriching. You have taught me a lot and I will always be grateful for that!

My gratitude also to Dr. Al-Samir and PD Dr. med. Endeward, you both have teach me a lot of things and you´ve being terrific co-workers.

I want to express my appreciation to all the coauthors which helped me with their time and knowledge during this process and also to Prof. Dr. Ngezahayo for all his suggestions and feedback.

Finally, I will like to thank DAAD and the International Affairs Office of the University of Costa Rica for giving me all the support for completing this goal.

"To my two mothers, who encourage me to pursue my dreams in life and one of them now inspires me from my heaven."

Index

Figure Index

Table Index

Abbreviation list

AQP: Aquaporin Protein

CO_2: Carbon dioxide

CA: Carbonic Anhydrase

CA_e: Extracellular carbonic anhydrase activity

CA_i: Intracellular/intraorganellar carbonic anhydrase activity

DIDS: 4,4'-Diisothiocyano-2,2'-stilbenedisulfonic acid

DNSA: 5-dimethylaminonaphtalene-1-sulfonamide

MDCK: Madin Darby Canine Kidney Cell line

P_{CO2}: Carbon dioxide permeability

PCE: Proximal Colon Epithelium

P_{HCO3}: Bicarbonate permeability

Zusammenfassung

Anpassung der CO_2-Permeabilität verschiedener Zellen und Organellen an ihren spezifischen Stoffwechsel

Mariela Eugenia Arias Hidalgo

Seit mehr als 20 Jahren haben sich Hinweise gehäuft, die dem Paradigma widersprechen, dass alle Zellmembranen hochdurchlässig für CO_2 (wie auch für andere Gase) sind. Es wurde gezeigt, dass die CO_2-Permeabilität (P_{CO2}) einer Lipidmembran hauptsächlich von zwei Faktoren abhängt: dem Cholesteringehalt der Membran und dem Einbau von zum CO_2-Transport fähigen Proteinen. Abhängig von der CO_2-Produktionsrate einer bestimmten Zelle, könnte ein zu niedriger P_{CO2} nachteilige Auswirkungen auf die Zell- und Körperhomöostase haben. Die Zielsetzung dieser Arbeit ist es folglich: 1- den P_{CO2} der Membranen dreier frisch isolierter Organellen/Zellen mit einem hohen oder normalen Sauerstoffverbrauch, und dementsprechender CO_2-Produktion, zu quantifizieren: Leber-Mitochondrien, Kardiomyozyten und Hepatozyten. 2- die Eigenschaften dieser Membranen zu identifizieren, die dem jeweiligen P_{CO2}-Wert zugrunde liegen, und schließlich, 3- herauszufinden, ob es eine Korrelation zwischen der CO_2-Permeabilität und der aeroben Stoffwechselrate der Zellen/Organellen gibt, d.h. ob es somit eine Anpassung des P_{CO2} an die CO_2-Produktionsrate gibt.

Für diese Dissertation wurden Kardiomyozyten, Hepatozyten und Leber-Mitochondrien von Lewis-Ratten isoliert und der P_{CO2} unter Verwendung der massenspektrometrischen ^{18}O-Austausch-Technik gemessen.

Mitochondrien haben den höchsten P_{CO2}, der je für eine biologische Membran gemessen wurde (0,3 cm/s), gefolgt von den Kardiomyozyten mit 0,1 cm/s und schließlich den Hepatozyten mit 0,03 cm/s. Der Sauerstoffverbrauch dieser Zellen und Organellen ergab sich aus der Literatur zu 1000 $nmol \cdot s^{-1} \cdot ml^{-1}$ für Mitochondrien, 297 $nmol \cdot s^{-1} \cdot ml^{-1}$ für Kardiomyozyten und 69 $nmol \cdot s^{-1} \cdot ml^{-1}$ für Hepatozyten. Aus einer Regressionsrechnung zwischen P_{CO2} und O_2-Verbrauch ergibt sich eine hochsignifikante positive Korrelation zwischen Sauerstoffverbrauch der Organellen/Zellen und ihrem P_{CO2}. Der P_{CO2} ist also offenbar an die jeweilige Stoffwechselrate sehr gut angepasst.

Der hohe P_{CO2} von Mitochondrien und Kardiomyozyten ist wohl vollständig durch ihren niedrigen Cholesteringehalt bedingt. Nur in Hepatozyten wurde ein kleiner Beitrag von DIDS-sensitiven CO_2-Kanälen gefunden. Die Hauptrolle bei der Anpassung des P_{CO2} an die metabolische Situation scheint also eine Variation des Cholesteringehalts der Zellmembranen zu spielen.

Abstract

Adaptation of the CO_2 permeability of various cells and organelles to their specific metabolic needs

Mariela Eugenia Arias Hidalgo

During the last 20 years, evidence has been accumulated that contradicts the paradigm that all cell membranes are highly permeable to CO_2 (as they are believed to be for other gases). It has been discovered that the CO_2 permeability (P_{CO2}) of a lipid membrane depends mainly on two factors: the cholesterol content of the membrane and the incorporation or absence of proteins capable of CO_2 transport. Depending on the CO_2 production rate of a certain cell, a low P_{CO2} could impair CO_2 release and have detrimental effects on cell and body homeostasis. Therefore, knowing that differences in P_{CO2} exist between different cell types, the aims of this work are: 1- to quantify the P_{CO2} of the membranes of cells/organelles freshly isolated from tissues with high and moderate oxygen consumptions and equivalent CO_2 productions, respectively. We have studied liver mitochondria, cardiomyocytes and hepatocytes; 2- to identify the characteristics of the membranes that constitute the basis of the different P_{CO2} values, and finally, 3- finding out if there is a correlation between the CO_2 permeability and the rate of aerobic metabolism of the cells/organelles, with the aim to test the hypothesis that P_{CO2} value of a membrane is adapted to a certain rate of CO_2 production.

For this dissertation, isolation of cardiomyocytes, hepatocytes and liver mitochondria of Lewis rats was performed, and the membrane P_{CO2} was determined using the mass-spectrometric ^{18}O exchange technique.

Mitochondria have the highest P_{CO2} ever measured for a biological membrane, 0.3 cm/s, followed by cardiomyocytes with 0.1 cm/s, and finally, hepatocytes with 0.03cm/s. The rates of oxygen consumption of these cells and organelles according to the literature is 1000 $nmol \cdot s^{-1} \cdot ml^{-1}$ for mitochondria, 297 $nmol \cdot s^{-1} \cdot ml^{-1}$ for cardiomyocytes, and 69 $nmol \cdot s^{-1} \cdot ml^{-1}$ for hepatocytes. From a regression calculation, there is a highly significant positive correlation between the P_{CO2} and the oxygen consumption of organelles or cells. This indicates that P_{CO2} is perfectly adapted to CO_2 production, ensuring that no limitation of CO_2 release by cells and organelles occurs.

The high P_{CO2} of mitochondria and cardiomyocytes seems to be essentially determined by the low cholesterol content of these membranes. Only in hepatocytes a small contribution of DIDS-sensitive CO_2 channels was found. The most important principle of how P_{CO2} is adapted to metabolism seems to be a variation of membrane cholesterol.

Introduction

It has been believed that CO_2 transport takes place freely by diffusion across the lipid phase of cell membranes. However, in the past 20 years evidence has accumulated that not all cell membranes behave as expected under this paradigm. The present study intends to determine the CO_2 permeability of a number of membranes from various interesting tissue cells and to study the molecular basis and the possible physiological significance of the different values of the CO_2 permeabilities found for these cells.

Mass spectrometric method to determine membrane CO_2 permeability

Most of the evidence on the variability of CO_2 permeabilities (P_{CO2}) has been produced using the mass spectrometric technique to measure P_{CO2} of plasma membranes (Wunder & Gros, 1998; Endeward & Gros, 2005; Endeward *et al.*, 2006, 2014; Itel *et al.*, 2012). With this method, utilizing the exchange of ^{18}O between HCO_3^-, CO_2 and H_2O, the rate of disappearance of $C^{18}O^{16}O$ from the extracellular fluid is followed by a mass spectrometer equipped with a special inlet system for fluids as first described by Itada & Forster (1977). From the time courses the permeabilities for CO_2 and HCO_3^- are obtained using the fitting procedure explained in Endeward & Gros (2005). In this system, the cells, organelles or vesicles to be studied are exposed to a solution of $C^{18}O^{16}O$ / $HC^{18}O^{16}O_2^-$ with a degree of ^{18}O-labelling of 1%. When carbonic anhydrase-containing cells or organelles are added to the chamber, they rapidly take up $C^{18}O^{16}O$, which is associated with a fall in extracellular $C^{18}O^{16}O$ (Figure 1, first phase). The speed of this process depends on the permeability of the membrane to CO_2 (P_{CO2}) and on the speed of the intracellular conversion of CO_2 to HCO_3^- that is catalyzed by the intracellular carbonic anhydrase. The slower phase following this first phase is dominated among other parameters by the permeability of the membrane for HCO_3^- (P_{HCO3^-}). Both permeabilities can be calculated by a fitting procedure from the time course of the entire curve of disappearance of $C^{18}O^{16}O$ as it occurs after the addition of cells (Figure 1). P_{CO2} derives predominantly from the first phase, P_{HCO3^-} mostly from the second phase. For this analysis, the intracellular carbonic anhydrase activity (CA_i) must be known and is determined independently in cell/organelle lysates, also by mass spectrometry. All experiments are terminated by the addition of an excess of CA in order to establish final isotopic equilibrium.
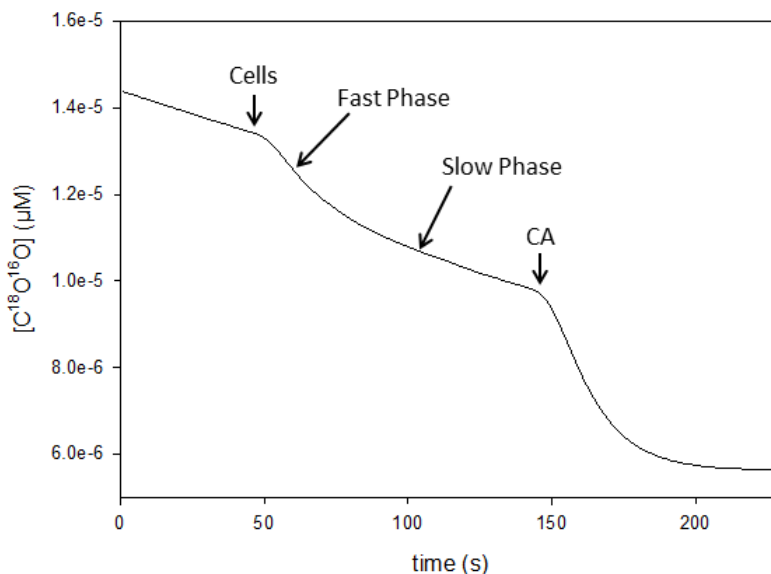
Figure 1: Original recording of a mass spectrometric experiment with isolated hepatocytes (in the presence of verapamil and extracellular carbonic anhydrase inhibitor, see below). The decay of the concentration of $C^{18}O^{16}O$ in the mass spectrometric reaction chamber is plotted semi-logarithmically versus time. After addition of the cells, a characteristic biphasic time course of the signal is seen, indicating that intact CA-containing cells have been added. The arrow "Cells" indicates where cell suspension was added, the arrow "CA" indicates where the experiment was terminated by the addition of excess CA. The Arrow "Fast Phase" points to the first fast phase developing after the addition of cells, the arrow "Slow Phase" points to the subsequent slower phase of the same process.

Parameters influencing P_{CO2}

The permeability to CO_2 of different natural and artificial membranes can be highly variable. For example, phospholipid bilayers have been reported to exhibit a very high CO_2 permeability (P_{CO2}) of 0.35 cm/s (Gutknecht *et al.*, 1977) or even 3.2 cm/s (Missner *et al.*, 2008), while other membranes such as the apical membrane of colon epithelium present a very low P_{CO2} of 0.0015 cm/s (Endeward & Gros, 2005).

It has been demonstrated that the amount of cholesterol in the membrane has a dramatic influence on the CO_2 permeability (Itel *et al.*, 2012). On the other hand, it has been shown that the movement of CO_2 occurs not only across the lipid phases of membranes; instead, protein gas channels present in the membrane can substantially improve the transport of this molecule across the membrane (Nakhoul *et al.*, 1998; Endeward *et al.*, 2006, 2008; Itel *et al.*, 2012).

We can then conclude that it appears that the two most important parameters influencing P_{CO2} of a biological membrane are: 1) the cholesterol content of the membrane and 2) the presence or absence of CO_2 channels.

Cholesterol content of the membrane

It has been observed that, when phospholipid vesicles or MDCK cell membranes are experimentally depleted of or enriched with cholesterol, they show drastic increases or decreases in P_{CO2}, respectively (Itel *et al.*, 2012; Kai & Kaldenhoff, 2014; Tsiavaliaris *et al.*, 2015). These data suggest that the amount of cholesterol in cell membranes is a crucial factor of P_{CO2}.

According to Itel *et al.* (2012), who measured P_{CO2} with the mass spectrometric technique, membranes with a cholesterol content under approximately 20 mol% possess a very high permeability (i.e. >0.1cm/s). If the amount of cholesterol is increased to 40%, the P_{CO2} decreases by a factor of 10 (0.01 cm/s), and if one increases the cholesterol content even further to 70%, as it is present in the apical membrane of colon epithelium, the P_{CO2} decreases by a factor of 100 (0.0015cm/s). The same findings were confirmed with the stopped-flow technique in which an increase in the cholesterol content of a vesicle from 0 to 50%, reduces the P_{CO2} at least by a factor or 10 (Tsiavaliaris *et al.*, 2015).

Differences in the cholesterol content of different biological membranes will have an incidence on the P_{CO2}. A few examples of this have been collected for red blood cells (Endeward *et al.*, 2006), MDCK cells (Itel *et al.*, 2012) and the apical membranes of colon epithelia (Endeward & Gros, 2005). Until now, no freshly isolated cells from tissues of greatly varying rates of oxygen consumption have been examined.

CO_2 channels

Most striking evidence for the involvement of protein channels in CO_2 transport has been obtained in the human red blood cell membrane, where proteins AQP1 (Endeward *et al.*, 2006) and Rhesus-associated glycoprotein (RhAG; Endeward *et al.*, 2008) are responsible for > 90% of the CO_2 transport. If these channels are inhibited, the P_{CO2} of the red cell membrane decreases by a factor of 10 from 0.15 cm/s to 0.015cm/s.

Another group has identified other aquaporin isoforms like AQP0, AQP4, AQP5, AQP6 and AQP9 (Geyer *et al.*, 2013*a*) and non-erythroid members of the family of Rhesus protein associated glycoproteins, RhBG and RhCG (Geyer *et al.*, 2013*b*), that are also capable of transporting CO_2. The expression and abundance of these proteins is different in every cell type and is not yet known if they also play such an important role for P_{CO2} as it happens with red blood cells.

Metabolism and P_{CO_2}

In all cells and mitochondria it is expected that a given O_2 consumption is associated with an equal CO_2 production. This requires that in these tissues, both gases meet no major diffusion resistance when passing through the cell membrane. The model presented by Endeward *et al.* (2014) considers the CO_2 production rate under maximal exercise conditions for a cardiomyocyte. Using Fick's law, this model predicts that permeabilities lower than 0.1 cm/s in conditions of maximal metabolism will exert a limiting effect on the release of CO_2 by these cells.

The heart and mitochondria possess the highest metabolic rates among mammalian tissues or organelles. The estimated oxygen consumption of the heart, under conditions of maximal aerobic exercise, is 0.4 ml O_2/(g·min), very high compared to other tissues and organs like the liver, which has an oxygen consumption of 0.05 ml O_2/(g·min) (both numbers from Schmidt & Thews, 1986). Determining the P_{CO_2} of these cell types and combining them with the data available for other cell types with lower metabolic rates (Itel *et al.*, 2012), will allow us to see if there is a correlation between aerobic metabolism and CO_2 permeability across cell membranes.

Therefore, the aim of this study is to measure CO_2 permeability of the membranes of cardiomyocytes and mitochondria (two systems with an exceptionally high rate of aerobic metabolism) and hepatocytes (as a control, a cell of moderate metabolic rate). Furthermore, it is intended to probe to which extent different membrane cholesterol contents and/or protein gas channels, such as aquaporins and Rhesus proteins, are involved in varying CO_2 permeabilities. This information is expected to yield new insights into the mechanism of gas exchange of cell membranes in active tissues and, specifically, allow us to see if there is a positive correlation between CO_2 permeability and metabolic rate.

Results

For this thesis, Lewis Rats were used to obtain the cells and organelles under the project numbers of the Niedersächsisches Landesamt für Verbraucherschutz und Lebensmittelsicherheit Nos. 33.9-13/1225 (cardiomyocytes), 2015/102 (mitochondria) and 15/2048 (hepatocytes).

In this section, intracellular/intraorganellar CA activities and P_{CO2} values of mitochondria, cardiomyocytes and hepatocytes will be presented and discussed. Also, the most important special problems that occurred during these measurements will be remarked on. The major goal is to establish the relationship between metabolism and P_{CO2}.

The results of mitochondria have been already published in Arias-Hidalgo *et al.*, 2016 and of cardiomyocytes in Arias-Hidalgo *et al.*, 2017. The results obtained for hepatocytes will be published as Arias-Hidalgo *et al*., "CO_2 permeability of rat hepatocytes and the influence of FC5-208A" (manuscript in preparation).

Estimation of the intracellular/intraorganellar carbonic anhydrase activity

Intracellular/intraorganellar CA activity (CA_i) must be known in order to be able to calculate the P_{CO2} of the cells and organelles from the mass spectrometric records (Endeward & Gros, 2005). This activity is estimated using the lysate from each preparation, also by means of mass spectrometry (Endeward & Gros, 2005). The following table summarizes the CA_i activity found for mitochondria, cardiomyocytes and hepatocytes.

Table 1: CA_i activity of mitochondria, cardiomyocytes and hepatocytes. The "n" reflects the number of rats.

Sample	CA_i
Mitochondria	675 (SD ± 151, n=8)[1]
Cardiomyocytes	5070 (SD ± 2140, n= 17)[2]
Hepatocytes	1898 (SD ± 591, n=8)

1. Arias-Hidalgo *et al.*, 2016, 2. Arias-Hidalgo *et al.*, 2017

P$_{CO2}$ of Mitochondria

In the case of mitochondria, transmission electron microscopy, dynamic light scattering and O$_2$ consumption experiments were performed to establish the morphological and functional conditions of the organelles in suspension. In all cases, the mitochondria from the rat liver were found to have a $\geq$ 70% normal and intact morphology, normal maximal oxygen consumption and a high respiratory control ratio (RCR). Thus, the mass spectrometric measurements were performed with mitochondria that were morphologically and functionally in very good condition (for more details see: Arias-Hidalgo *et al.*, 2016).

To assess the P$_{CO2}$, experiments with control organelle suspensions, pre-incubation with FC5-208A (an extracellular CA (CA$_e$) inhibitor) or with DIDS (an AQP1- and RhAG-gas channel inhibitor) were performed. In all three cases a permeability 0.3 cm/s was found, with no significant difference between any of the treatments (Figure 2).
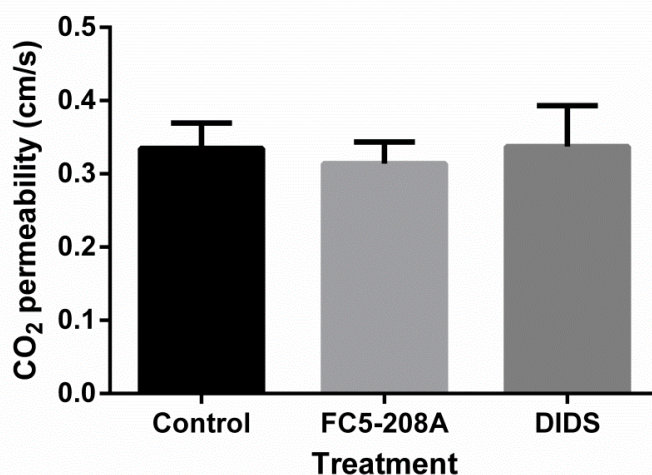
Figure 2: CO$_2$ permeability of mitochondria in suspension and the effect of extracellular CA inhibitor FC5-208A ($2.5 \cdot 10^{-5}$ M) and the CO$_2$ channel inhibitor DIDS ($1.0 \cdot 10^{-4}$ M). ANOVA p=0.29. From left to right n=24, n=10, n=5. Bars represent SD. (Arias-Hidalgo *et al.*, 2016)

P$_{CO2}$ of Cardiomyocytes

All our cardiomyocyte cell suspensions had a low vitality of around 6% on average (2-14%). The method we use to estimate the P$_{CO2}$ requires that only living cells are capable of giving a mass-spectrometric signal. To check if non-vital cells could be interfering with our findings, two experiments were performed.

The first one was to carry out mass-spectrometric recordings with completely non-vital cell suspensions. These non-vital cells were studied under control conditions and also with addition of Triton, or extra- or intracellular CA inhibitors, respectively. The non-vital cell suspensions (0% vitality) were obtained occasionally, when the heart cannulation took longer than 5 minutes, or when there were problems during the perfusion. The mass spectrometric records were analyzed using a semi logarithmic plot ($C^{18}O^{16}O$ signal logarithmized, time non-logarithmized) and the slope of these plots after the addition of non-vital cells (with and without Triton or CA inhibitors) was compared with the initial slope of the uncatalyzed rate of the decay of $C^{18}O^{16}O$ as it occurred before the addition of cells. If a ratio of these slopes equal to 1 is found, it means that there is no difference between the initial slope (uncatalyzed reaction) and the slope after the addition of cells, and therefore it follows that the added cells possess no CA activity accelerating the reaction.

The results summarized in Table 2 shows that after the addition of non-vital cells there is no change in the rate of the reaction (1st column). The same is found when non-vital cells are lysed with Triton (2nd column), pre-incubated with extracellular CA inhibitor FC5-208A (3rd and 4th column), or the extra- plus intracellular CA inhibitor ethoxzolamide (5th column). This means that non-vital cardiomyocytes lack of extracellular as well as intracellular CA activity, which could interfere with the mass spectrometric technique to measure P_{CO2} of living cardiomyocytes.

Table 2: Ratios of the slopes of mass spectrometric recordings before and after addition of non-vital cardiomyocytes in suspension. (Arias-Hidalgo *et al.*, 2017)

Treatment	NVCS	NVCS + Triton	NVCS + FC5-208A	FC5-208A, 5 min pre-incubation	Ethoxzolamide, 5 min pre-incubation
Mean ratio	1.06	1.08	1.04	1.02	0.99
SD	± 0.04	± 0.05	± 0.05	± 0.02	± 0.05
n	13	4	5	3	3

The second approach, to establish the potential influence of non-vital cardiomyocytes on the mass spectrometric measurements, was staining the cell suspensions with DNSA. This experiment showed a marked difference in DNSA staining between vital and non-vital cardiomyocytes. As is apparent in Figure 3, we found a strong fluorescence in living cardiomyocytes (rectangularly shaped) but none in the non-vital rounded cells. This confirms that CA is present only in living cardiomyocytes. Thus, two lines of evidence show that non-vital cardiomyocytes are devoid of CA, meaning that they will not contribute to the mass spectrometric signal and have no influence on the signal generated by the vital cells.
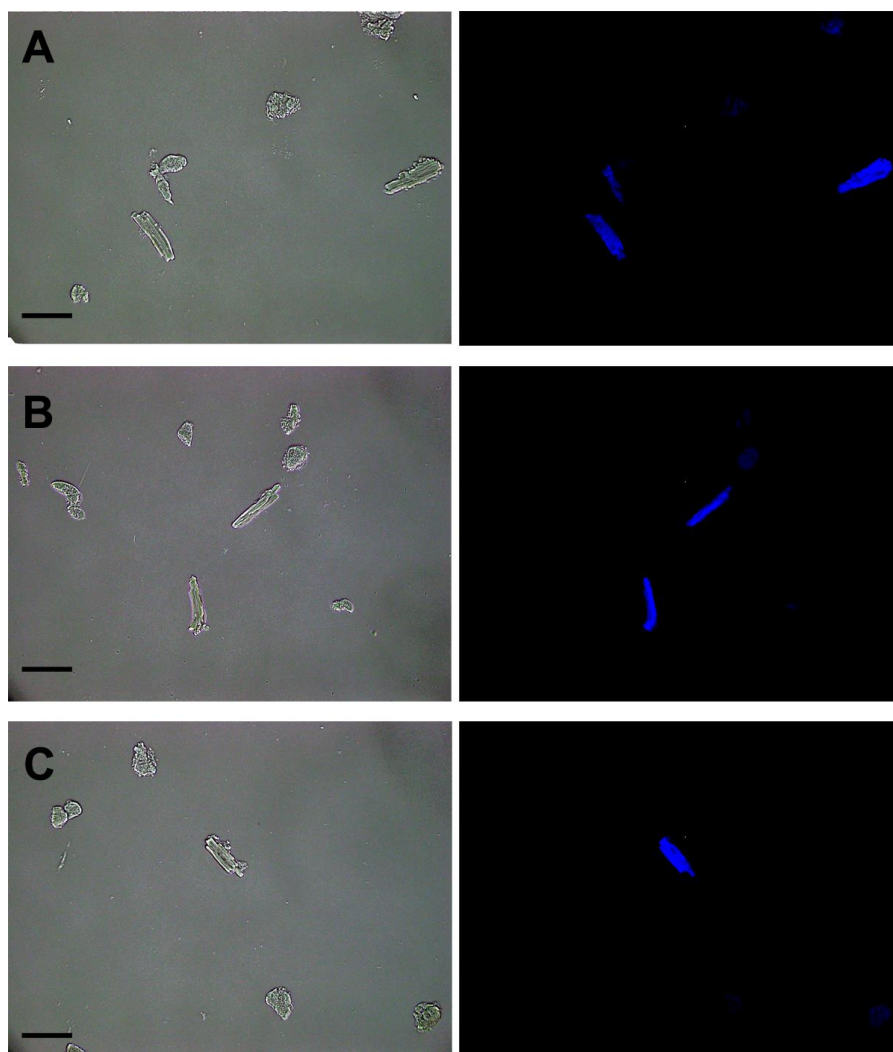
Figure 3: DNSA staining of a suspension of isolated cardiomyocytes. A, B, C represent three views from a partially vital cardiomyocyte suspension. On the left, the three sections viewed by phase contrast microscopy, on the right, the same sections viewed in the DNSA fluorescence mode (DNSA concentration $1.0 \cdot 10^{-5}$M). Comparing phase contrast and fluorescence pictures, it is apparent that the living cardiomyocytes, which conserve their rectangular shape, are intensely stained for carbonic anhydrase, while the rounded non-vital cardiomyocytes are unstained and thus contain no CA. In phase contrast microscopy no red blood cells, and in fluorescence microscopy no stained cells other than living cardiomyocytes are visible. Bars 100μm. (Arias-Hidalgo *et al.*, 2017).

P_{CO2} was again estimated in control experiments without any additions, and with cells preincubated in FC5-208A or DIDS, respectively. In this case, a significant difference between experiments under control conditions and with FC5-208A was found (Figure 4). The effect of FC5-208A indicates that vital cardiomyocytes possess an extracellular CA (CA_e) that will affect the mass spectrometric signal and distort the calculation of permeabilities. Therefore, the experiments in the presence of DIDS had also to be repeated with a simultaneous incubation in FC5-208A, to check if perhaps an effect of DIDS was obscured by the effect of extracellular CA. As seen in Figure 5, P_{CO2} in the presence of FC5-208A (0.10 cm/s ($\pm$ 0.06; n =15)), does not differ from the value of 0.11 cm/s ($\pm$ 0.07, n=7) found in the presence of FC5-208A plus DIDS. This shows that DIDS has no significant effect on the CO_2 permeability. It also shows that 0.10 rather than 0.2 cm/s is the correct P_{CO2} of cardiomyocytes.
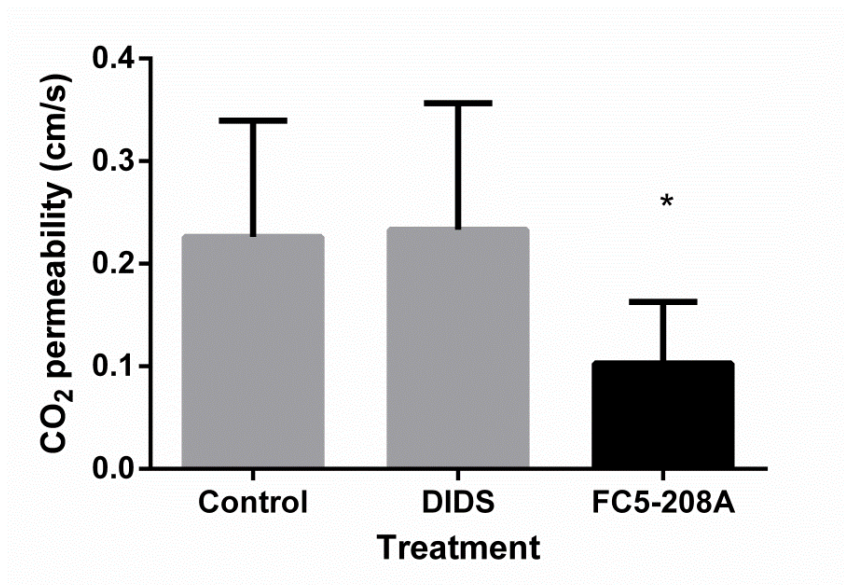
Figure 4: CO_2 permeability of cardiomyocyte suspensions and the effect of inhibitors. Under control conditions P_{CO2} was 0.23 cm/s ($\pm$ 0.11; n =14). $1 \cdot 10^{-4}$ M DIDS had no effect and yielded a P_{CO2} of 0.23 cm/s ($\pm$ 0.12; n =7). However, $2.5 \cdot 10^{-5}$ M of the extracellular CA inhibitor FC5-208A reduced P_{CO2} significantly to 0.10 cm/s ($\pm$ 0.06; n =15). n from left to right: 16, 7, 13. Bars are SD. ANOVA yields P=0.0016. With Dunnett's posttest FC5-208A is significantly different from control (*), DIDS has no effect. (Arias-Hidalgo *et al*., 2017)
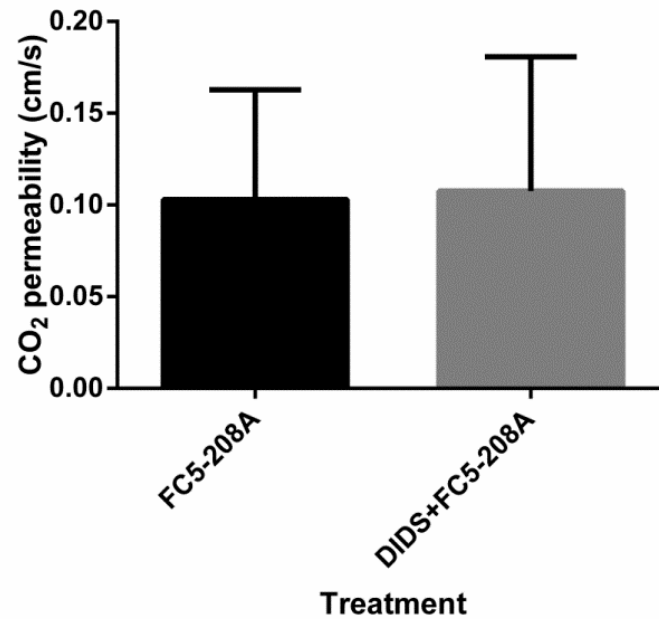
Figure 5: CO_2 permeabilities of cardiomyocytes pre-incubated with $2.5 \cdot 10^{-5}$ M extracellular CA inhibitor FC5-208A, without and with $1 \cdot 10^{-4}$ M DIDS. n from left to right: 15, 7. Bars represent SD. Student's t test: p=0.88. The right-hand column shows that in the presence of FC5-208A, as in its absence (Fig. 4), DIDS has no effect on P_{CO2}. (Arias-Hidalgo *et al.*, 2017)

P_{CO2} of Hepatocytes

During the fitting procedure of control experiments with freshly isolated hepatocytes from the rat, most of the P_{CO2} values did not reach convergence ($P_{CO2} \geq 0.1$cm/s). However, when incubating cells in FC5-208A (the CA_e inhibitor), the permeability on the other hand became extremely low ($P_{CO2} \sim 0.01$cm/s). This observation would be explicable, in case the supposedly extracellular CA inhibitor would enter the cell interior and inhibit CA_i in addition to CA_e. We note that the extracellular inhibitor FC5-208A is usually impermeable to cell membranes because it is a polyvalent organic cation (Perut *et al.*, 2015). In the case of the hepatocytes – unlike to what we see with cardiomyocytes, mitochondria and also erythrocytes – we observe upon addition of FC5-208A to an ongoing mass spectrometric control experiment, an upward shift of the record (see Figure 6 A, 2nd arrow). All other cells mentioned show either no effect in this experiment or a downward shift if there is extracellular CA present. A computer simulation performed in our laboratory (data not published) indicates that such an upward shift upon addition of a CA inhibitor occurs only, if the inhibitor enters the cells and inhibits intracellular CA.

This is confirmed in Fig. 6B, where, instead of FC5-208A, we add the highly membrane-permeable CA inhibitor ethoxzolamide, which as predicted leads to a strong upwards shift of the recorded curve. Thus, both the model calculation and the experiment of Figure 6B indicate clearly that in the case of hepatocytes FC5-208A crosses the cell membrane and inhibits intracellular CA.
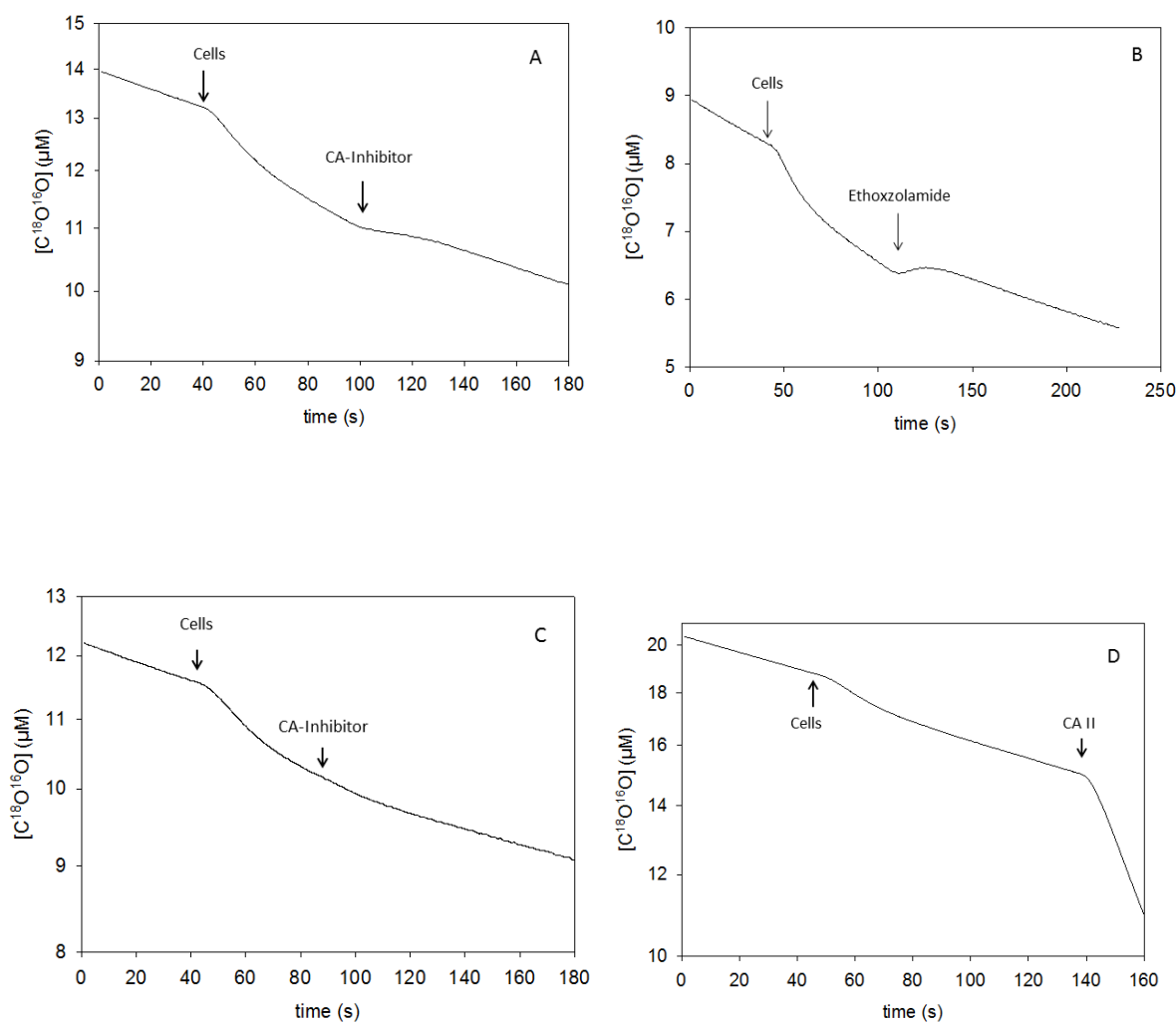
Figure 6: Original mass spectrometric recordings of liver cells under different conditions. A- Hepatocyte suspension under control conditions with addition of $5 \cdot 10^{-5}$ M CA$_e$ inhibitor FC5-208A during the ongoing experiment (second arrow). B- Identical experiment as in A, but with addition of the permeable CA inhibitor ethoxzolamide instead of FC5-208A to the ongoing experiment (second arrow). C- Hepatocytes preincubated for 5min in 20 μM Verapamil and measured under this condition. Addition of $5 \cdot 10^{-5}$ M FC5-208A to the ongoing experiment (second arrow). D- Hepatocytes preincubated with 20 μM Verapamil were added into the solution in the measuring chamber that contained 20 μM Verapamil plus $5 \cdot 10^{-5}$ M FC5-208A (first arrow). Isotopic equilibrium was finally established at the end of the experiment by addition of excess CA (second arrow). This was the standard way in which all experiments were performed.

The first step to solve this problem was searching for possible transporters in the hepatocyte membrane that might be able to transport the inhibitor into the cell. Rat liver expresses OCT1 (Wang *et al.*, 2015), an organic cation transporter, which would be a candidate for the uptake of FC5-208A by hepatocytes. Verapamil, a known OCT1 inhibitor, was used to block this transporter with a concentration of 20 μM, which is 32 times its IC_{50} for Metformin (Ahlin *et al.*, 2011), 14 times greater than the IC_{50} described for serotonin (Boxberger *et al.*, 2014) and 6 times the I_{50} for tetraethylammonium (TEA; Zhang *et al.*, 1998), in order to achieve a nearly complete inhibition. After 5min incubation of the cell suspensions with Verapamil (Figure 6C), addition of the FC5-208A during the ongoing experiment did not lead anymore to the upwards "bump" in the mass spectrometric record. This shows that no inhibition of intracellular CA occurred anymore (Figure 6C). Of course, the inhibition of extracellular CA persisted. After these findings, pre-incubation of cells with Verapamil was included in all the experiments in order to be able to use the FC5-208A for inhibition of extracellular CA only. Thus, it was possible to determine the P_{CO2} for the hepatocytes without the distorting influence of extracellular CA activity. Figure 6D shows that in the presence of both, Verapamil and FC5-208A, we obtained the usual record for or organelle or cell suspensions as may be seen in Arias-Hidalgo *et al.* (2016, 2017).

For the standard determinations of hepatocyte P_{CO2}, cells were pre-incubated with Verapamil, but the equally necessary extracellular CA inhibitor was added to the measuring chamber before starting the experiments. Thus the cells were exposed to FC5-208A only in the moment they were pipetted into the measuring chamber. This procedure was chosen to minimize the possibility of the FC5-208A entering the cells. With this precaution, we found the P_{CO2} to be 0.03 cm/s (±0.01, n=8 rats). In the presence of $1 \cdot 10^{-4}$ M DIDS, this value fell to 0.02 cm/s (±0.006, n=8 rats) as can be seen in Figure 7, which shows a significant effect of DIDS on P_{CO2} (P=0.017).
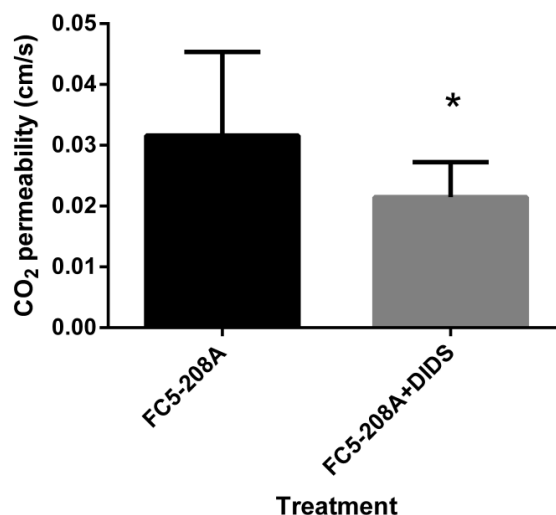
Figure 7: P_{CO2} of rat hepatocytes and the effect of DIDS. In both cases the concentration of FC5-208A was $5 \cdot 10^{-5}$ M and that of DIDS $1 \cdot 10^{-4}$ M. * indicates a significant difference (Student's paired t-test, t=3.098, df=7, p=0.017).

Correlation between metabolism and P_{CO2} and the relationship of these parameters with membrane cholesterol.

Table 3 summarizes the information about P_{CO2} and oxygen consumption for mitochondria, cardiomyocytes and hepatocytes (this work). Additionally data for MDCK cells and the basolateral membrane of proximal colon epithelia (PCE) were included.

Table 3: Oxygen consumption and P_{CO2} of different cell types and mitochondria.

Type of cell/organelle	Rate of Oxygen Consumption ($nmol \cdot s^{-1} \cdot ml^{-1}$)	P_{CO2} (cm/s)
MDCK	12[a]	0.017[e]
Basolateral membrane PCE	54.7[b]	0.022[f]
Rat Hepatocytes	69.3[c]	0.03
Rat Cardiomyocytes	297[d]	0.1[g]
Mitochondria	1000[a]	0.3

a-Arias-Hidalgo *et al.*, 2016 **b**-Converted from Del Castillo *et al.*, 1991 **c**- Converted from Foy *et al.* 1994   **d**- Converted from Schmidt & Thews, 1986   **e**-Itel *et al.*, 2012 **f**-Endeward & Gros, 2005 **g**-Arias-Hidalgo *et al.*,2017.

The sequence of values in Table 3 shows clearly that membranes of cells or organelles with a high O_2 consumption show a higher P_{CO_2} than cells with lower metabolism. Actually, Figure 8 shows that there is an excellent and practically linear correlation between P_{CO_2} and O_2 consumption (or CO_2 production). This might suggest that there is an adaptation of membrane P_{CO_2} to the rate of aerobic metabolism.

As discussed above, P_{CO_2} depends basically on two factors: cholesterol content of the membrane and the presence of CO_2 channels. Itel *et al*. (2012) have already explained that there is a negative correlation between the P_{CO_2} and the cholesterol content of the membrane of liposomes. Here, we are able to show the same correlation, but for freshly isolated intact cells and organelles, confirming his observations that membrane cholesterol content correlates negatively with the value of P_{CO_2} (Figure 9). It is apparent that cholesterol is the major determinant of the CO_2 permeability of many cells from mammalian tissues. In the data of Figure 9, CO_2 channels have no influence, except a very minor one in the case of hepatocytes.
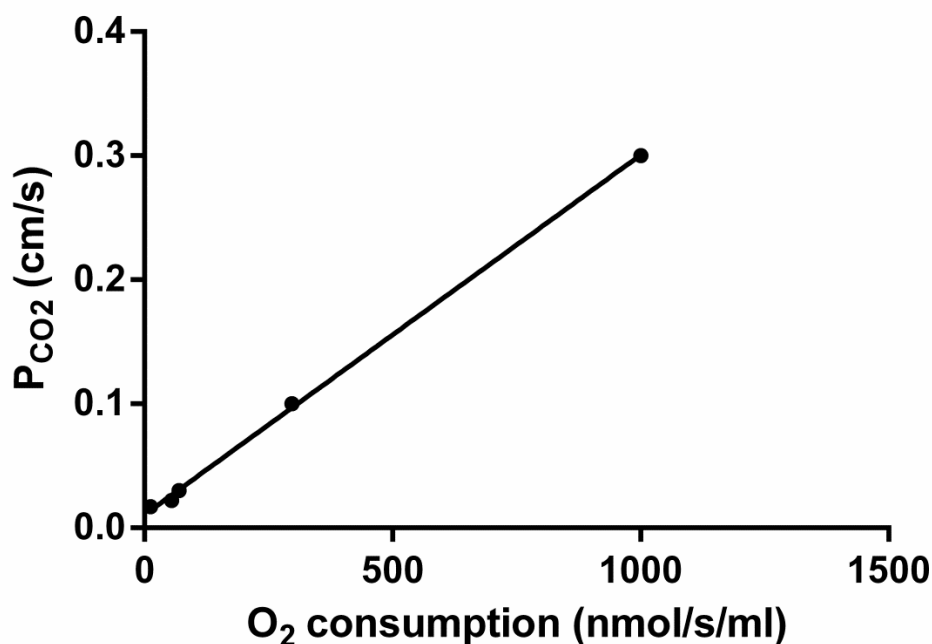
Figure 8: Linear regression between P_{CO_2} and O_2 consumption for (from left to right) MDCK cells, the basolateral membrane of colon epithelium, hepatocytes, cardiomyocytes, and mitochondria. R=0.99, p<0.0001.
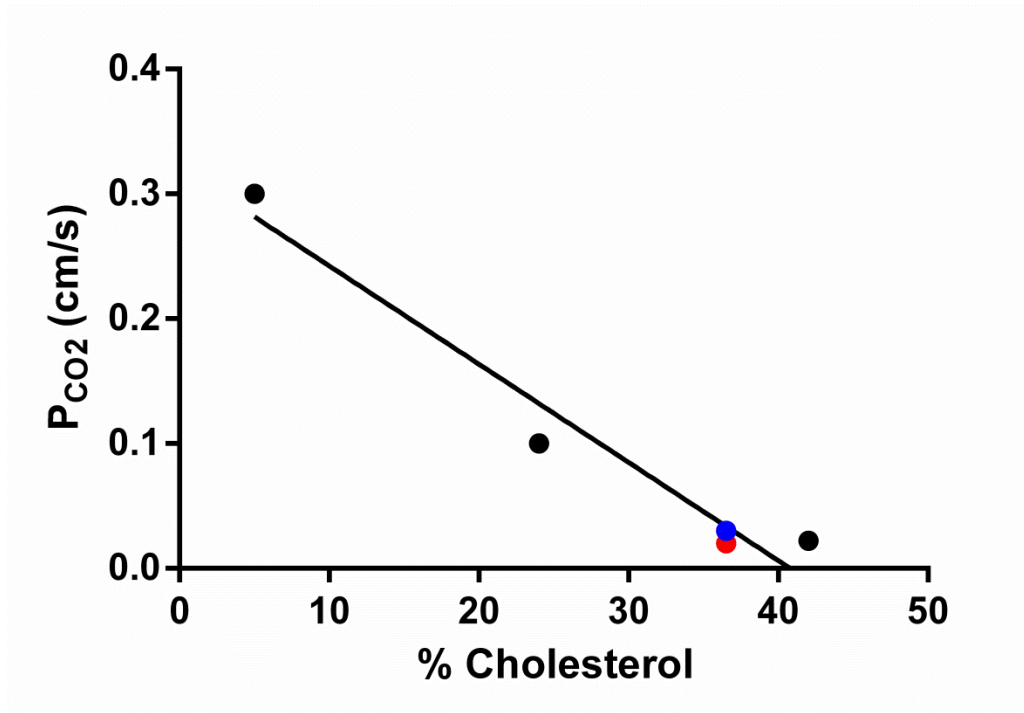
Figure 9: Linear regression between P_{CO_2} and cholesterol content of the membrane for (from left to right) mitochondria, cardiomyocytes, hepatocytes and the basolateral membrane of colon epithelium. In red (•) is the permeability of hepatocytes with DIDS, and in blue (•) the hepatocyte permeability without DIDS. R=0.97, p=0.004.

If we plot two of the three parameters of Figure 8 and Figure 9 in a different combination, namely O_2 consumption versus membrane cholesterol, we see again a good correlation (Figure 10). Note that the data in Figure 10 contain some additional data from the literature that could not be included in Figure 8 and Figure 9, because P_{CO_2} has not been measured. The way of looking at the data as implemented in Figure 10 might lend itself to the speculation that it is the rate of oxidative metabolism that determines membrane cholesterol. The rate of oxidative metabolism would then be a candidate mechanism for the apparently excellent adaptation of P_{CO_2} to O_2 consumption/CO_2 production of a cell. However, this is highly speculative and no data seem available in the literature to support this idea.
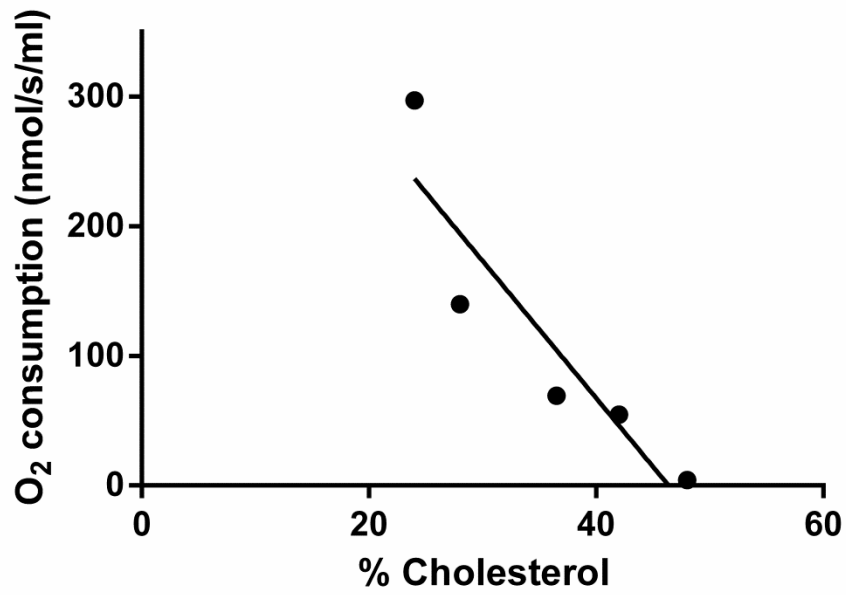
Figure 10: Linear regression of O_2 consumption versus the cholesterol content of membranes primary isolated cells. Data point from left to right are: cardiomyocytes, skeletal muscle (Schmidt & Thews, 1986; Williams & Smith, 1989) , hepatocytes, basolateral membrane of proximal colon ephitelia, neutrophils (Proctor, 1979; Wright *et al.*, 1997). R=0.91 p=0.03.

Discussion

Intracellular carbonic anhydrase activity of mitochondria, hepatocytes and cardiomyocytes

It is known that the rat liver mitochondria possess CA V in their matrix. The activity inside the rat liver mitochondria was estimated by Vincent & Silverman (1982), who reported a value of 700, very similar to the 675 that we report here, but they also described that the CA activity is distributed between the matrix and the space between the inner and outer membrane. This latter observation could not be confirmed by our experiments because the CA inhibitor FC5-208A (mol.wt. 376.81) is expected to be able to enter the space between the two membranes through the porins but should not have access to the matrix. As we show in Figure 2, FC5-208A has no effect on the calculated CO_2 permeability of mitochondria. If there was significant extra-matrix CA in these mitochondria, we would expect a marked change of the mass spectrometric signal upon addition of the inhibitor. Thus, the present results show that CA is localized entirely in the mitochondrial matrix space. The latter conclusion is in agreement with the observations of Balboni & Lehninger (1986) in rat liver mitoplasts, which lack of the outer membrane, and still exhibit a similar rapid uptake of CO_2 into the matrix as intact liver mitochondria.

In the case of rat hepatocytes, several membrane-bound and cytoplasmic carbonic anhydrases have been described. CAIV is the membrane-bound form present on the plasma membrane and the endoplasmic reticulum, and CAII and CAIII are in the cytoplasm (Ono *et al.*, 1992; Dodgson *et al.*, 1993). Using the data published by Ono *et al.* (1992) and assuming an overall protein concentration of 200 mg/ml, rat hepatocytes have a CA activity of 1,400 which is in good agreement with the value of 1,898 obtained from our lysates.

Mitochondria and hepatocytes show a quite good agreement between the CA activities obtained in our experiments and the ones found in the literature. The situation is not so uniform in the case of cardiomyocytes. Using the cardiomyocyte lysate data of Villafuerte *et al.* (2014) together with the information they give, and in addition assuming an overall protein concentration of 200 mg/ml for heart tissue, we arrive at a CA activity of undiluted heart homogenate of between 600-6000 from their data. This is in agreement with our value of 5000 for isolated vital cardiomyocytes. On the other hand, Schroeder *et al.* (2013) report an intracellular CA activity for Wistar rat hearts of only 2.7, which is orders of magnitude lower than the present value and absolutely incompatible with our mass spectrometric results.

If we calculate the minimum CA activity necessary to explain our recordings by setting arbitrarily the P_{CO_2} so high that the membrane offers no noticeable resistance to CO_2 diffusion (i.e $P_{CO_2} \geq 10$; Endeward & Gros, 2005; Endeward *et al.*, 2014), we calculate a CA_i of 3,740, which represents the minimum CA activity necessary to explain the mass spectrometric results (Arias-Hidalgo *et al.*, 2017). The CA_i activity of ~5000 is probably almost completely due to intracellular membrane-bound CA, as is the case in hearts of other species (Bruns & Gros, 1992; bovine; Geers *et al.*, 1992; rabbit). The expression of cytosolic CAII in cardiomyocytes normally occurs at very low levels (Brown *et al.*, 2012; Alvarez *et al.*, 2013; Torella *et al.*, 2014). This is confirmed by Arias-Hidalgo *et al.* (2017), who use DNSA fluorescence staining and confocal imaging to demonstrate that CA is not distributed homogeneously in the cell but associated with structures. The pattern this staining shows is consistent with an association of the CA with the longitudinal system of the sarcoplasmic reticulum.

Mechanistic basis of the P_{CO_2} of mitochondria, hepatocytes and cardiomyocytes

The influence of CO_2 channels

In mitochondria and cardiomyocytes we find no effect of DIDS and therefore no contribution of DIDS-sensitive CO_2 channels to P_{CO_2}. In the case of mitochondria, the only known aquaporin is AQP8 (Calamita *et al.*, 2005), and this AQP is no CO_2 channel (Geyer *et al.*, 2013*a*). Cardiomyocytes, on the other hand, express several AQPs (Butler *et al.*, 2006) but only AQP1 and AQP4 are candidates for CO_2 transport (Geyer *et al.*, 2013*a*). Nevertheless, AQP4 has not yet been found at the protein level in rat heart (Butler *et al.*, 2006) and AQP1 occurs only in cardiac endothelium but not in the sarcolemma of adult rats (Nielsen *et al.*, 1993; Netti *et al.*, 2014).

In hepatocytes, on the other hand, P_{CO_2} is reduced by a third in the presence of DIDS (from 0.03 cm/s to 0.02 cm/s). From the known CO_2 channels (Geyer *et al.*, 2013*a*), only AQP9 is known to be expressed in the plasma membrane (Huebert *et al.*, 2002). Therefore, AQP9 could be participating in CO_2 transport. Unfortunately, information about the DIDS sensitivity of this channel is not available. Another possibility is that rat hepatocytes also express the non-erythroid forms of Rhesus proteins, RhBG and RhCG, which have been described in the mouse liver (Liu *et al.*, 2001; Weiner *et al.*, 2003). Both Rhesus proteins are also capable of transporting CO_2 (Geyer *et al.*, 2013*b*), but again, there is no information about the DIDS sensitivity of these channels.

Therefore, we do have a DIDS effect, which means that there are DIDS-sensitive CO_2 channels involved, but we are not able to specify which specific protein contributes to hepatocyte CO_2 permeability.

The influence of membrane cholesterol

Itel *et al.* (2012) have shown that the amount of cholesterol present in the membrane of liposomes has a very strong effect on P_{CO2}; the lower the cholesterol the higher the permeability. This is shown impressively in Figure 11(black dots), where it is seen that P_{CO2} of liposomes decreases by at least two orders of magnitude when membrane cholesterol increases from 0 to 70%. The red data points in Figure 11 illustrate that the present results, for membranes of intact cells and mitochondria, agree remarkably well with the results of Itel *et al.,* (2012) for artificial liposomes. Mitochondrial membranes, with only 3% moles cholesterol/moles total membrane lipid (Alberts *et al.*, 2011), exhibit the highest permeability ever reported for a biological membrane, 0.3 cm/s (Arias-Hidalgo *et al.*, 2016). Rat cardiomyocytes possess a membrane cholesterol between 19% (de Jonge *et al.*, 1996) and 26% moles cholesterol/moles of total membrane lipids (Ma *et al.*, 1995), and exhibit a P_{CO2} of 0.1 cm/s (Arias-Hidalgo *et al.*, 2017). In the case of hepatocytes, the permeability of 0.02 cm/s (permeability in the presence of DIDS, thus probably excluding the contribution of CO_2 channels) also corresponds quite well with their membrane cholesterol content that amounts to about 36.5%, the average from the available determinations in the literature (Storch & Schachter, 1984; Mahler *et al.*, 1988; Burger *et al.*, 2007). Figure 11 includes in addition previously published pairs of P_{CO2} and membrane cholesterol for the basolateral membrane of proximal colon epithelium and for the apical membrane of proximal colon epithelium, both from the guinea pig (Endeward & Gros, 2005). It is apparent that there is an excellent agreement of the relations between P_{CO2} and membrane cholesterol for biological membranes on the one hand, and for artificial liposomes on the other hand. Thus, Figure 11 confirms that membrane cholesterol is an extremely important parameter determining membrane P_{CO2}. Moreover, Figure 11 shows that for a large number of cells, if not for most, cholesterol is the most dominating determinant of P_{CO2}. As will be discussed below, it appears that the incorporation of CO_2 channels into biological membranes, in order to achieve a sufficiently high CO_2 permeability, is rather an exception than a rule. Most cells seem to owe their specific P_{CO2} value to the cholesterol in their membranes.

In this discussion of cholesterol effects on P_{CO2}, it is important to state that we present mean values of cholesterol as well as P_{CO2} for the whole membrane of the cell. In many cases the cell membrane will not exhibit homogeneous distribution of cholesterol and thus not homogeneous CO_2 permeabilities. It remains to be studied how specific regions of the cell membrane, like lipid rafts, behave.
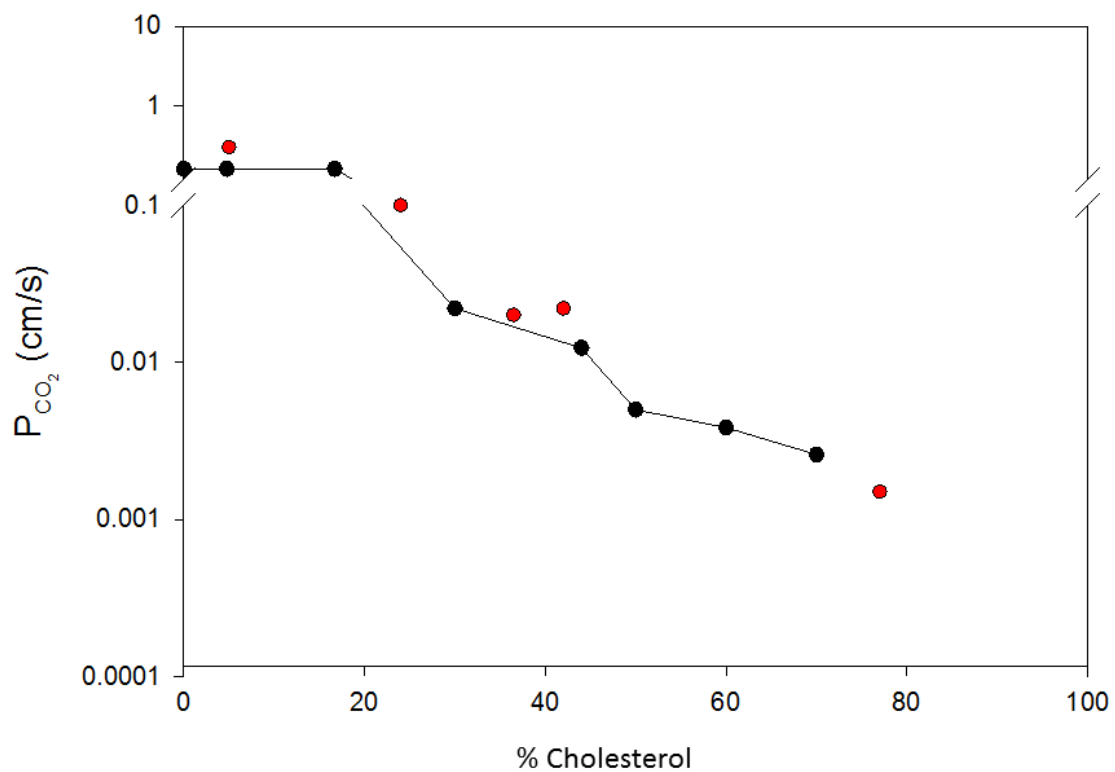
Figure 11: Effect of cholesterol on CO_2 permeability. In black (•)are plotted the results obtained by Itel *et al.*, 2012 for lipid vesicles loaded with cholesterol, and in red (•) the results, from left to right, for mitochondria, cardiomyocytes, hepatocytes (this work), basolateral membrane of the proximal colon epithelium (Endeward & Gros, 2005), and apical membrane of the proximal colon epithelium (Endeward & Gros, 2005).

The biological adaptation of membrane CO_2 permeability to the rate of O_2 consumption

Arias-Hidalgo *et al.* (2016) have described an approach to estimate the efficiency of CO_2 release by various cells or organelles of highly different sizes. They calculate a "whole cell /organelle CO_2 membrane conductance, C_M" as the product of membrane CO_2 permeability times cellular/organellar membrane area, $P_{CO2} \cdot A = C_M$. They relate this parameter to the "whole cell/organelle CO_2 production, $\dot{V}_{CO2}$" and use the ratio $P_{CO2} \cdot A / \dot{V}_{CO2}$ as a measure of the efficiency of CO_2 release of the cell or organelle. The ratios resulting for the cells/organelles studied here plus that for MDCK cells are shown in Table 4. It should be noted that wherever applicable the maximal oxygen consumptions were used to represent $\dot{V}_{CO2}$.

Table 4: Ratio between CO_2 membrane conductance and CO_2 production for several cell types and mitochondria.

Cell/Organelle	$C_M/\dot{V}_{CO2}$ (cm^3/nmol)
Mitochondria (maximally activated)	98*
MDCK cells	5.7*
Hepatocytes	2.33
Heart (maximal oxygen consumption)	1.37

*(Arias-Hidalgo *et al.*, 2016)

It is seen that mitochondria possess a $C_M/\dot{V}_{CO2}$ almost 20 times greater than that of any of the cells of Table 4. MDCK cells, hepatocytes and cardiomyocytes present ratios in the same order of magnitude and thus similar efficiencies of CO_2 release. With these values, we can conclude that mitochondria are maximally optimized for the release of CO_2 in comparison to cells, including cells of especially high metabolic rate such as cardiomyocytes. Of course it must be noted that the specific oxygen consumption of activated mitochondria of about 1000 nmol/s/ml is considerably higher than that of maximally working cardiomyocytes, which have about 300 nmol/s/ml. The lower values of $C_M/\dot{V}_{CO2}$ for cells compared to mitochondria, however, do not imply that CO_2 release by the cells is insufficient, as will be explained below. The conclusion here is simply that mitochondria possess an exceptionally optimized CO_2 release mechanism.

Endeward *et al.* (2014), using a simple mathematical model, have studied at which value P_{CO2} becomes critical for the release of CO_2 by a respiring cell. They found that, for cells producing CO_2 at a rate of that of the maximally working heart, CO_2 permeabilities < 0.1cm/s will begin to impair CO_2 release, with a serious effect being exerted by a P_{CO2} of 0.01 cm/s. In this work, we obtain a permeability of 0.1 cm/s for cardiomyocytes, which can be considered non-limiting even under conditions of maximal respiration. Applying this same calculation to cells with lower metabolism such as hepatocytes, we find that only P_{CO2} values <0.01cm/s are expected to become limiting for an adequate CO_2 exchange, while a permeability of 0.03 cm/s as found here, allows an unimpeded CO_2 release by these cells. Although the cells of Table 4 have quite different P_{CO2} values, their P_{CO2} value offers no limitation to the CO_2 release under the conditions given by their respective rates of oxygen consumption or CO_2 production. Thus, we can conclude that the P_{CO2} of various cell types seems to be perfectly adapted to the specific metabolic activity of each cell type, such that usually the cell membrane constitutes no noticeable barrier to CO_2 release.

Exceptions to the rule

We have shown above that there is a positive correlation between aerobic metabolism and P_{CO2}. Cells from tissues with higher metabolic rate and mitochondria have a higher CO_2 permeability, and vice versa, showing the principle of biological adaptation of membrane CO_2 permeability to the functional needs of each cell. This principle has been shown to apply to several cells, perhaps even to most cells, but there are at least two exceptions from this principle.

The first example we will to address is some epithelial cells. These cells are polarized and show very different characteristics between their apical and basolateral membranes. A specific example is the epithelial cells of the guinea pig proximal colon (another one would be the gastric epithelium). The apical membrane in this case has an extremely high cholesterol content (Meyer zu Düttingdorf *et al.*, 1999) combined with a very low P_{CO2} of 0.0015cm/s (Endeward & Gros, 2005), while the basolateral membrane has a lower cholesterol content (Meyer zu Düttingdorf *et al.*, 1999) and a much higher P_{CO2} of 0.02 (Endeward & Gros, 2005).

The very low apical P_{CO2} seems surprising in view of the fact that colon epithelium has an average –but not very low – rate of aerobic metabolism. We believe that the differences of P_{CO2} between apical and basolateral membranes relate to the different physiological role each of the two membranes has. Endeward & Gros (2005) described that the P_{CO2} of the apical membrane constitutes a very effective barrier against the high CO_2 concentration found in the lumen of this part of the intestine and therefore protects the cell interior from a high CO_2 partial pressure, which would constitute a severe acid load for the epithelial cell. The basolateral membrane, on the other hand, is expected to be in charge of the nutrient and gas exchange of these cells, so this explains that the P_{CO2} of these membranes fit in with what is to be expected on the basis of the metabolism of these cells (Figure 8, 2nd point from left).

The second example, where the principle of Figure 8 does not seem to hold, are red blood cells, which lack mitochondria and depend in their metabolism mainly on anaerobic glycolysis (Schmidt & Thews, 1986), a process that does not produce CO_2. In this case, red blood cells have not a high aerobic metabolism but they possess nevertheless a high P_{CO2} of 0.15 cm/s due to the strong expression of the two CO_2 channels AQP1 and RhAG. This property is of course due to the red cells' physiological role of gas transport. The high CO_2 permeability of the erythrocyte membrane allows an efficient exchange of CO_2 (and perhaps O_2) between red blood and the lung and tissue.

Final remarks

From our work we can conclude that most cells present a P_{CO2} that correlates with their aerobic metabolism and that cholesterol seems to play the central role in the adaptation of P_{CO2} to the aerobic metabolism. There are, however, exceptions like the case of red blood cells. Therefore it will also be interesting to analyze pneumocytes which have similar oxygen consumption to hepatocytes and colonocytes, but participate crucially in gas exchange. This example of a special cell might give an indication, whether perhaps it is in general the membrane cholesterol that adapts P_{CO2} to CO_2 production, and whether it is CO_2 channels that adapt P_{CO2} to special tasks as gas exchange in red cells.

It is known that cholesterol on the cell membrane is highly controlled by homeostatic mechanisms and that protein channels are expressed according to the genetic programming of each cell type. It remains to be asked if CO_2 acts as an evolutionary force that controls the cholesterol/phospholipid ratio of cells membranes, allowing cells to achieve an optimal P_{CO2} without compromising their other structural and functional roles.

Key Points of this Work

1. A general correlation between cholesterol content of the membrane and P_{CO_2} is confirmed.

2. Cardiomyocytes and mitochondria exhibit a high P_{CO_2} due to the low cholesterol of their membranes.

3. Only in the case of hepatocytes, a minor contribution of DIDS-sensitive CO_2 channels to P_{CO_2} was found.

4. Evidence in favor of a correlation between P_{CO_2} and aerobic metabolism of cells and organelles is presented. Most of the cells show the novel biological principle of adaptation of membrane CO_2 permeability to their rate of CO_2 production.

5. Cholesterol seems to play a dominant role in the adaptation of P_{CO_2} to the aerobic metabolism of cells and organelles.

6. In mitochondria and cells, although they have quite different P_{CO_2} values, P_{CO_2} is never limiting for their individual maximal CO_2 release under physiological conditions.

7. Mitochondria seem exceptionally well adapted to CO_2 release.

8. Apical membranes of proximal colon cells and erythrocyte membranes represent exceptions from the principle of metabolic adaptation of P_{CO_2}, and show how a specialized physiological role of a cell can also have an influence on P_{CO_2}.

References

Ahlin G, Chen L, Lazorova L, Chen Y, Ianculescu AG, Davis RL, Giacomini KM & Artursson P (2011). Genotype-dependent effects of inhibitors of the organic cation transporter, OCT1: predictions of metformin interactions. *Pharmacogenomics J* **11,** 400–411.

Alberts B, Johnson A, Lewis J, Raff M, Roberts K & Walter P (2011). *Molekularbiologie der Zelle*, 5th edn. Wiley-VCH, Weinheim.

Alvarez B V, Quon AL, Mullen J & Casey JR (2013). Quantification of carbonic anhydrase gene expression in ventricle of hypertrophic and failing human heart. *BMC Cardiovasc Disord* **13,** 2.

Arias-Hidalgo M, Al-Samir S, Weber N, Geers-Knörr C, Gros G & Endeward V (2017). CO2 Permeability and Carbonic Anhydrase Activity of Rat Cardiomyocytes. *Acta Physiol (Oxf)* Apr 20. doi: 10.1111/apha.12887. [Epub ahead of print].

Arias-Hidalgo M, Hegermann J, Tsiavaliaris G, Carta F, Supuran CT, Gros G & Endeward V (2016). CO_2 and HCO_3^- Permeability of the Rat Liver Mitochondrial Membrane. *Cell Physiol Biochem* **39,** 2014–2024.

Balboni E & Lehninger a L (1986). Entry and exit pathways of CO2 in rat liver mitochondria respiring in a bicarbonate buffer system. *J Biol Chem* **261,** 3563–3570.

Boxberger KH, Hagenbuch B & Lampe JN (2014). Common Drugs Inhibit Human Organic Cation Transporter 1 (OCT1) -Mediated Neurotransmitter Uptake. 990–995.

Brown BF, Quon A, Dyck JRB & Casey JR (2012). Carbonic anhydrase II promotes cardiomyocyte hypertrophy. *Can J Physiol Pharmacol* **90,** 1599–1610.

Bruns W & Gros G (1992). Membrane-bound carbonic anhydrase in the heart. *Am J Physiol - Hear Circ Physiol* **262,** 577–584.

Burger H.M, Abel S, Snijman PW, Swanevelder S & Gelderblom WCA (2007). Altered lipid parameters in hepatic subcellular membrane fractions induced by fumonisin B1. *Lipids* **42,** 249–261.

Butler TL, Au CG, Yang B, Egan JR, Tan YM, Hardeman EC, North KN, Verkman a S & Winlaw DS (2006). Cardiac aquaporin expression in humans, rats, and mice. *Am J Physiol Heart Circ Physiol* **291,** H705-13.

Calamita G, Ferri D, Gena P, Liquori GE, Cavalier A, Thomas D & Svelto M (2005). The inner mitochondrial membrane has aquaporin-8 water channels and is highly permeable to water. *J Biol Chem* **280,** 17149–17153.

Del Castillo JR, Ricabarra B & Sulbarán-Carrasco MC (1991). Intermediary metabolism and its relationship with ion transport in isolated guinea pig colonic epithelial cells. *Am J Physiol* **260,** C626-34.

Dodgson SJ, Quistorff B & Ridderstråle Y (1993). Carbonic anhydrases in cytosol, nucleus, and membranes of rat liver. *J Appl Physiol* **75,** 1186–1193.

Endeward V, Al-Samir S, Itel F & Gros G (2014). How does carbon dioxide permeate cell membranes? A discussion of concepts, results and methods. *Front Physiol* **4,** 382.

Endeward V, Cartron J-P, Ripoche P & Gros G (2008). RhAG protein of the Rhesus complex is a CO2 channel in the human red cell membrane. *FASEB J* **22,** 64–73.

Endeward V & Gros G (2005). Low carbon dioxide permeability of the apical epithelial membrane of guinea-pig colon. *J Physiol* **567,** 253–265.

Endeward V, Musa-Aziz R, Cooper GJ, Chen L-M, Pelletier MF, Virkki L V, Supuran CT, King LS, Boron WF & Gros G (2006). Evidence that aquaporin 1 is a major pathway for CO2 transport across the human erythrocyte membrane. *FASEB J* **20,** 1974–1981.

Foy BD, Rotem A, Toner M, Tompkins RG & Yarmush ML (1994). A device to measure the oxygen uptake rate of attached cells: importance in bioartificial organ design. *Cell Transplant* **3,** 515–527.

Geers C, Krüger D, Siffert W, Schmid A, Bruns W & Gro G (1992). Carbonic anhydrase in skeletal and cardiac muscle from rabbit and rat. *Biochem J* **282,** 165–171.

Geyer RR, Musa-Aziz R, Qin X & Boron WF (2013*a*). Relative CO(2)/NH(3) selectivities of mammalian aquaporins 0-9. *Am J Physiol Cell Physiol* **304,** C985-94.

Geyer RR, Parker MD, Toye AM, Boron WF & Musa-Aziz R (2013*b*). Relative CO2/NH3 Permeabilities of Human RhAG, RhBG and RhCG. *J Membr Biol* **246,** 915–926.

Gutknecht J, Bisson M a & Tosteson FC (1977). Diffusion of carbon dioxide through lipid bilayer membranes: effects of carbonic anhydrase, bicarbonate, and unstirred layers. *J Gen Physiol* **69,** 779–794.

Huebert RC, Splinter PL, Garcia F, Marinelli RA & Larusso NF (2002). Expression and localization of aquaporin water channels in rat hepatocytes. Evidence for a role in canalicular bile secretion. *J Biol Chem* **277,** 22710–22717.

Itada N & Forster RE (1977). Carbonic anhydrase activity in intact red blood cells measured with 18O exchange. *J Biol Chem* **252,** 3881–3890.

Itel F, Al-Samir S, Öberg F, Chami M, Kumar M, Supuran CT, Deen PMT, Meier W, Hedfalk K, Gros G & Endeward V (2012). CO2 permeability of cell membranes is regulated by membrane cholesterol and protein gas channels. *FASEB J* **26,** 5182–5191.

de Jonge HW, Dekkers DH, Bastiaanse EM, Bezstarosti K, van der Laarse A & Lamers JM (1996). Eicosapentaenoic acid incorporation in membrane phospholipids modulates receptor-mediated phospholipase C and membrane fluidity in rat ventricular myocytes in culture. *J Mol Cell Cardiol* **28,** 1097–1108.

Kai L & Kaldenhoff R (2014). A refined model of water and CO_2 membrane diffusion: effects and contribution of sterols and proteins. *Sci Rep* **4,** 6665.

Liu Z, Peng J, Mo R, Hui C & Huang CH (2001). Rh type B glycoprotein is a new member of the Rh superfamily and a putative ammonia transporter in mammals. *J Biol Chem* **276,** 1424–1433.

Ma Z, Meddings JB & Lee SS (1995). Cardiac plasma membrane physical properties and β-adrenergic receptor function are unaltered in portal-hypertensive rats. *Hepatology* **22,** 188–193.

Mahler SM, Wilce PA & Shanley BC (1988). Studies on Regenerating Liver and Hepatoma Plasma-Membranes .1. Lipid and Protein-Composition. *Int J Biochem* **20,** 605–611.

Meyer zu Düttingdorf H, Sallmann H, Glockenthör U, von Engelhardt W & Busche R (1999). Isolation and lipid composition of apical and basolateral membranes of colonic segments of guinea Pig. *Anal Biochem* **269,** 45–53.

Missner A, Kugler P, Saparov SM, Sommer K, Mathai JC, Zeidel ML & Pohl P (2008). Carbon Dioxide Transport through Membranes. *J Biol Chem* **283,** 25340–25347.

Nakhoul NL, Davis BA, Romero MF & Boron WF (1998). Rapid communication. *Appl Phys* **365,** 363–365.

Netti VA, Vatrella MC, Chamorro MF, Ros??n MI, Zotta E, Fellet AL & Balaszczuk AM (2014). Comparison of cardiovascular aquaporin-1 changes during water restriction between 25- and 50-day-old rats. *Eur J Nutr* **53,** 287–295.

Nielsen S, Smith BL, Christensen EI & Agre P (1993). Distribution of the aquaporin CHIP in secretory and resorptive epithelia and capillary endothelia. *Proc Natl Acad Sci U S A* **90,** 7275–7279.

Ono Y, Ridderstråle Y, Forster RE, Chu ZG & Dodgson SJ (1992). Carbonic anhydrase in the membrane of the endoplasmic reticulum of male rat liver. *Proc Natl Acad Sci U S A* **89,** 11721–11725.

Perut F, Carta F, Bonuccelli G, Grisendi G, Di Pompo G, Avnet S, Sbrana FV, Hosogi S, Dominici M, Kusuzaki K, Supuran CT & Baldini N (2015). Carbonic anhydrase IX inhibition is an effective strategy for osteosarcoma treatment. *Expert Opin Ther Targets* **19,** 1593–1605.

Proctor RA (1979). Endotoxin in vitro interactions with human neutrophils: Depression of chemiluminescence, oxygen consumption, superoxide production, and killing. *Infect Immun* **25,** 912–921.

Schmidt RF & Thews G (1986). *Physiologie des Menschen*, 23rd edn. Springer Verlag, Berlin Heidelberg.

Schroeder M a., Ali M a., Hulikova A, Supuran CT, Clarke K, Vaughan-Jones RD, Tyler DJ & Swietach P (2013). Extramitochondrial domain rich in carbonic anhydrase activity improves myocardial energetics. *Proc Natl Acad Sci* **110,** E958–E967.

Storch J & Schachter D (1984). Dietary induction of acyl chain desaturases alters the lipid composition and fluidity of rat hepatocyte plasma membranes. *Biochemistry* **23,** 1165–1170.

Torella D, Ellison GM, Torella M, Vicinanza C, Aquila I, Iaconetti C, Scalise M, Marino F, Henning BJ, Lewis FC, Gareri C, Lascar N, Cuda G, Salvatore T, Nappi G, Indolfi C, Torella R, Cozzolino D & Sasso FC (2014). Carbonic anhydrase activation is associated with worsened pathological remodeling in human ischemic diabetic cardiomyopathy. *J Am Heart Assoc* **3,** e000434.

Tsiavaliaris G, Itel F, Hedfalk K, Al-Samir S, Meier W, Gros G & Endeward V (2015). Low CO2 permeability of cholesterol-containing liposomes detected by stopped-flow fluorescence spectroscopy. *FASEB J* **29,** 1780–1793.

Villafuerte FC, Swietach P, Youm J-B, Ford K, Cardenas R, Supuran CT, Cobden PM, Rohling M & Vaughan-Jones RD (2014). Facilitation by intracellular carbonic anhydrase of Na+ -HCO3- co-transport but not Na+ / H+ exchange activity in the mammalian ventricular myocyte. *J Physiol* **592,** 991–1007.

Vincent SH & Silverman DN (1982). Carbonic anhydrase activity in mitochondria from rat liver. *J Biol Chem* **257,** 6850–6855.

Wang L, Prasad B, Salphati L, Chu X, Gupta A, Hop CECA, Evers R & Unadkat JD (2015). Interspecies variability in expression of hepatobiliary transporters across human, dog, monkey, and rat as determined by quantitative proteomics. *Drug Metab Dispos* **43,** 367–374.

Weiner ID, Miller RT & Verlander JW (2003). Localization of the ammonium transporters, Rh B glycoprotein and Rh C glycoprotein, in the mouse liver. *Gastroenterology* **124,** 1432–1440.

Williams KD & Smith DO (1989). Cholesterol conservation in skeletal muscle associated with age and denervation-related atrophy. *Brain Res* **493,** 14–22.

Wright LC, Nouri-Sorkhabi MH, May GL, Danckwerts LS, Kuchel PW & Sorrell TC (1997). Changes in cellular and plasma membrane phospholipid composition after lipopolysaccharide stimulation of human neutrophils, studied by 31P NMR. *EurJBiochem* **243,** 328–335.

Wunder MA & Gros G (1998). 18O exchange in suspensions of red blood cells: determination of parameters of mass spectrometer inlet system. *Isotopes Environ Health Stud* **34,** 303–310.

Zhang L, Schaner ME & Giacomini KM (1998). Functional characterization of an organic cation transporter (hOCT1) in a transiently transfected human cell line (HeLa). *J Pharmacol Exp Ther* **286,** 354–361.

Article 1

CO$_2$ and HCO$_3^-$ Permeability of the Rat Liver Mitochondrial Membrane

Authors: <u>Mariela Arias-Hidalgo</u>, Jan Hegermann, Georgios Tsiavaliaris, Fabrizio Carta, Claudiu T. Supuran, Gerolf Gros, Volker Endeward

Candidate's contribution:

I have performed the isolation of mitochondria for all the experiments, protein quantification and the mass spectrometric experiments to determine the O$_2$ consumption, CO$_2$ and bicarbonate permeability of these organelles, as well as the calculation of the results in MatLab and the statistical analysis. I also wrote the first draft of this publication, made the graphs and most of the images for the manuscript, and worked in the later editing of the manuscript.

Original Paper

CO_2 and HCO_3^- Permeability of the Rat Liver Mitochondrial Membrane

Mariela Arias-Hidalgo[a]   Jan Hegermann[b]   Georgios Tsiavaliaris[c]   Fabrizio Carta[d]
Claudiu T. Supuran[d]   Gerolf Gros[a]   Volker Endeward[a]

[a]Abt. Molekular- und Zellphysiologie, AG Vegetative Physiologie 4220, Medizinische Hochschule Hannover, Hannover, [b]Abt. Funktionelle und Angewandte Anatomie, Elektronenmikroskopie 8840, Medizinische Hochschule Hannover, Hannover, [c]Abt. Biophysikalische Chemie 4350, Medizinische Hochschule Hannover, Hannover, Germany; [d]NEUROFARBA Dipart., Pharmaceutical and Nutraceutical Chemistry, University of Florence, Sesto Fiorentino, Italy

Abstract
Background/Aims: Across the mitochondrial membrane an exceptionally intense exchange of O_2 and CO_2 occurs. We have asked, 1) whether the CO_2 permeability, $P_{M,CO2}$, of this membrane is also exceptionally high, and 2) whether the mitochondrial membrane is sufficiently permeable to HCO_3^- to make passage of this ion an alternative pathway for exit of metabolically produced CO_2. ***Methods:*** The two permeabilities were measured using the previously published mass spectrometric ^{18}O exchange technique to study suspensions of mitochondria freshly isolated from rat livers. The mitochondria were functionally and morphologically in excellent condition. ***Results:*** The intramitochondrial CA activity was exclusively localized in the matrix. $P_{M,CO2}$ of the inner mitochondrial membrane was 0.33 (SD ± 0.03) cm/s, which is the highest value reported for any biological membrane, even two times higher than $P_{M,CO2}$ of the red cell membrane. $P_{M,HCO3-}$ was $2 \cdot 10^{-6}$ (SD ± $2 \cdot 10^{-6}$) cm/s and thus extremely low, almost 3 orders of magnitude lower than $P_{M,HCO3-}$ of the red cell membrane. ***Conclusion:*** The inner mitochondrial membrane is almost impermeable to HCO_3^- but extremely permeable to CO_2. Since gas channels are absent, this membrane constitutes a unique example of a membrane of very high gas permeability due to its extremely low content of cholesterol.

© 2016 The Author(s)
Published by S. Karger AG, Basel

Introduction

Mitochondria, the organelles responsible for cellular respiration, convert O_2, ADP and energy substrates into ATP, CO_2 and water. Their O_2 consumption together with their - about identical - CO_2 production requires that both gases meet no major diffusion resistance

Dr. Gerolf Gros

Abt. Molekular- und Zellphysiologie, AG Vegetative Physiologie – 4220 –Medizinische Hochschule Hannover, 30625 Hannover, (Germany)
Fax +49-511-532 2938, E-Mail Gros.Gerolf@MH-Hannover.de

KARGER

Arias-Hidalgo et al.: Mitochondrial CO_2 Permeability

when passing through the mitochondrial membrane from/into the mitochondrial matrix. While the O_2 permeability of the mitochondrial membrane has not been accessible to direct determination, Elder and Lehninger [1] and Balboni and Lehninger [2] have presented qualitative evidence indicating that the inner mitochondrial membrane is permeable to CO_2 but not to HCO_3^-. In view of the extremely high rate of CO_2 production per mitochondrial volume, one must postulate then that the mitochondrial membrane possesses an unusually high permeability for CO_2. We ask here whether and by which mechanism the mitochondrial membrane does indeed achieve a high permeability to CO_2. This question arises, because several biological membranes have been reported to possess low CO_2 permeabilities (0.017 cm/s for the cell lines MDCK and tsA201, or even 0.0015 cm/s for the apical membrane of colonic epithelium [3, 4]). Others, such as the red blood cell membrane, on the other hand possess a much higher CO_2 permeability of 0.15 cm/s [5, 6].

For methodological reasons, it has so far not been possible to determine the permeability of the mitochondrial membrane for CO_2 quantitatively. Only more recently, the mass spectrometric ^{18}O exchange technique developed in our lab [4] has made it feasible to tackle this problem. This method is suitable to determine $P_{M,CO2}$ and $P_{M,HCO3^-}$ not only of cells but also of vesicles and organelles [3, 7]. Thus, we determine here the CO_2 permeability along with the bicarbonate permeability of the mitochondrial membrane.

We wanted to answer two questions: 1) Does the mitochondrial membrane indeed possess a very high CO_2 permeability as expected from its exceptionally high rate of CO_2 exchange? 2) If the CO_2 permeability does turn out to be very high, what is the mechanistic basis for this property in view of other less permeable biological membranes? 3) Does the bicarbonate permeability of the mitochondrial membrane allow a significant permeation of HCO_3^-, as an alternative pathway to CO_2? This latter question is still controversial, as Vincent and Silverman [8] have reported a high HCO_3^- permeability, similar to that of the human red blood cell membrane, while Dodgson et al. [9] find a value at least two orders of magnitude lower than found in red cells.

Materials and Methods

Solutions

Homogenization medium (HM buffer). 0.32 M Sucrose, 1 mM EDTA and 10 mM Tris-HCl and pH adjusted to 7.4.

O_2 and CO_2 Buffers. The "O_2 buffer" (for measurement of mitochondrial O_2 consumption) consists of 125 mM KCl, 20 mM MOPS, 5 mM KH_2PO_4 and 1 mM $MgCl_2$. The "CO_2 buffer" (for the measurement of ^{18}O exchange) consists of the same components as the O_2 buffer, but has 25 mM KCl less [10]. Both buffers were filtered through a Millipore filter with pore size 0.2 μm.

Lysate Buffer. 60 mM NaCl, 20 mM Hepes, 23.7 mM HSO_4 and pH adjusted to 7.4.

Isolation of Mitochondria

All experiments were performed using male Lewis rats between 250 and 300 g of body weight with permission of the local authorities for animal experimentation. Animals were anesthetized with carbon dioxide and killed by cervical dislocation. The liver was removed within 5 minutes, washed with ice cold homogenization medium, cut into pieces and homogenized with a Potter-Elvehjem homogenizer. Homogenization and centrifugation steps were performed as described by Fernandez-Vizarra et al. [11, 12].

An initial centrifugation step was performed at 1000 g for 5 min at 4°C and supernatant was taken and aliquots transferred into several 1.5 ml Eppendorf tubes. These samples were then centrifuged at 15,000 g for 2 min at 4°C, supernatant was discarded and the pellets of 2 tubes were combined and resuspended in HM buffer. This process was repeated until there was only one tube containing the entire sample. This tube was centrifuged once more, the supernatant was discarded and the pellet was resuspended in O_2 buffer to be used for further experiments.

KARGER

Arias-Hidalgo et al.: Mitochondrial CO$_2$ Permeability

Characterization of the mitochondrial samples

Protein content. The final mitochondrial pellet was resuspended in O$_2$ buffer to a volume of 1000 µl. 10 µl of this suspension were taken for determination of protein content using the Total Protein Kit, Micro Lowry, Peterson's Modification, from Sigma (Sigma-Aldrich, Taufkirchen, Germany). Two determinations of protein content were performed for each sample.

Parameters. We used the protein concentrations of the mitochondrial suspensions to derive mitochondrial matrix volume and inner membrane surface area form the data published by Schwerzmann et al. [13], using their numbers of 1.6 µl/mg protein for matrix volume and 521 cm^2/mg protein for inner membrane surface area. The protein concentration of the suspensions was also used to determine the number of mitochondria per volume, using the figure $8.7 \cdot 10^9$ mitochondria per mg of mitochondrial protein [13].

Electron microscopy. The final mitochondrial pellet was resuspended in a 10-fold volume of fixation buffer (150 mM HEPES, pH 7.35, containing 1.5 % formaldehyde and 1.5 % glutaraldehyde) at RT. Fixation was 30 min at RT and overnight at 4°C. Mitochondria were postfixed in 1% osmium tetroxide 2 h at RT and 4% uranyl acetate at 4°C overnight. After dehydration in acetone, samples were embedded in EPON. 50 nm thick sections were poststained with 4% uranyl acetate and lead citrate [14] and observed in a Morgagni TEM (FEI), operated in the bright field mode. Images were recorded at 80 kV using a 2K side mounted Veleta CCD camera, binned to 1K.

Dynamic Light scattering (DLS). DLS studies were performed using a Viscotek 802 instrument (Viscotek Corporation) equipped with a single mode fiber optics and a 50 mW diode laser (λ = 832 nm) at 20°C. The mitochondrial preparation was diluted 1000-fold in O$_2$ buffer containing 0.1 %w/v BSA. Prior to dilution the O$_2$ buffer was filtered through a syringe filter (Minisart®) with a pore size of 0.2 µm (Sartorius, Germany). Polystyrene beads of 1 µm diameter (Molecular probes) and a concentration of 1×10^7 beads per ml were used as a control. The purity of the mitochondrial suspension was estimated from the area of the mitochondrial peak fraction relative to the total area of all peak fractions including that of the contaminants.

Mass spectrometric assays

A chamber with a volume of 2.2 ml was used that was attached to the high vacuum of the mass spectrometer via the previously published inlet system [4]. This chamber had a water-jacket that kept the solutions at 37°C, and contained a stirrer that mixed the content continuously. The pH was adjusted to 7.4 and monitored during the whole procedure with a pH electrode. 50 µl of mitochondrial suspension was used in each experiment.

Oxygen consumption. O$_2$ consumption of mitochondrial suspensions was measured by monitoring over time the concentration of physically dissolved O$_2$ in the fluid of the mitochondrial suspension in the mass spectrometer's chamber. The O$_2$ signal produced by the mass spectrometer was proportional to the O$_2$ concentration in the sample. Initially, the sample was equilibrated with air. After the chamber was closed, a decline of O$_2$ concentration in the sample occurred due to mitochondrial respiration and was recorded via the mass spectrometer. The slopes of the recordings represent the O$_2$ consumption $\dot{V}_{O_2}$. Each measurement consisted of the following phases, as seen in Fig. 1: (1) $\dot{V}_{O_2}$ of the suitably diluted native mitochondrial

Fig. 1. Original mass spectrometric recording of an oxygen consumption measurement of a mitochondrial suspension. Substrates 5mM glutamate and 1mM malate (second arrow) and 0.3 mM ADP (third and fourth arrow) were added. RCR was calculated using the ratio between oxygen consumption values of the state III (after addition of ADP) and state IV (after ADP has been consumed).

Arias-Hidalgo et al.: Mitochondrial CO_2 Permeability
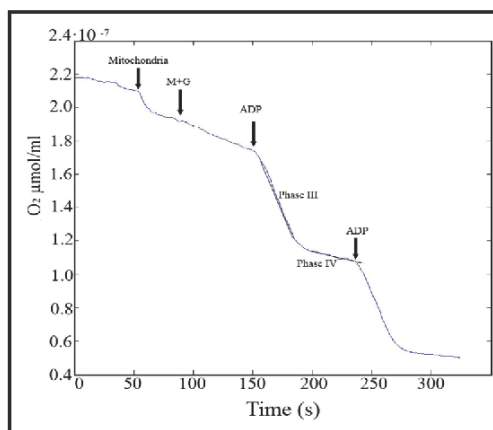
suspension, (2) $\dot{V}_{O2}$ after addition of glutamate and malate to give final concentrations of 5 and 1 mM, respectively, (3) $\dot{V}_{O2}$ after addition of ADP at a final concentration of 0.3 mM (giving state III respiration), (4) $\dot{V}_{O2}$ after the added ADP has been consumed (giving state IV respiration). Specific $\dot{V}_{O2}$ values and the respiratory control ratio (RCR = slope of state III / slope of state IV) allowed us to assess the functional integrity of the mitochondria [10].

Estimation of CO_2 permeability. The mass spectrometric chamber was filled with isotonic "CO_2 buffer" that contained 25 mM ^{18}O-labelled HCO_3^- as described before [4]. The pH was adjusted to 7.40 at 37°C. The mass spectrometer followed the concentration of $C^{18}O^{16}O$ in the chamber fluid. Due to the exchanges of ^{18}O with water, the $C^{18}O^{16}O$ concentration declined over time. After addition of the mitochondrial sample into the chamber, this decline was accelerated, yielding a first fast phase followed by a second slower phase, as is seen in Fig. 4. The acceleration was due to the exchange of ^{18}O between the pools of CO_2 and water inside the mitochondria, which was sped up by intramitochondrial carbonic anhydrase (CA). After the second phase of $C^{18}O^{16}O$ decline had been recorded for a sufficiently long time, a high concentration of CA was added to the chamber to establish final isotopic equilibrium (see Fig. 4). The two phases after addition of mitochondria seen in Fig. 4 were used to derive the CO_2 permeability ($P_{M,CO2}$) of the mitochondrial membrane in the manner described previously [4].

Inhibitors used in several experiments were: extracellular carbonic anhydrase inhibitor 2,4,6-trimethyl-1-(4-sulfamoyl-phenyl)-pyridinium perchlorate salt (FC5-208A; [15]) in a final concentration of $2.5 \cdot 10^{-5}$ M, and the inhibitor of the gas channels aquaporin-1 and RhAG 4.4′-Diisothiocyanato-2.2′-stilbenedisulfonate (DIDS) in a final concentration of 1.0×10^{-4} M [16, 6]. Mitochondrial samples were preincubated with inhibitor(s) for 5 min.

Determination of intramitochondrial carbonic anhydrase activity. Mitochondria were kept frozen overnight and thawed the next day. 1 μl of Triton 10% was added to each 100 μl of mitochondrial suspension. 22 μl of the same Triton solution were also added into the measuring chamber of the mass spectrometer containing "lysate buffer" with 25 mM labelled bicarbonate. The experiment was then terminated by the addition of excess CA to establish final isotopic equilibrium. This record was analyzed to obtain the carbonic anhydrase activity and then related to the mitochondrial volume estimated for each sample to obtain the activity inside the mitochondrium. CA activity A was defined as acceleration factor (A+1) of the uncatalysed hydration velocity minus 1. In other words, the total rate of CO_2 hydration v_{CO2} is given by $k_{CO2} \cdot (A+1) \cdot [CO_2]$, where k_{CO2} is the uncatalysed rate constant of CO_2 hydration, and $[CO_2]$ is the concentration of dissolved CO_2.

Statistical Analysis

Data are presented as means and ± SD. For comparisons between more than 2 groups with one independent variable, we used one way ANOVA. Dunnett's post-test was used to allow comparisons with the control group.

Results

Characterization of the mitochondrial preparations

We worked with mitochondrial suspensions containing 32 (SD ± 4; n = 8) mg protein/ml. The oxygen consumption (state III) was 97 (SD ± 38; n = 28) nmol O_2/min/mg protein and the RCR was around 10 (SD ± 5; n = 8). State three respiration rates and RCR values were in the range of literature values for liver mitochondria [10, 13, 17, 18]. In transmission electron microscopy, the mitochondria appeared morphologically intact and little other material was seen (Fig. 2). The average shortest diameter of the mitochondrial profiles obtained by electron microscopy was 0.73 (SD ± 0.11, n=18) μm (the average longest diameter was 0.89 (SD ± 0.13) μm). In addition, we determined the size of the mitochondria by DLS. Fig. 3B shows a measurement of a preparation yielding an average radius of 0.44 (SD ± 0.12) μm (Fig. 3B). Averaging the radii from several DLS measurements using different dilutions of the mitochondrial suspension and various scanning rates of acquisition gave a final diameter of 0.98 (SD ± 0.18, n = 12) μm. The short diameter of 0.73 μm from electron microscopy is in excellent agreement with the value given by Schwerzmann et al. [13], and all

KARGER

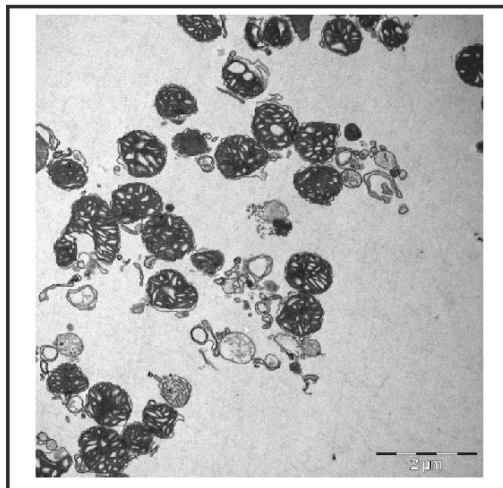Arias-Hidalgo et al.: Mitochondrial CO_2 Permeability

Fig. 2. Electron microscopic image of isolated mitochondria. Their shape and structure are well preserved, and only moderate contamination with other membranes or other cellular components is found. Complete bar = 2μm.

Fig. 3. DLS experiments of radii distribution and relative abundance of particles. (A) Size distribution histogram of polystyrene beads reveal a mean average radius of 0.47 ± 0.11 μm, which agrees well with the manufacturer's specification when taking the uncertainty of the DLS derived intensity size distribution of approximately 10 to 15% into account. (B) Representative size distribution histogram of a mitochondrial preparation. The mean average radius of the mitochondria is 0.44 ± 0.12 μm (main peak distribution). Low and high molecular weight contaminations of the mitochondrial preparation with proteins and other cellular components are shown as distributions of the minor peaks. The error corresponds to the half-width of the peak size. The relative purity of the mitochondrial preparation is found to be approximately 70%.

diameters mentioned are in the range given in the literature [19]. In addition to the overall radius, the DLS measurement allows us by quantification of the areas of the DLS peaks to give an estimate of the purity of the sample. This value was approximately 70%, a figure compatible with the degree of purity seen in the electron micrograph of Fig. 2. This is considered a very satisfactory degree of purity.

Determinations of mitochondrial CO_2 and HCO_3^- permeability

Among the measurements of ^{18}O-exchange in mitochondrial suspensions (Fig. 4), we performed 32 experiments with control conditions, and 12 with each of the inhibitors, FC5-208A and DIDS, respectively. The CO_2 permeability values obtained from the fitting procedure [4] were either between 0.3 and 0.4 cm/s, or they were > 400 cm/s and did not reach convergence. This shows that a) the permeability of the mitochondrial membrane is > 0.3 cm/s, b) it may be even higher than 0.4 cm/s, but this cannot be demonstrated because the method becomes insensitive to $P_{M,CO2}$ above ~ 0.4 cm/s. In the case of control measurements of mitochondria in the absence of inhibitors, 8 out of 32 measurements did not converge and $P_{M,CO2}$ in these 8 measurements thus appeared to be > 0.4 cm/s. In the presence of the extracellular CA inhibitor FC5-208A 2 out of 12 measurements did not converge, and in the case of experiments in the presence of DIDS 7 out of 12 measurements did not converge. The results shown in Fig. 5 are based on the $P_{M,CO2}$ values obtained up to a value of about 0.4 cm/s. So, in most cases, the calculated $P_{M,CO2}$ values range between 0.3 and 0.4 cm/s. Thus, at least in the control experiments and those in the presence of FC5-208A, the means given in Fig. 5 should be fairly reliable and the
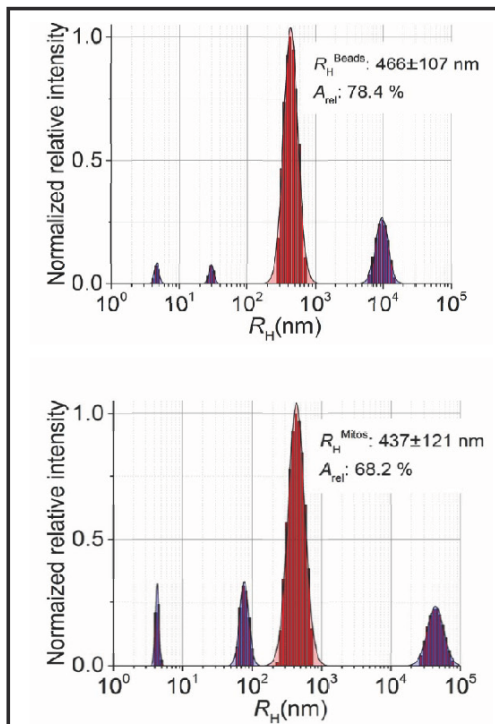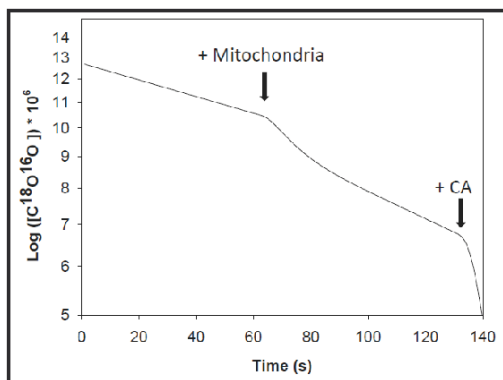
KARGER

Fig. 4. Original mass spectrometric recording of an experiment with rat liver mitochondria. Mass 46 ($C^{18}O^{16}O$) is plotted logarithmically versus time. 1st arrow indicates addition of mitochondrial suspension to reaction chamber, 2nd arrow indicates addition of an excess of carbonic anhydrase to establish final isotopic equilibrium.
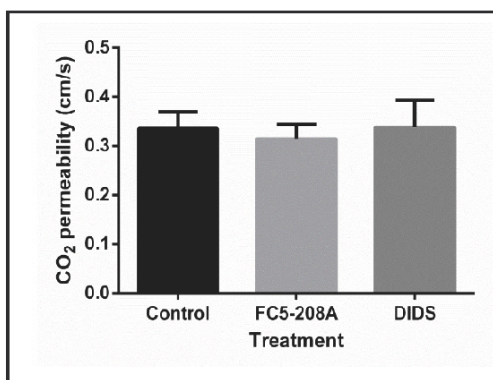

Fig. 5. CO_2 permeability of mitochondria in suspension and the effect of extracellular CA inhibitor FC5-208A ($2.5 \cdot 10^{-5}$ M) and the CO_2 channel inhibitor DIDS ($1.0 \cdot 10^{-4}$ M). ANOVA p = 0.29. From left to right n = 24, n = 10, n = 5. Bars represent SD.

true values should not be significantly higher than shown.

From control experiments, we calculated a mean bicarbonate permeability of $2 \cdot 10^{-6}$ cm/s (SD $\pm 2 \cdot 10^{-6}$ cm/s, n = 39). This is a very low value compared to red cells [6] but it is still significantly different from 0 (p < 0.0001). Mean intra-matrix CA activity was found to be 675 (SD $\pm$ 151, n = 8). This activity is high, yet still a little less than 5% of the exceptionally high human intraerythrocytic CA activity.

The mitochondrial CO_2 permeability we obtain under control conditions is 0.33 cm/s (SD $\pm$ 0.03; n =24; Fig. 5), which is twice as high as the value of 0.15 cm/s reported for the human red cell membrane [5, 6]. Because extracellular CA activity could interfere with the $P_{M,CO2}$ calculations, we performed experiments in the presence of FC5-208A, a membrane-impermeable and thus extracellular and extramitochondrial CA inhibitor. Organelles pre-incubated with FC5-208A exhibit the same permeability of 0.32 cm/s (SD $\pm$ 0.03; n =10), indicating that no extramitochondrial CA is present in our mitochondrial suspensions. Finally, we performed experiments with DIDS, a CO_2 channel inhibitor (of aquaporin 1 and RhAG [5, 6, 16]), and obtained a $P_{M,CO2}$ of 0.34 cm/s (SD $\pm$ 0.06; n = 5), again identical to control $P_{M,CO2}$.

Discussion

Stereological Mitochondrial Parameters

The calculation of $P_{M,CO2}$ from the two phases of $C^{18}O^{16}O$ decline seen in Fig. 4 requires knowledge of the mitochondrial matrix volume and the surface of the inner mitochondrial membrane [4]. These values have been determined for rat liver mitochondria by Schwerzmann et al. [13], who report a matrix volume of 1.6 µl/mg mitochondrial protein and a surface area of the inner membrane of 521 cm^2/mg protein. Matrix volume rather than total mitochondrial volume and inner membrane rather than outer mitochondrial membrane were chosen, because a) all mitochondrial CA is present in the matrix (see below), and b) the outer mitochondrial membrane has large pores und thus is less likely to offer a significant resistance towards permeation of CO_2 as well as HCO_3^- in comparison to the inner mitochondrial membrane. For the mitochondrial matrix volume, various estimates have been obtained. Besides the value employed here, 1.6 µl/mg protein as reported by Schwerzmann et al. [13], Halestrap and Quinlan [20] obtained values of 0.46 and 1.68 µl/mg

KARGER

(where they preferred the estimate of 0.46 µl/mg). Cohen et al. [21] reported matrix volumes between 0.85 and 1.4 µl/mg, and Vincent and Silverman [8] found a value of 1.4 µl/mg. We tested the effect of assumed matrix volumes of 1 µl/mg and 0.46 µl/mg on the calculated CO_2 permeabilities, and found for both these values average $P_{M,CO2}$ values remaining between 0.2 and 0.4 cm/s, i.e. very similar to the $P_{M,CO2}$ value calculated with a matrix volume of 1.6 µl/mg. Thus, the $P_{M,CO2}$ values of Fig. 5 do not depend very much on the value chosen from this range of mitochondrial matrix volumes. This is due to the fact that, at the given experimental CA activity of the mitochondrial lysate, the calculated intra-matrix CA activity increases as mitochondrial volume decreases, and these two changes largely compensate each others' opposite effects on $P_{M,CO2}$.

Imperfect Purity of Mitochondrial Preparation

As discussed above, the present mitochondrial preparation is not entirely pure, the contaminations amounting to 30% according to DLS measurements (Fig. 3). On the other hand, we use here the mitochondrial parameters derived from another study, that of Schwerzmann et al. [13], which raises the question to which extent their parameters are applicable to our preparations. A first consideration concerns the present preparation technique. This technique is almost identical to the one used by Schwerzmann et al. [13], with one major exception: we did not include the final step used by Schwerzmann et al. [13], Percoll gradient centrifugation intended to reduce microsomal contamination. We tested the effect of this step and found no improvement of the purity of the preparation, but an impairment of the functional properties of the mitochondria after Percoll. Therefore, this step was omitted. This suggests that the purity of the present preparation may be similar to that of Schwerzmann et al. [13]. A second consideration concerns the hypothesis that the data of Schwerzmann et al. [13] refer to a 100% pure preparation, while 30% of the protein of our preparation is not due to mitochondria. Which error in our estimate of $P_{M,CO2}$ would this situation cause? 30% contaminating proteins would reduce the mitochondrial volume and surface as calculated from Schwerzmann's data [13] by 30%, and at the same time increase calculated intra-matrix CA activity by 30%. As mentioned above, the reduction in volume and the increase in activity largely compensate each other, such that the average $P_{M,CO2}$ of a representative group of experiments is calculated to fall from 0.32 cm/s to 0.29 cm/s, an error negligible in view of the limitations of the present method. In conclusion, even if there is a major difference between the purities of the preparations of Schwerzmann et al. [13] and of this paper, this has no relevant effect on the value of mitochondrial $P_{M,CO2}$. The same holds for $P_{M,HCO3^-}$.

Mitochondrial Carbonic Anhydrase Activity

For rat liver mitochondria at 37°C we report here an intra-matrix CA activity of 675, indicating that the intra-matrix rate of CO_2 hydration is accelerated over its uncatalysed value by a factor 675+1 = 676. For guinea pig liver mitochondria at 25°C, Dodgson et al. [9] have reported a standard k_{cat} of 0.13 ml/s/mg protein. Using the above matrix volume of 1.6 µl/mg, this gives an activity of 2030 in the matrix of these mitochondria. The difference between this value and the present one can be due to the difference in species and/or to the difference in temperatures. For rat liver mitochondria at 25°C, Vincent and Silverman [8] report a mitochondrial CA activity of 700, very similar to our value at 37°C. However, they conclude from digitonin subfractionation experiments that about one half of this CA activity is located in the space between inner and outer mitochondrial membrane, and only the other half in the matrix. We cannot confirm this latter conclusion, as the membrane-impermeable inhibitor FC5-208A (mol.wt. 376.81) should be able to enter the space between the two membranes through the porins but should not have access to the intra-matrix space. As apparent from Fig. 5, FC5-208A has no effect on calculated CO_2 permeability, which means that the mass spectrometric signal is not detectably altered by the presence of FC5-208A. If there were significant extra-matrix CA in these mitochondria, we would expect a marked change of the mass spectrometric signal upon addition of the inhibitor. Thus, the present

KARGER

Arias-Hidalgo et al.: Mitochondrial CO_2 Permeability

results yield CA activities that are in a range similar to previously reported values, but show that CA is localized entirely in the mitochondrial matrix space. The latter conclusion is in agreement with the observations of Balboni and Lehninger [2], who observed that rat liver mitoplasts, which are devoid of the outer mitochondrial membrane and the intermembrane space, exhibit a similar rapid uptake of CO_2 into the matrix as intact liver mitochondria.

The localization of CA within the mitochondrium is relevant for the present study, because the ^{18}O exchange technique observes the exchange of CO_2 and HCO_3^- between the compartment containing the CA and the surrounding space devoid of CA [7]. If the space containing the CA is the matrix, and both the space between the two mitochondrial membranes and the extramitochondrial space are free of CA, then the permeabilities measured here for CO_2 as well as HCO_3^- should refer to the sum of the diffusion resistances of the inner and the outer mitochondrial membrane. In view of the fact that the outer membrane has large pores and is known to be quite permeable, it is likely that our permeability results essentially reflect the properties of the inner mitochondrial membrane.

Low Mitochondrial Bicarbonate Permeability

Williams [22] has early on postulated that it is HCO_3^- rather than that CO_2 leaves the mitochondrial matrix. Elder & Lehninger [1] and Balboni and Lehninger [2] have presented several lines of evidence indicating that it is more likely that CO_2 is the permeating species. In view of this discussion it is of interest to know what the permeability of the (inner) mitochondrial membrane for HCO_3^- is. This question has been studied by Dodgson et al. [9], who used the same ^{18}O-exchange technique that we apply here. Their approach differs from the present one by the theoretical treatment. They consider the membrane permeability for CO_2 to be infinite and derive the two parameters intramitochondrial CA activity and membrane bicarbonate permeability from mass spectrometric recordings such as the one shown in Fig. 4 (see method in [23]). In our treatment the intramitochondrial CA activity is determined independently, and the two parameters membrane $P_{M,CO2}$ and $P_{M,HCO3^-}$ are derived from the mass spectrometric recordings [4]. Therefore, the results for $P_{M,HCO3^-}$ obtained by Dodgson et al. [9] and in the present paper are not strictly comparable, even if the experimental mass spectrometer recordings were identical. However, since we find here an exceptionally high CO_2 permeability of the mitochondrial membrane, it can be expected that assuming it to be infinite does not affect the calculated value of $P_{M,HCO3^-}$ very much. Thus, it is not surprising that our value for $P_{M,HCO3^-}$, $2 \cdot 10^{-6}$ cm/s, is well within the range of values between 10^{-6} and 10^{-5} cm/s reported by Dodgson et al. [9]. These values are almost three orders of magnitude lower than the $P_{M,HCO3^-}$ of about 10^{-3} cm/s in human red cells, which possess the chloride-bicarbonate exchanger AE1 in their membrane [6, 24, 25]. The present mitochondrial $P_{M,HCO3^-}$ of $2 \cdot 10^{-6}$ cm/s is about as low as the $P_{M,HCO3^-}$ of hagfish red cells, which lack the AE1 and have been reported to exhibit a $P_{M,HCO3^-}$ of $<< 10^{-5}$ cm/s [26]. Both bicarbonate permeabilities can be considered to be close to zero. This would be clearly lower than the mitochondrial $P_{M,HCO3^-}$ of $9 \cdot 10^{-5}$ cm/s reported by Vincent and Silverman [8], but would agree with the reports of Chappell and Crofts [27] and Elder and Lehninger [1], who concluded that bicarbonate is virtually impermeable in the inner mitochondrial membrane. In summary, we confirm here the concept of Elder and Lehninger [1] and Balboni and Lehninger [2] that bicarbonate does not play a significant role in mediating the transfer of CO_2 - HCO_3^- across the mitochondrial membrane.

High Mitochondrial CO_2 Permeability, Significance and Mechanism

Physiological Significance. If CO_2 is the only form in which all species of the $CO_2/HCO_3^-/H_2CO_3/CO_3^{2-}$ system can pass the inner mitochondrial membrane, then all CO_2 produced from O_2 inside the mitochondrion has to permeate this membrane in the form of CO_2. If we take oxygen consumptions as an approximation of CO_2 production rates, we can use the state III mitochondrial oxygen consumption measured in this study, , $\dot{V}_{O2}$ = 97 nmol O_2/min/mg protein (see Results). We convert this to $\dot{V}_{O2}$ per volume using the matrix volume of 1.6 µl/mg, and obtain a $\dot{V}_{O2}$ per matrix volume of ~ 1000 nmol/s/ml. One can now compare this

KARGER

2022

Arias-Hidalgo et al.: Mitochondrial CO_2 Permeability

figure with the O_2 consumption of a cell line in culture, MDCK, which exhibits a low oxygen consumption of 1.25 fmol/min/cell [28]. Converting this number to $\dot{V}_{O2}$ per cell volume, we obtain about 12 nmol/s/ml. This is a 100x lower specific $\dot{V}_{O2}$ than that of mitochondria.

Mitochondria seem to be well adapted to the high $\dot{V}_{CO2}$ by their high $P_{M,CO2}$ of 0.3 cm/s, whereas MDCK cells are obviously able to sufficiently release their CO_2, produced at a 100x lower rate, in spite of their much lower $P_{M,CO2}$ of 0.017 cm/s [3]. However, the size and surface area of a mitochondrion and a MDCK cell are greatly different. In order to obtain a rough estimate of the efficiencies in releasing CO_2 achieved by mitochondria vs. MDCK cells, we can calculate the ratio of whole organelle/cell CO_2 membrane conductance, C_M, over whole cell/organelle CO_2 production, $\dot{V}_{CO2}$. Membrane conductances are given by $P_{M,CO2} \cdot A$, A representing the total membrane area of the single cell or organelle. For mitochondria one obtains $C_M = 0.3$ cm/s $\cdot$ 6.0·10^{-8} cm² = 1.8·10^{-8} cm³/s (A taken from [13]), for MDCK cells C_M = 0.017 cm/s 7·10^{-6} cm² = 12·10^{-8} cm³/s (A calculated from a cell diameter of 15μm assuming a spherical shape of the MDCK cell). $\dot{V}_{CO2}$ per mitochondrion with a matrix volume of 1.84·10^{-13} cm³ [13] is obtained from the above $\dot{V}_{CO2}$ per volume to be 1.84·10^{-10} nmol/s. $\dot{V}_{CO2}$ of a MDCK cell is obtained analogously to be 12 nmol/s/cm³ 1.77·10^{-9} cm³ = 2.1·10^{-8} nmol/s (the cell volume being calculated from the diameter of 15 μm). For the ratio of C_M over $\dot{V}_{CO2}$ we obtain then for mitochondria: $C_M/\dot{V}_{CO2}$ = 1.8·10^{-8} cm³/s / 1.84·10^{-10} nmol/s = 98 cm³/nmol, and for MDCK cells: $C_M/\dot{V}_{CO2}$ = 12·10^{-8} cm³/s / 2.1·10^{-8} nmol/s = 5.7 cm³/nmol.

Thus, mitochondria possess an almost 20 times greater membrane CO_2 conductance per rate of CO_2 production than MDCK cells. We conclude that mitochondria possess an especially perfect optimization of CO_2 release across their membranes when compared to MDCK cells. This advantage would disappear, if the mitochondrial membrane had a similarly low CO_2 permeability as MDCK cells have.

Mechanism of High CO_2 Permeability of Mitochondria. Several authors have shown that a major parameter determining the permeability of phospholipid and cell membranes is the cholesterol content of the membrane [3, 29-31]. Itel et al. [3], Kai and Kaldenhoff [30] and Tsiavaliaris et al. [31] have shown that the CO_2 permeability of liposomes and artificial phospholipid membranes – like that of cell membranes – is in addition governed by the presence or absence of membrane gas channels. The content of cholesterol can reduce $P_{M,CO2}$ from > 0.16 cm/s in the absence of cholesterol to ~ 0.002 cm/s in the presence of 70% mol% cholesterol per total lipids, i.e. by at least two orders of magnitude [3, 29]. This finding implies that cell membranes with a normal cholesterol content of 30-40% can have a rather low CO_2 permeability, such as for example MDCK cells with a $P_{M,CO2}$ of 0.017 cm/s [3]. In tissues with a high metabolic rate, such as the heart, such a permeability would be limiting for cellular CO_2 release [7]. Thus, it is important that cell membranes in such tissues acquire a substantially higher membrane $P_{M,CO2}$. Itel et al. [3] have shown in artificial phospholipid membranes that an effective means to achieve this is to incorporate protein gas channels into the membrane. Incorporating the gas channel aquaporin 1, they were able to increase $P_{M,CO2}$ in a membrane containing 50 mol% cholesterol up to 10-fold. Thus, in tissues of high metabolic rate $P_{M,CO2}$ can become high in spite of a high cholesterol content of the membrane, which may be needed for other reasons such as establishing the desired mechanical properties of the membrane [32] or because of cholesterol's general barrier function [33].

The mitochondrial membrane seems to constitute an example in which a novel constellation of the two above parameters leads to an unusually high CO_2 permeability. Mitochondrial membranes (inner as well as outer) have an extremely low cholesterol content, amounting to an about 40-fold lower value compared to the cholesterol levels in plasma membranes [34, 35]. This per se is expected to impart a high $P_{M,CO2}$ to the mitochondrial membrane, which on the basis of the data of Itel et al. [3] can easily assume the value reported here, 0.3 cm/s. On the other hand, the mitochondrial membrane does not seem to possess any known protein gas channel. This is compatible with the lack of an effect of DIDS on $P_{M,CO2}$ as seen in Fig. 5; DIDS has been shown to be an effective gas channel inhibitor [16] both for aquaporin 1 and for Rhesus-associated glycoprotein [5, 6]. Furthermore, while many aquaporin isoforms have been shown to function as protein gas channels [36], the

KARGER

only isoform known to be present in mitochondria, aquaporin 8 [37, 38], does not conduct CO_2 [36]. The available evidence thus points to the mitochondrial membrane exhibiting a very high CO_2 permeability due to extremely low cholesterol content in spite of the absence of gas channels.

Acknowledgments

Disclosure Statement

None of the authors declares any conflict of interest.

References

1   Elder JA, Lehninger AL: Respiration-dependent transport of carbon dioxide into rat liver mitochondria. Biochemistry 1973;12:976-982.
2   Balboni E, Lehninger AL: Entry and exit pathways of CO2 in rat liver mitochondria respiring in a bicarbonate buffer system. J Biol Chem 1986;261:3563-3570.
3   Itel F, Al-Samir S, Öberg F, Chami M, Kumar M, Supuran CT, Deen PMT, Meier W, Hedfalk K, Gros G, Endeward V: CO2 permeability of cell membranes is regulated by membrane cholesterol and protein gas channels. FASEB J 2012;26:5182-5191.
4   Endeward V, Gros G: Low carbon dioxide permeability of the apical epithelial membrane of guinea-pig colon. J Physiol 2005;15:253-265.
5   Endeward V, Musa-Aziz R, Cooper GJ, Chen LM, Pelletier MF, Virkki LV, Supuran CT, King LS, Boron WF, Gros G: Evidence that aquaporin 1 is a major pathway for CO2 transport across the human erythrocyte membrane. FASEB J 2006;20:1974-1981.
6   Endeward V, Cartron JP, Ripoche P, Gros G: RhAG protein of the Rhesus complex is a CO2 channel in the human red cell membrane. FASEB J 2008;22:64-73.
7   Endeward V, Al-Samir S, Itel F, Gros G: How does carbon dioxide permeate cell membranes? A discussion of concepts, results and methods. Front Physiol 2014;4:382.
8   Vincent SH, Silverman DN: Carbonic anhydrase activity in mitochondria from rat liver. J Biol Chem 1982; 257: 6850-6855.
9   Dodgson SJ, Forster RE, Storey BT, Mela L: Mitochondrial carbonic anhydrase. Proc Natl Acad Sci USA 1980;77:5562-5566.
10 Ono Y, Lin L, Storey BT, Taguchi Y, Dodgson SJ, Forster RE: Continuous measurement of 13C16O2 production from [13C] pyruvate by intact liver mitochondria: effect of HCO-3. Am J Physiol 1996;270:C98-C106.
11 Fernández-Vizarra E, Lopez-Perez MJ, Enriquez JA: Isolation of biogenetically competent mitochondria from mammalian tissues and cultured cells. Methods 2002;26:292–297.
12 Fernández-Vizarra E, Ferrín G, Pérez-Martos A, Fernández-Silva P, Zeviani M, Enríquez JA: Isolation of mitochondria for biogenetical studies: An update. Mitochondrion 2010;10:253–262.
13 Schwerzmann K, Cruz-Orive LM, Eggman R, Sänger A, Weibel ER. Molecular architecture of the inner membrane of mitochondria from rat liver: a combined biochemical and stereological study: J Cell Biol 1986;102:97-103.
14 Reynolds ES: The use of lead citrate at high pH as an electron-opaque stain in electron microscopy. J Cell Biol 1963;17:208-213.

KARGER

Arias-Hidalgo et al.: Mitochondrial CO_2 Permeability

15 Perut F, Carta F, Bonuccelli G, Grisendi G, Di Pompo G, Avnet S, Sbrana FV, Hosogi S, Dominici M, Kusuzaki K, Supuran CT, Baldini N: Carbonic anhydrase IX inhibition is an effective strategy for osteosarcoma treatment. Expert Opin Ther Targets 2015;19:1593-1605.

16 Forster RE, Gros G, Lin L, Ono Y, Wunder M: The effect of 4,4'-diisothiocyanato-stilbene-2,2'-disulfonate on CO2 permeability of the red blood cell membrane. Proc Natl Acad Sci USA 1998;95:15815-15820.

17 Traaseth N, Elfering S, Solien J, Haynes V, Giulivi C: Role of calcium signaling in the activation of mitochondrial nitric oxide synthase and citric acid cycle. Biochim Biophys Acta 2004;1658:64-71.

18 Kantrow SP, Taylor DE, Carraway MS, Piantadosi CA: Oxidative metabolism in rat hepatocytes and mitochondria during sepsis. Arch Biochem Biophys 1997;345:278–288.

19 Alberts B, Johnson A, Lewis J, Raff M, Roberts K, Walter P: Molekularbiologie der Zelle. John Wiley & Sons, 2011.

20 Halestrap A, Quinlan PT: The intramitochondrial volume measured using sucrose as an extramitochondrial marker overestimates the true matrix volume determined with mannitol. Biochem J 1983;214:387-393.

21 Cohen NS, Cheung C, Raijman L: Measurements of mitochondrial volumes are affected by the amount of mitochondria used in the determinations. Biochem J 1987;245:375-379.

22 Williams GR: Dynamic aspects of the tricarboxylic acid cycle in isolated mitochondria. Can J Biochem 1965;43:603-615.

23 Itada N, Forster RE: Carbonic anhydrase activity in intact red blood cells measured with 18O exchange. J Biol Chem 1977;252:3881-3890.

24 Dodgson SJ, Forster RE: Carbonic anhydrase activity of intact erythrocytes from seven mammals. J Appl Physiol Respir Environ Exerc Physiol 1983;55:1292-1298.

25 Al-Samir S, Papadopoulos S, Scheibe RJ, Meißner JD, Cartron JP, Sly WS, Alper SL, Gros G, Endeward V: Activity and distribution of intracellular carbonic anhydrase II and their effects on the transport activity of anion exchanger AE1/SLC4A1. J Physiol 2013;591:4963-4982.

26 Peters T, Forster RE, Gros G: Hagfish (Myxine Glutinosa) red cell membrane exhibits no bicarbonate permeability as detected by 18O exchange. J Exp Biol 2000; 203: 1551–1560.

27 Chappel JB, Crofts AR: In Regulation of Metabolic Processes in Mitochondria. Tager JM, Papa S, Quagliarello E and Slater EC (eds). Elsevier; Amsterdam, 1966, pp. 293-314.

28 Guarino RD, Dike LE, Haq TA, Rowley JA, Pitner JB, Timmins MR: Method for determining oxygen consumption rates of static cultures from microplate measurements of pericellular dissolved oxygen concentration. Biotechnol Bioeng 2004;86:775-787. Erratum in: Biotechnol Bioeng 2005;91:392.

29 Hub JS, Winkler FK, Merrick M, de Groot BL: Potentials of mean force and permeabilities for carbon dioxide, ammonia, and water flux across a Rhesus protein channel and lipid membranes. J Am Chem Soc 2010;132:13251-13263.

30 Kai L, Kaldenhoff R: A refined model of water and CO2 membrane diffusion: effects and contribution of sterols and proteins. Sci Rep 2014;4:6665.

31 Tsiavaliaris G, Itel F, Hedfalk K, Al-Samir S, Meier W, Gros G, Endeward V: Low CO2 permeability of cholesterol-containing liposomes detected by stopped-flow fluorescence spectroscopy. FASEB J 2015;29:1780-1793.

32 Khelashvili G, Johner N, Zhao G, Harries D, Scott HL: Molecular origins of bending rigidity in lipids with isolated and conjugated double bonds: the effect of cholesterol. Chem Phys Lipids 2014;178:18-26.

33 Hill WG, Zeidel ML: Reconstituting the barrier properties of a water-tight epithelial membrane by design of leaflet-specific liposomes. J Biol Chem 2000;275:30176-30185.

34 Horvath SE, Daum G: Lipids of mitochondria. Prog Lipid Res 2013;52:590-614.

35 Paradies G, Ruggiero FM: Effect of aging on the activity of the phosphate carrier and on the lipid composition in rat liver mitochondria. Arch Biochem Biophys 1991;284:332–337.

36 Geyer R, Musa-Aziz R, Qin X, Boron WF: Relative CO2/NH3 selectivities of mammalian aquaporins 0–9. Am J Physiol Cell Physiol 2013;304:985–994.

37 Calamita G, Ferri D, Gena P, Liquori GP, Cavalier A, Thomas D, Svelto M: The inner mitochondrial membrane has aquaporin-8 water channels and is highly permeable to water. J Biol Chem 2005;280:17149–17153.

38 Molinas SM, Trumper L, Marinelli RA: Mitochondrial aquaporin-8 in renal proximal tubule cells: evidence for a role in the response to metabolic acidosis. Am J Physiol Renal Physiol 2012;303:F458-F466.

KARGER

Article 2

CO$_2$ Permeability and Carbonic Anhydrase Activity of Rat Cardiomyocytes

Authors: <u>Mariela Arias-Hidalgo</u>, Samer Al-Samir, Natalie Weber, Cornelia Geers-Knörr, Gerolf Gros[§], Volker Endeward

Candidate's contribution:

I have performed the isolation of cardiomyocytes and the mass spectrometric experiments to determine CO$_2$ and bicarbonate permeability of these cells, as well as the calculation of the results in MatLab, and the statistical analysis. Also I performed the DNSA experiments with phase contrast, fluorescent and confocal microscopy in collaboration with Dr. Samer Al-Samir. I also wrote the first draft of this publication, made the graphs, edited the mass spectrometric records for the manuscript, and worked in the subsequent editing of the manuscript.

ACTA PHYSIOLOGICA

CO$_2$ permeability and carbonic anhydrase activity of rat cardiomyocytes

M. Arias-Hidalgo, S. Al-Samir, N. Weber, C. Geers-Knörr, G. Gros and V. Endeward

Molekular- und Zellphysiologie and AG Vegetative Physiologie, Medizinische Hochschule Hannover, Hannover, Germany

Abstract

Aim: To determine the CO$_2$ permeability (P$_{CO2}$) of plasma membranes of cardiomyocytes. These cells were chosen because heart possesses the highest rate of O$_2$ consumption/CO$_2$ production in the body.

Methods: Cardiomyocytes were isolated from rat hearts using the Langendorff technique. Cardiomyocyte suspensions exhibited a vitality of 2–14% and were studied by the previously described mass spectrometric ^{18}O-exchange technique deriving P$_{CO2}$. We showed by mass spectrometry and by carbonic anhydrase (CA) staining that non-vital cardiomyocytes are free of CA and thus do not contribute to the mass spectrometric signal, which is determined exclusively by the fully functional vital cardiomyocytes.

Results: Lysed cardiomyocytes yielded an intracellular CA activity for vital cells of 5070; that is, the rate of CO$_2$ hydration inside the cell is accelerated 5071-fold. Using this number, analyses of the mass spectrometric recordings from cardiomyocyte suspensions yield a P$_{CO2}$ of 0.10 cm s^{-1} (SD $\pm$ 0.06, n = 15) at 37 °C.

Conclusion: In comparison with the P$_{CO2}$ of other cells, this value is quite high and about identical to that of the human red cell membrane. As no major protein CO$_2$ channels such as aquaporins 1 and 4 are present in rat cardiac sarcolemma, the high P$_{CO2}$ of this membrane is likely due to its low cholesterol content of about 0.2 (mol cholesterol)·(mol total membrane lipids)$^{-1}$. Previous work predicted a P$_{CO2}$ of $\geq$0.1 cm s^{-1} from this level of cholesterol. We conclude that the low cholesterol establishes a P$_{CO2}$ high enough to render the membrane resistance to CO$_2$ diffusion almost negligible, even under conditions of maximal O$_2$ consumption of the heart.

Keywords carbonic anhydrase, cardiomyocyte, membrane CO$_2$ permeability.

The permeability of biological membranes to CO$_2$ (P$_{CO2}$) can be modulated over more than two orders of magnitude. Values reported so far vary between 0.3 cm s^{-1} for the mitochondrial membrane and 0.001 cm s^{-1} for the apical membrane of colon epithelium.[1,2] Itel *et al.*,[3] Hub *et al.*,[4] and Kai and Kaldenhoff[5] have shown that the modulation of P$_{CO2}$ is achieved by variations in membrane cholesterol content and absence/presence of protein gas channels in the membrane. What is the biological purpose of the adaptability of P$_{CO2}$ in such a wide range? It appears plausible that the value of P$_{CO2}$ may be related to the CO$_2$ flux that occurs across the cell membrane considered. Endeward *et al.*,[6] have presented a model calculation showing that, for a tissue exhibiting the maximal O$_2$ consumption/CO$_2$ production of the heart under conditions of heavy exercise of 0.4 mL CO$_2$ g tissue^{-1} min^{-1},[7] a cell membrane

P_{CO2} of ≥ 0.1 cm s^{-1} is required, if membrane permeation of CO_2 is to be a non-limiting process. For cells with markedly lower rates of CO_2 production, a much lower P_{CO2} would be sufficient to achieve this. For example, MDCK cells in culture have an oxygen consumption of 0.02 mL O_2 g^{-1} min^{-1}[1,2] that is 1/20 of the maximal O_2 consumption of the heart, and a P_{CO2} of only 0.017 cm s^{-1}.[3] Cardiomyocytes, which have the highest maximal metabolic rate among the tissues of the body, appeared to be an ideal model, therefore, to study whether P_{CO2} is well adapted to the situation of a very high metabolic rate. A high P_{CO2}, as seems desirable in this case, can always be established by low membrane cholesterol,[2] but this entails loss of cholesterol's general barrier function and its effect on mechanical stability of the membrane. In cases where this is disadvantageous, a high P_{CO2} can be achieved in spite of high cholesterol by the incorporation of protein gas channels. An example for this latter situation is the red blood cell membrane, which loses 90% of its CO_2 permeability, when the protein gas channels are absent or inhibited.[8]

It may be noted that, aside from a relation of P_{CO2} to the metabolic rate, there can be other factors that make specific P_{CO2} values advantageous. One so far described example of this is the red blood cell, which has a low metabolic rate but an exceptionally high rate of O_2 and CO_2 exchange, rendering its high P_{CO2} of 0.15 cm s^{-1} essential.[8,9] Another case is the colon epithelium, which has an average metabolic rate but whose cell interior needs to be protected from very high CO_2 partial pressures in the colonic lumen (up to 0.5 atm).[1] This protection is achieved by the extremely low P_{CO2} of the apical membrane of 0.001 cm s^{-1}, in combination with a much higher P_{CO2} of the basolateral membrane of 0.02 cm s^{-1}.[1] In the heart, we expect that it is only the necessities of the rates of oxidative metabolism that determine the functionally desirable P_{CO2} of the cardiomyocyte membrane.

Results

Characterization of the rat cardiomyocytes

Vital cardiomyocytes had a length of 103 μm (SD ± 22) and width of 20 μm (±6.7). Volume was 12 220 μm^3 (±3900), surface area was 4870 μm^2 (±1070) and surface-to-volume (S/V) ratio was 4920 cm^{-1} (±800) (numbers derived from 294 cells). The average number of cardiomyocytes obtained per heart preparation was 2.3 × 10^6; their average vitality was 6%.

The average cellular carbonic anhydrase activity was 5070 (SD ± 2250; number of experiments

$n = 35$), when all activities measured in lysates were attributed to the vital cells only (see below).

All mass spectrometric measurements determining P_{CO2} and activity measurements were carried out with suspensions of cardiomyocytes.

Non-vital cell experiments

Because the fraction of vital cells in our preparations was low, and the measurements were carried out with mixtures of vital and non-vital cells, it was important to know the carbonic anhydrase activities of vital vs. non-vital cells. For this purpose, we studied cardiomyocyte suspensions that contained exclusively non-vital cells. Such preparations were obtained occasionally when the time interval between opening of the thorax and start of coronary perfusion had become too long; that is, the cardiac tissue was hypoxic for longer than usual. We added the suspensions into the mass spectrometer chamber and analysed the slopes of the mass spectrometric records using a semilogarithmic scale. It should be pointed out that the present mass spectrometric technique does not give a change in signal, neither with intact cells nor in lysates, when no carbonic anhydrase is present.[6] Figure 1a shows the slope after the addition of the non-vital cells (arrow in Fig. 1a), which may be compared with the slope before the addition of cells. As seen in Table 1, first column 'NVCS', the ratio between both slopes is about 1. This means that there is no difference between the slope of the uncatalysed rate of the reaction $HC^{18}O^{16}O_2 + H^+ \leftrightarrow H_2{}^{16}O + C^{18}O^{16}O$ or $H_2{}^{18}O + C^{16}O_2$ and the slope after the addition of a non-vital cell suspension. This is in contrast to the change in slope seen after the addition of lysate of vital cells as apparent in Figure 1b. In addition to the lack of a change in slope, there is in Figure 1a also no biphasic time course of $C^{18}O^{16}O$ appearing after the addition of the cells, as it would be characteristic for intact CA-containing cells and is illustrated for a vital cell experiment in Figure 1c.

All results for non-vital cell preparations are summarized in Table 1. Non-vital cells produce no change in slope of the mass spectrometric record even after they have been lysed in the presence of 0.1% Triton X-100 (Table 1, second column 'NVCS+Triton'). This means that the non-vital cells possess no CA accelerating this reaction, neither intra- nor extracellularly. This conclusion is confirmed by the observation that neither the extracellular CA inhibitor FC5-208A (Table 1, third and fourth columns) nor the membrane-permeable intracellular CA inhibitor ethoxzolamide (Table 1, fifth column) has any effect on the slopes seen after the addition of non-vital cells. In conclusion, there is no CA activity in non-vital cells
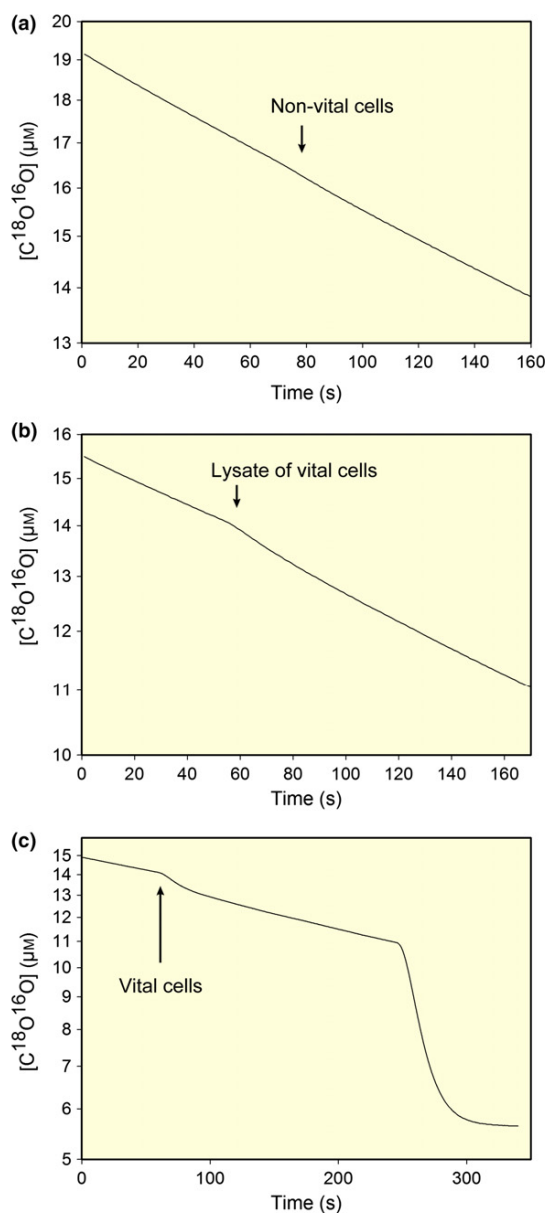
Figure 1 Original recordings of mass spectrometric experiments with isolated cardiomyocytes. The decay of the concentration of $C^{18}O^{16}O$ in the mass spectrometric reaction chamber is plotted semilogarithmically vs. time. (a) Non-vital cardiomyocytes, cell density 2.2×10^6 cells mL^{-1} and vitality 0%. After the addition of cells, almost no change in the slope of the mass spectrometric signal is seen, and also no biphasic decay of $C^{18}O^{16}O$ as in Figure 1c is apparent. (b) Lysate of vital cells. Cell density before lysis was 0.3×10^6 cells mL^{-1}, and vitality was 3%. After the addition of lysate, an increase in the slope of the time course of $C^{18}O^{16}O$ is seen. (c) Vital cell suspension was 0.23×10^6 cells mL^{-1}, and vitality 7%. After the addition of the cells, the characteristic biphasic time course of the signal is seen, indicating that intact CA-containing cells have been added. Arrows indicate where cell suspension/lysate was added.

that could affect the time course of $C^{18}O^{16}O$ observed with the mass spectrometric technique. This implies that the presence of non-vital cells will not affect the mass spectrometric signal produced by vital cardiomyocytes, meaning that the presence of non-vital cells in the present cardiomyocyte suspensions does not disturb the analysis of the vital cardiomyocytes.

To further check the concept that non-vital cardiomyocytes possess no CA and thus do not contribute to the mass spectrometric signal, we stained the present cardiomyocyte suspensions with the sulphonamide DNSA, which exhibits blue fluorescence when bound to CA.[10] The three examples of details from cardiomyocyte suspensions (Fig. 2a c) viewed by phase-contrast microscopy (panels on the left) and by fluorescence microscopy (panels on the right) show clearly that living intact, rod-shaped cardiomyocytes emit strong blue fluorescence, while the rounded non-vital cardiomyocytes exhibit no fluorescence. In phase-contrast microscopy, no other cells than cardiomyocytes are recognizable, and likewise in the fluorescence mode, no other cells than cardiomyocytes exhibit DNSA staining. In summary, two different approaches indicate that in our preparation only intact living cardiomyocytes possess carbonic anhydrase, and thus, only these cells can contribute to the mass spectrometric signal such as that given in Figure 1c.

CO₂ and HCO₃⁻ permeabilities of cardiomyocytes

Records from 'vital' cardiomyocyte suspensions with vitalities varying between 2 and 14%, such as the one shown in Figure 1c, were used to derive the permeabilities of CO_2 and HCO_3^-. Cell vitality remained stable during the time interval of *ca.* 1 h, in which the mass spectrometric permeability measurements were taken. Figure 3 shows the results for P_{CO2} from a first set of measurements. Under control conditions, P_{CO2} was 0.23 cm s^{-1} ($\pm$0.11; $n = 14$). 1×10^{-4} M DIDS had no effect and yielded a P_{CO2} of 0.23 cm s^{-1} ($\pm$0.12; $n = 7$). However, 2.5×10^{-5} M of the extracellular CA inhibitor FC5-208A reduced P_{CO2} significantly to 0.10 cm s^{-1} ($\pm$0.06; $n = 15$). The effect of FC5-208A indicates that vital cardiomyocytes possess an extracellular CA that will affect the mass spectrometric signal and disturb the calculation of permeabilities. We have therefore repeated these measurements with FC5-208A present under control conditions as well as in the presence of DIDS. As shown in Figure 4, P_{CO2} values of 0.10 cm s^{-1} ($\pm$0.06; $n = 15$) in the presence of 2.5×10^{-5} M FC5-208A, and 0.11 cm s^{-1} ($\pm$0.07, $n = 7$) in the presence of 2.5×10^{-5} M FC5-208A plus 1×10^{-4} M DIDS, were obtained. This latter result shows that DIDS has

45

CO$_2$ permeability of cardiomyocytes · M Arias-Hidalgo et al.   Acta Physiol 2017

Table 1 Ratios of the slopes of mass spectrometric recordings before and after addition of non-vital cardiomyocyte suspension

Treatment	NVCS	NVCS + Triton	NVCS + FC5-208A	FC5-208A, 5-min pre-incubation	Ethoxzolamide, 5-min pre-incubation
Mean ratio	1.06	1.08	1.04	1.02	0.99
SD	±0.04	±0.05	±0.05	±0.02	±0.05
n	13	4	5	3	3

Slope ratios after the addition of 100% non-vital cell suspension (NVCS) into the mass spectrometric reaction chamber, non-vital cells with 0.1% Triton X-100 added, non-vital cells with 2.5×10^{-5} M of the extracellular carbonic anhydrase inhibitor FC5-208A added directly before the measurement or after 5-min pre-incubation with FC5-208A, or non-vital cells 5-min pre-incubation with 1×10^{-4} M membrane-permeable CA inhibitor ethoxzolamide. The non-vital cell suspensions had an average cell density of 3.5×10^6 mL^{-1}. SD, standard deviation, n number of preparations. ANOVA $P > 0.05$. None of the ratios given are significantly different from 1.0, indicating that there is no CA activity present in all conditions.
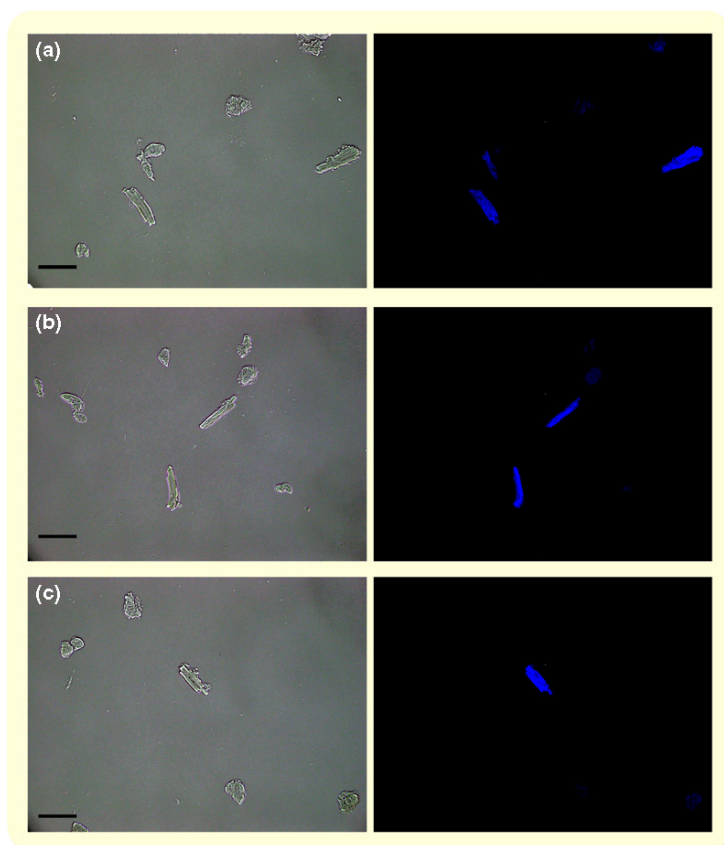

Figure 2 DNSA staining of a suspension of (vital) cardiomyocytes. a, b, c represent three views from a partially vital cardiomyocyte suspension. On the left, the three sections viewed by phase-contrast microscopy and, on the right, DNSA fluorescence (DNSA concentration 1.0×10^{-5} M) of the same sections. Comparing phase-contrast and fluorescence pictures, it is apparent that the living cardiomyocytes, which conserve their rectangular shape, are intensely stained for carbonic anhydrase, while the rounded non-vital cardiomyocytes are unstained and thus contain no CA. In phase-contrast microscopy no red blood cells and in fluorescence microscopy no stained cells other than living cardiomyocytes are visible. Bars 100 μm.

no significant effect on the CO$_2$ permeability of cardiomyocytes (Student's t-test, $P = 0.88$). It also shows that 0.10 rather than 0.2 cm s^{-1} is the correct P_{CO2} of cardiomyocytes.

P_{HCO3-} is found to be 2.1×10^{-3} cm s^{-1} ($\pm 2.0 \times 10^{-3}$, $n = 15$) in the presence of FC5-208A, and 2.6×10^{-3} cm s^{-1} ($\pm 2.6 \times 10^{-3}$, $n = 7$) in the presence of both FC5-208A and DIDS. Thus, DIDS in this case does not seem to reduce P_{HCO3-}, which may be related to the involvement of NBCn1 in cardiac sarcolemmal HCO$_3^-$ transport, a transporter that is

not DIDS sensitive,[11,12] and/or to the substantial scatter in the present data for P_{HCO3-}.

Discussion

Properties of present cardiomyocyte preparation

For the present purpose, it is essential to have a suspension of cardiomyocytes rather than the usual preparation of cardiomyocytes attached to the surface of a culture plate. As evident from the literature, this
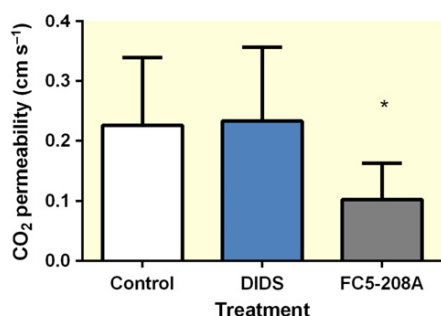
Figure 3 CO$_2$ permeability of cardiomyocyte suspensions and the effect of inhibitors. *n* from left to right: 16, 7, 13. Bars are SD. ANOVA yields *P* = 0.0016. With Dunnett's post-test, FC5-208A is significantly different from control (*), and DIDS has no effect.
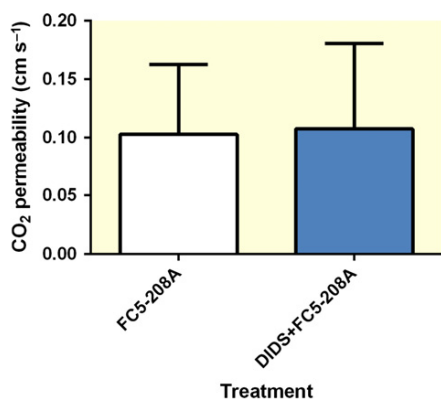

Figure 4 CO$_2$ permeabilities of cardiomyocytes pre-incubated with extracellular CA inhibitor FC5-208A. *n* from left to right: 15, 7. Bars represent SD. Student's *t*-test: *P* = 0.88. Left-hand column shows that in the presence of FC5-208A, as in its absence (Fig. 3), DIDS has no effect on P$_{CO2}$.

implies that many cells are lost over time. When adult cardiomyocytes are not adherent to a surface but remain in suspension, a majority lose vitality within hours.[13 15] For this reason, the vitalities seen here are not greater than 6% on average (2 14%). They fall to this value within about 1 h after the first centrifugation of the crude suspension of freshly isolated cardiomyocytes, and then remain at this level of vitality between 2 and 4 h after the first centrifugation. In this condition, the vital cells retain the characteristic rod-like shape, while the non-vital cells have become rounded, as seen in Figure 2. Another feature of the non-vital cells is seen in Figure 5a,b, which show isolated cardiomyocytes from this study stained for α-myosin. It is apparent that the vital rod-shaped cells exhibit longitudinally oriented myofilaments and clearly visible cross-striations. In contrast, the rounded cells, while still expressing α-myosin, have lost all

structural properties of myofilaments, an observation in general agreement with the literature.[13,16,17] The vital cells of the present preparation, on the other hand, can be demonstrated to be functionally intact from their ability to contract upon electrical stimulation. Rod-shaped cardiomyocytes were attached to laminin-coated glass coverslips and stimulated by electrodes as described in Mutig *et al.*,[18] Representative traces of a stimulation-induced calcium transient and the associated contraction are shown in Figure 5c,d. Quantification of the shortening of the sarcomeres during contraction yielded (i) for a stimulation frequency of 1 Hz, a diastolic sarcomere length of 1.819 ± 0.048 (SD) μm, which fell during contraction by 0.075 ± 0.042 μm (four rats, 59 cells), (ii) for a frequency of 3 Hz, a diastolic length of 1.813 ± 0.050 μm, reduced during contraction by 0.080 ± 0.044 μm (four rats, 60 cells), and (iii) for a frequency of 5 Hz, a diastolic length of 1.800 ± 0.054, reduced by 0.086 ± 0.041 μm during contraction (four rats, 57 cells). Thus, the myocytes contracted with amplitudes increasing from 4.1% at 1 Hz to 4.8% at 5 Hz. In conclusion, the rod-shaped vital cardiomyocytes used here for the mass spectrometric measurements are clearly functional both in terms of Ca^{2+} transient and in terms of contractile behaviour.

Carbonic anhydrase activity of vital cardiomyocytes

We report here a carbonic anhydrase activity of cardiomyocytes of 5070 at 37 °C, a number indicating that the rate of CO$_2$ hydration in a myocyte is accelerated over the uncatalysed rate by a factor of 5070 + 1. This number refers to the whole cell after lysis with Triton and encompasses the contributions by all cytosolic and all membrane-bound forms of CA. This includes intra- as well as extracellular carbonic anhydrase. The present CA activity seems to be exclusively due to isolated cardiomyocytes, as the isolation procedure removes all other cell types such as endothelial cells and erythrocytes by repeated low-speed centrifugation.[19] Microscopic inspection of the suspensions of isolated cardiomyocytes showed complete absence of red cells, and the DNSA staining as shown in Figure 2 revealed that no cells other than intact cardiomyocytes are stained for CA. Our figure for cardiomyocyte CA activity is in rough agreement with the number one can derive from the measurements of whole myocardium homogenate reported by Villafuerte *et al.*,[20] If one assumes that the Sprague Dawley rat hearts used by them had an overall protein concentration of 200 mg mL ^{1}, one can estimate that their reported lysate CA activities indicate a whole-cell activity of between 600 and 6000, a range consistent with our above figure for Lewis rat cardiomyocytes.
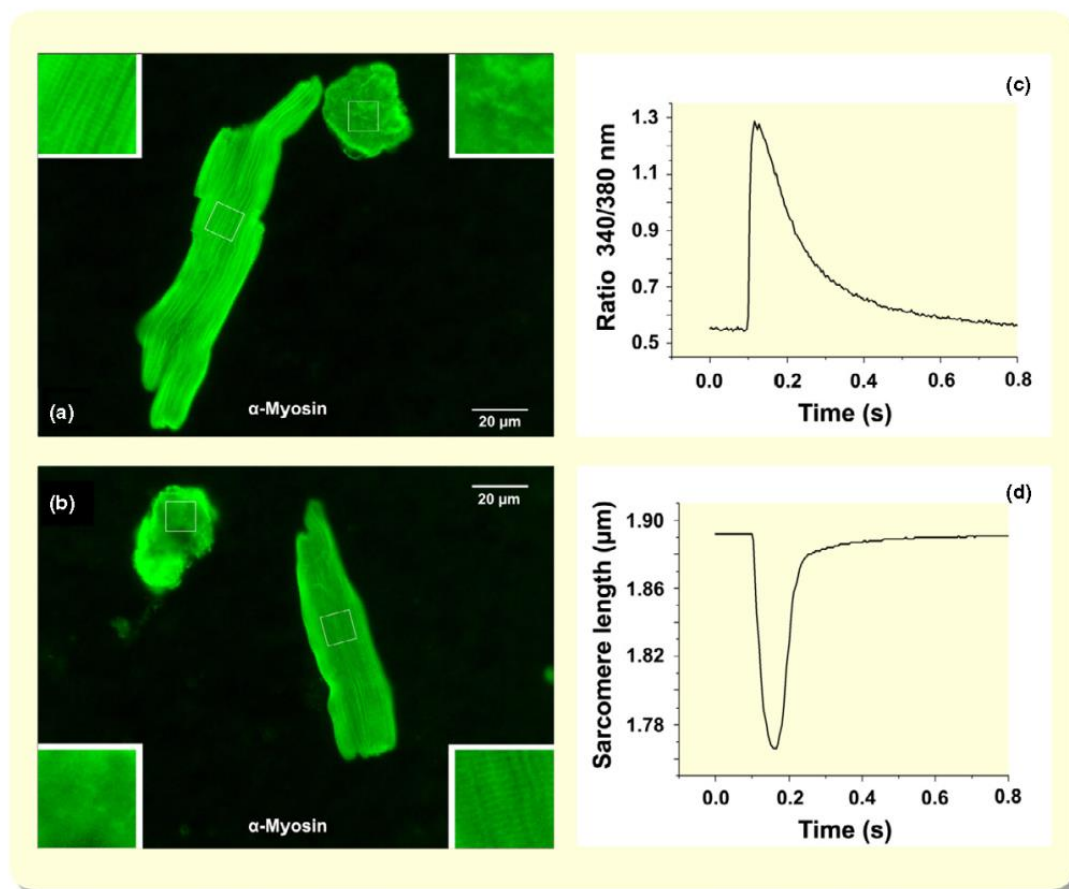
Figure 5 α-Myosin staining and excitation–contraction coupling in isolated rat cardiomyocytes. (a,b) Immunocytochemical demonstration of α-myosin in vital (rod-shaped) and non-vital (rounded) cardiomyocytes. Filament structure and cross-striations are clearly seen in vital cells, but lost in non-vital cells. Framed sections appear in greater magnification to the left or the right of the frames respectively. (c) Ca^{2+} transient of a vital cardiomyocyte elicited by an electrical pulse, Ca^{2+} concentration expressed as the ratio of Fura-2 fluorescence after excitation at 340 and 380 nm. (d) Time course of the sarcomere length during the contraction associated with the Ca^{2+} transient shown in (c).

The number of about 5000 is, however, in marked contrast to the number reported by Schroeder *et al.*,[21] who derived from ^{13}C magnetic resonance spectroscopy an average CA activity in the cytoplasm of ventricular myocytes from Wistar rats of only 2.7. We note that the present mass spectrometric results are incompatible with an activity of this order of magnitude. We can calculate a minimum CA activity necessary to explain the present mass spectrometric recordings of the decay of C^{18}O^{16}O (Fig. 1c) by setting P$_{CO2}$ arbitrarily high enough to render the membrane resistance for CO$_2$ negligible, that is to P$_{CO2} \geq 10$ cm s^{-1}.[1,6] This yields a minimum intracellular CA activity of 3740 (SD ± 1710; $n = 31$; significantly different from 5070 with $P < 0.01$) in intact cardiomyocytes, ruling out a substantially lower CA activity for these cells.

It has been reported that a multitude of CA isoforms is present in the myocardium. While often cytosolic CA has not been detectable in heart homogenates after correction for CA attributable to residual red blood cells (rabbit, Geers *et al.*,[22]; rat, Moynihan[23]), it has been shown that some cytosolic CA II is expressed in normal cardiomyocytes, probably at very low levels.[24 26] In addition, mRNA of cytosolic CA XIII has been observed in mouse heart,[27] but protein expression of CA XIII in hearts has not been studied. Scheibe *et al.*,[28] have presented a comprehensive immunocytochemical study on mouse hearts, in which the presence of CA XIV and CA IV in the sarcolemma was demonstrated. In addition, however, Scheibe *et al.*,[28] found that most of these membrane-bound CAs plus the membrane-bound CA IX are associated with intracellular membranes of longitudinal and
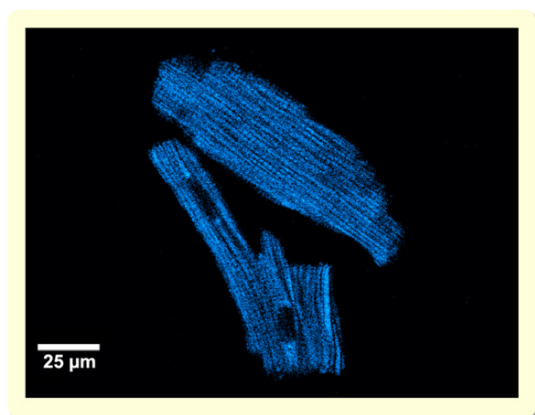
Figure 6 Confocal image of DNSA-stained vital rat cardiomyocytes. Blue fluorescence results from DNSA bound to carbonic anhydrase. The fluorescence pattern is compatible with staining of the sarcoplasmic reticulum, especially the longitudinal system. The dark areas within cells represent nuclei. No contribution of mitochondria to the staining is expected, as heart mitochondria do not possess carbonic anhydrase activity.[31]

terminal sarcoplasmic reticulum and T tubules. This is in agreement with Sender *et al.*,[29] who found CA IV in rat und human hearts to be associated with sarcolemma as well as sarcoplasmic reticulum and T tubules. It is also in agreement with Geers *et al.*,[22] who found an especially high activity of membrane-bound CA activity in rabbit heart, several-fold higher than they observed in other striated muscles. Furthermore, this agrees with Bruns and Gros,[30] who found a majority of the CA of bovine hearts to be associated with intracellular membranes and sarcolemma and whose DNSA staining pictures suggest that most of this CA is intracellular rather than sarcolemmal. This view is confirmed for the present intact isolated cardiomyocytes by the present confocal images of DNSA-stained cells as seen in Figure 6. It is apparent that at better resolution the blue fluorescence is not homogeneous as in Figure 2, but exhibits an intracellular structure with a longitudinal orientation. This pattern is compatible with staining of the sarcoplasmic reticulum.[32 34]

For the present study, it is of interest whether there is a significant difference between the actual intracellular CA activity and the activity derived from whole lysate, because we use the latter to represent the former in our analysis of the ^{18}O exchange data. Correct derivation of CO_2 and bicarbonate permeabilities from the present mass spectrometric recordings requires knowledge of the true intracellular CA activity. Thus, it is important to assess whether a significant part of the total CA of whole-cell lysates is associated with the sarcolemma, and thus

extracellular, and functionally not accessible in the intracellular space. The results of Scheibe *et al.*,[28] and those of Bruns and Gros[30] indicate that by far most of the CA is intracellular. This is supported by the DNSA staining of the present cardiomyocytes (Fig. 2), which show a strong and nearly homogeneous intracellular staining without any visibly pronounced staining intensity in the region of the sarcolemma. This is also seen in the confocal image of the present cardiomyocytes in Figure 6, which shows strongly stained intracellular structures without marked sarcolemmal staining. In the following, we will attempt to quantitatively estimate the contribution of the extracellular sarcolemmal CA to the activities measured in whole-cell lysate. Bruns and Gros[30] have produced highly purified sarcolemmal vesicles from bovine hearts and found their specific CA activity to be 15 U mL mg ^{1}, where 1 mL means 1 mL of sarcolemmal vesicle suspension and 1 mg means 1 mg of sarcolemmal membrane protein. The plasma membrane of many cells, including red blood cells, has a ratio of membrane protein to membrane lipid of about 1 : 1.[35] Therefore, we adopt here the estimate of membrane protein per membrane area, 4.6×10^{-12} (mg membrane protein)·(μm^2 membrane area)^{1}, as determined for red cell ghosts by Dupuy and Engelmann.[36] Further, we use the cardiomyocyte parameters single cardiomyocyte volume 12 220 μm^3 and cardiomyocyte surface area 4870 μm^2, as given above. With these parameters, we calculate that one single cardiomyocyte possesses 2.2×10^{-8} mg of membrane protein. This corresponds to 1.8 mg sarcolemmal membrane protein per mL cardiomyocyte volume. By multiplication with the above specific sarcolemmal CA activity, one obtains a contribution of sarcolemmal CA activity to the overall cardiomyocyte CA activity of 27 activity units. This is no more than 0.5% of the total overall activity of 5070 activity units. In other words, the contribution of extracellular sarcolemmal CA to the whole cardiomyocyte lysate activity is negligible. Thus, 5070 is a reliable estimate of the intracellular activity of cardiomyocytes.

We must also ask how easily the intracellular membrane-bound CAs are functionally accessible from the cytoplasm. As discussed by Scheibe *et al.*,[28] two of the three CA isoforms mentioned above, CA XIV and CA IX, have their active centre oriented towards the space outside the sarcoplasmic reticulum, that is towards the cytoplasmic space. Moreover, the sarcoplasmic reticulum membrane is expected to be easily permeable for CO_2 due to its low cholesterol content,[3,37] and likely also to bicarbonate by its established transport pathway for anions,[38] which is due to a non-selective monovalent anion channel.[39] Thus, it can be expected that not only intracellular CA IX and CA XIV but

also intracellular CA IV is functionally accessible from the cytoplasm and therefore contributes to cytoplasmic CA activity. The latter conclusion is compatible with the report by Schneider *et al.*,[40] who found that intracellular membrane-bound CA IV contributes to intracellular CA activity in oocytes and in mouse neurones.

The intracellular CA activity of ~5000 found here speeds up the uncatalysed half-time of CO_2 hydration from 5 s to 1 ms. This is physiologically meaningful for at least two groups of cellular functions. Intracellular CA can substantially facilitate intracellular CO_2 diffusion and thus CO_2 elimination from the cardiomyocyte.[41] However, in cells of the intracellular diffusion distances of cardiomyocytes, a CA activity of 5000 is required for half-maximal facilitation, and an activity <1000 would be without any effect (Gros *et al.*,[42]; V. Endeward and G. Gros, unpublished). Do inhibition of intramyocytic CA and the associated lack of intracellular facilitated CO_2 diffusion impair cardiac performance? Clinical or slightly above-clinical doses of acetazolamide did not affect maximal cardiac output in horses[43] and did not affect exercise tolerance in humans.[44] However, doses of acetazolamide considerably above-clinical ones resulted in a strong reduction in exercise tolerance in rats.[44] It appears conceivable but has not been studied with such doses of acetazolamide that in this latter case maximal cardiac output may have been reduced due to the inhibition of cardiomyocyte CA. It should be noted here that permeation of acetazolamide, especially across sarcolemma, is probably slow,[45] so fully inhibitory effects of acetazolamide within striated muscle cells may often not be reached *in vivo*. Another function of intracardiomyocyte CA has been pointed out by Spitzer *et al.*,[46], who found that this CA helps to accelerate intracellular effective H^+ mobility and intracellular dissipation of acid. In addition to these functions related to intracellular transport processes, CA activity is essential for the numerous acid base-exchanging membrane transporters of the heart by providing a rapidly accessible intracellular source (or sink) for H^+ and HCO_3^-. For this reason, many epithelia that intensely secrete or absorb acids or bases possess high intracellular CA activities.[47,48] For example, it can be estimated from the data of Stiel *et al.*,[49] that gastric mucosa has an intracellular CA activity of ~10 000. Thus, the present cardiomyocyte CA activity seems to be adequately high for the functions mentioned.

No carbonic anhydrase activity in non-vital cardiomyocytes

The above figure for intracardiomyocyte CA activity depends on the premise that non-vital cells exhibit no

CA activity. This is crucial not only for the activity attributed to vital cardiomyocytes but also for the interpretation of the mass spectrometric recordings, which are taken to represent vital cells alone. We have established this fact (i) by studying ^{18}O exchange in suspensions of 100% non-vital cells and (ii) by DNSA staining of the usual mixture of 2 14% vital cardiomyocytes and a majority of non-vital cells. 100% non-vital cardiomyocytes resulted from cardiac tissue hypoxia, when the time interval between opening the thorax and start of the perfusion was >5 min or when perfusion was obstructed by air bubbles. Figure 1 and Table 1 demonstrate that non-vital cell suspensions at normal densities did not produce a significant mass spectrometric signal, neither under control conditions nor in the presence of Triton X-100. Also, extra- as well as intracellular CA inhibitors did not have any influence on the mass spectrometric recording. This shows clearly that non-vital cardiomyocytes no longer possess CA activity. DNSA staining of partly vital cardiomyocyte suspensions as shown in Figure 2 confirm this. Only vital cells, whose characteristic shape is preserved, show DNSA staining, while the rounded non-vital cells exhibit no staining whatsoever. Because, as discussed above, most of the intracellular CA of cardiomyocytes is associated with intracellular membranes, the loss of CA may indicate the known damage to and loss of sarcoplasmic reticulum and T tubules linked to the process of conversion of vital to non-vital cardiomyocytes.[17] We conclude that non-vital cardiomyocytes do not contribute to the mass spectrometric signal due to their complete lack of CA.

CO_2 permeability of cardiomyocytes

The effect of the extracellular carbonic anhydrase inhibitor FC5-208A on P_{CO2} shows that the mass spectrometric signal is affected by some extracellular CA, which is likely due to the sarcolemmal extracellular CA of intact cardiomyocytes. It is unlikely that this CA is enzyme released from non-vital cells as the above studies indicate that our preparations of non-vital cardiomyocytes have no CA at all. It is essential that the extracellular CA activity is suppressed in order to obtain correct estimates of P_{CO2}. The P_{CO2} thus determined turns out to be 0.10 cm s^{-1} (Figs 3 and 4).

This P_{CO2} value is similar to the P_{CO2} of about 0.15 cm/s reported for human red blood cells.[8,9] It is about 10 times higher than the P_{CO2} of 0.015 cm s^{-1} of MDCK cells[3] and 100 times higher than the P_{CO2} of 0.0015 cm s^{-1} of the apical epithelial membrane of colon epithelium.[1] Endeward *et al.*,[6] have presented a model calculation showing that a P_{CO2} of

0.1 cm s $^{-1}$ is about the minimum membrane permeability necessary to ensure an unimpaired release of CO_2 from the maximally metabolizing cardiomyocyte (specific oxygen consumption 0.4 mL g tissue $^{-1}$ min $^{-1}$). Thus, two cell types with a very high rate of gas exchange, red cells and cardiomyocytes, share a P_{CO2} of about 0.1 cm s $^{-1}$. This value can be considered very high and is only exceeded by the P_{CO2} of the mitochondrial membrane, which exhibits the highest P_{CO2} reported so far for a biological membrane, 0.33 cm s $^{-1}$.[2]

Mechanism of high CO_2 permeability of cardiac sarcolemma. Itel *et al.*,[3] have shown that two major factors determine the CO_2 permeability of a biological membrane, the cholesterol content and the possible incorporation of protein gas channels. Cholesterol has an extremely powerful effect on membrane P_{CO2} in that it can lower P_{CO2} from >0.16 cm s $^{-1}$ to 0.0028 cm s $^{-1}$, when its membrane content is increased from 0 to 70% (moles cholesterol)·(moles of total membrane lipid) $^{-1}$.[3] A second strong influence can be exerted by the incorporation of gas channels into the membrane. Itel *et al.*,[3] have shown that reconstitution of aquaporin 1 into liposomes can increase P_{CO2} 10-fold. Thus, a high P_{CO2} can be achieved in biological membranes either by low cholesterol or by the insertion of protein gas channels.

Rat hearts have been reported to express the RNA for AQP1, AQP6, AQP7 and AQP11.[50] Purified rat cardiomyocytes showed RNA mainly for AQP1, and to a minor extent for AQP3, AQP4, AQP5, AQP7 and AQP11. While protein expression could be demonstrated for AQP1, AQP4 protein was not detectable in the rat heart,[50] and AQP3 and AQP7 show no CO_2 permeability.[51] The major potential CO_2 channel in heart is thus AQP1. This AQP, however, is essentially localized in the heart endothelium, but not in the sarcolemma.[52][54] Because the CO_2 pathway of AQP1 has been shown to be strongly inhibited by DIDS,[8,9] the present data, which exhibit no effect of DIDS on P_{CO2}, also indicate that AQP1 is not present and does not act as a CO_2 channel in the cardiomyocyte membrane. We conclude that cardiac sarcolemma likely expresses no significant amounts of a CO_2 channel.

Why then is P_{CO2} of this membrane so high? It has been reported that cardiomyocyte membranes have a low cholesterol content compared to many other cell membranes. This may seem surprising as cholesterol affords mechanical stability to membranes. However, it also causes membrane rigidity, which may be speculated to be disadvantageous for a muscle cell undergoing substantial deformation during contraction. Membrane cholesterol expressed in

(mol cholesterol)·(mol total lipid) $^{-1}$ has been reported to be between 0.19,[55] 0.25,[56] and 0.26[57] for rat cardiomyocytes. Weglicki *et al.*,[58] found a similar ratio of 0.23 in dog cardiomyocytes. All these values around 0.2 mol mol $^{-1}$ are not expected to significantly affect P_{CO2} of a phospholipid membrane as demonstrated in phospholipid vesicles by Itel *et al.*,[3] Pure phospholipid membranes exhibit a P_{CO2} of ≥0.16 cm s $^{-1}$.[3,6] Thus, the present high P_{CO2} of 0.1 cm s $^{-1}$ can be easily explained on the basis of the especially low cholesterol content of cardiomyocytes. We conclude that the high P_{CO2} of cardiac sarcolemma contributes to an adequate CO_2 transport in heart muscle with its very high metabolic rate. This property is similar to the case of the mitochondrial membrane[2] achieved through low membrane cholesterol rather than through incorporation of gas channels.

Materials and methods

Cardiomyocyte isolation

The following protocol is adapted from the one used by Niederbichler *et al.*,[59] All experiments were performed using male Lewis rats between 250 and 300 g body weight and were approved by the Niedersächsisches Landesamt für Verbraucherschutz und Lebensmittelsicherheit.

The heart perfusion and the cardiomyocyte isolation were performed using sterile techniques. Animals were anaesthetized with isoflurane, anticoagulated with 1000 U of heparin sodium, and a bilateral thoracotomy was performed. The distal aortic arch was cannulated and secured to the cannula, then together with the entire heart removed from the thorax and mounted on a Langendorff perfusion system.

Initiation of heart perfusion took place within 30 s of removal of the organ from the animal. All the perfusion solutions were supplemented with taurine (2-aminoethanesulphonic acid, intended to dampen increases in intracellular Ca^{2+}, thus protecting isolated cardiomyocyte preparations[60]) and BDM (2,3-butanedione monoxime, intended to inhibit myosin ATPase and thereby prolong cardiomyocyte viability[61]), equilibrated with 95% O_2/5% CO_2, and pH adjusted to 7.4 at 37 °C. The perfusion started with 1 mM calcium-containing Krebs–Henseleit buffer (KHB) for 5 min, followed by 5-min perfusion with a calcium-free KHB. Enzyme digestion was then performed with 92 mg collagenase type II (260 U mg $^{-1}$; Worthington Biochem. Corp., CellSystems Biotechnologie Vertrieb, Troisdorf, Germany) and 13 mg hyaluronidase from bovine testes (Sigma, Deisenhofen, Germany) that were added to 150 mL perfusate volume. After 10 min, 1.8 mL of 100 mM $CaCl_2$ was added to this

perfusate, yielding a calcium concentration of 1.2 mM, and perfusion was continued for 10 min. The heart was then removed from the cannula, and the atrium was cut away. The ventricles were gently minced and resuspended in 10 mL of calcium-containing enzyme solution.

The tissue suspension was further dispersed by repeated aspiration into a sterile glass pipette. Then, the suspension was allowed to stand for 5 min at room temperature, during which time the remaining coarse pieces of tissue settled down. Thereafter, the supernatant was pipetted off and centrifuged at 60 g for 60 s. The pellet was washed first with 10 mL Ca^{2+}-containing KHB supplemented with 2% bovine serum albumin (BSA) and then with Ca^{2+}-KHB with 6% BSA. After each washing step, the suspension was centrifuged at 60 g for 60 s and the supernatant was discarded. This procedure was repeated two more times with the remaining heart pieces, using smaller-diameter glass pipettes each time. All the collected single-cell suspensions were combined and resuspended in DMEM, centrifuged again and resuspended in a bicarbonate-free buffer containing 117 mM NaCl, 5.7 mM KCl, 1.2 mM NaH_2PO_4, 0.66 mM $MgSO_4*7H_2O$, 10 mM glucose, 5 mM Na-pyruvate, 10 mM creatine, 20 mM Hepes and 1.25 mM $CaCl_2*H_2O$. After one more centrifugation step, the supernatant was discarded and the final pellet suspended in an equal volume of the same buffer. This suspension was used for the subsequent experiments.

Cardiomyocyte density was determined using a microscope; cell viability was assessed from cell morphology and from trypan blue dye exclusion. Myocytes with a rodlike shape, clearly defined edges and visible striations usually represent viable cells, whereas cells without these characteristics are non-viable.

For the intracellular volume and surface determination, the length and width of the nearly rectangular cells were determined and volume and surface area were calculated for ellipsoids as described by Sorenson *et al.*,[62]

Contraction records, Ca^{2+} transients and immunocytochemistry

For functional analysis and immunocytochemical studies, cardiomyocytes were resuspended in DMEM (D5796; Sigma) and M199 (12350-039; Thermo Fisher, Schwerte, Germany) supplemented with 10 mmol L^{-1} L-glutathione (G4251; Sigma), 0.2 mg mL^{-1} BSA (A3803; Sigma), 1% antibiotic solution (penicillin/streptomycin; Thermo Fisher, 10 000 U m^{-1}), pH 7.4 at 37 °C.

The cardiomyocytes were then plated onto laminin-coated glass coverslips (Roche, 11243217001, Mannheim, Germany) and incubated for 3 h at 37 °C, 5%

CO_2. After 2 h, dead cells were removed and fresh supplemented M199 was added.

Single-cell sarcomere contraction and relaxation analysis. The single-cell contraction and relaxation analysis was performed using a variable-rate CCD video camera system (MyoCam®; IonOptix Corp., Milton, MA, USA) as described previously.[18] Briefly, a coverslip with adherent cardiomyocytes was placed into a custom-made perfusion chamber and perfused at 37 ± 0.5 °C with Hepes buffer containing in mmol/L: NaCl 117, KCl 5.7, NaH_2PO_4 1.2, $MgSO_4$ 0.66, glucose 10, sodium pyruvate 5, creatine 10, Hepes 20, EGTA 0.01, $CaCl_2$ 1.25, pH 7.4.[63]

The cardiomyocytes were electrically stimulated with MyoPacer® EP Cell Stimulator (IonOptix Corp.) and changes in sarcomere length at 1 Hz, 3 Hz and 5 Hz were recorded. For contraction analysis, 20–30 single twitches were averaged and diastolic sarcomere length and contraction amplitude were calculated using IonWizard® software (IonOptix Corp.).

Analysis of intracellular Ca^{2+} transients. Intracellular Ca^{2+} transients of single cardiomyocytes were recorded simultaneously with sarcomere shortening using a dual-excitation fluorescence photomultiplier system (IonOptix Corp.) as described previously.[18] Briefly, cardiomyocytes were loaded with 2 μM Fura-2 AM (Invitrogen™ Corp., Molecular probes®, Eugene, OR, USA) and incubated for 30 min at 37 °C, 5% CO_2. Then, cells were rinsed twice for 15 min., and fluorescence measurements were taken as described previously.[18] Ratio transients were analysed and diastolic ratio and ratio amplitude, together with a number of kinetic parameters, were calculated using IonWizard® software.

Myosin immunocytochemistry. Fluorescent staining of cardiomyocytes was performed as described previously.[64] Briefly, after fixation and permeabilization, cardiomyocytes were incubated for 1 h with rabbit anti-α-MyHC (rabbit-α-huMYH6, polyclonal, Bio-Genes, Berlin) primary antibody, rinsed with PBS without Ca^{2+}/Mg^{2+} (L1825; BioChrom, Berlin, Germany) for 15 min. and incubated for another hour with a specific goat anti-rabbit secondary antibody Alexa Fluor 488 (polyclonal, A11008; Thermo Fisher, Dreieich, Germany) respectively. Fluorescent images were recorded using an Olympus IX51 microscope and processed with cellSens (Olympus Corp., Tokyo, Japan) and IMAGEJ software packages.

DNSA staining

5-Dimethylaminonaphthalene-1-sulphonamide (DNSA) has a SO_2NH_2 attached to an aromatic

nucleus that binds to carbonic anhydrase forming a highly fluorescent complex that can be detected by fluorescence microscopy.[10,65] Suitably diluted cell suspensions were incubated for 10 min with a final concentration of 1.0×10^{-5} M DNSA; an aliquot was placed on a glass slide and covered with a cover slip. A fluorescence microscope Keyence Biozero BZ-9000 Generation II (Keyence Deutschland, Neu-Isenburg, Germany) was used to observe DNSA fluorescence. Excitation filter was 360/40, emission filter 460/50, dichroic mirror 400 (DAPI filter set OP-66834). Exposure time of the DNSA-incubated specimen to the exciting light was 0.5 s. Objective was S Plan Fluro 20×/0.45. Pictures were captured by the BZ Image Application (Keyence). We studied vital cell suspensions (average vitality 6%) and fully non-vital cell suspensions.

For confocal imaging of DNSA-stained cardiomyocytes, cells were plated onto laminin-coated glass coverslips (Roche, 11243217001) and incubated for 1 h at 37 °C, 5% CO_2. Afterwards, dead cells were washed away with fresh supplemented M199. This was allowed to drip off and 20 μL of 10^{-5} M DNSA in PBS was added to the cells on the coverslips. Coverslips were then put inversely onto a glass microscope slide. Images were acquired with an Olympus FluoView 1000 confocal microscope (Olympus, Shinjuku, Japan) with a 40× objective. DNSA-stained cells were imaged using a 405-nm laser for excitation. Emission was recorded from 440 to 520 nm.

Mass spectrometric assays

We have previously reported how the CO_2 permeability of plasma membranes can be determined for cells in suspension using a mass spectrometric method.[1,6,9,66,67] In principle, cells are exposed to a solution of $C^{18}O^{16}O/HC^{18}O^{16}O_2$ with a degree of labelling with ^{18}O of 1%. In a first phase, carbonic anhydrase-containing cells rapidly take up $C^{18}O^{16}O$. The kinetics of this process depends on the permeability of the membrane to CO_2 and on the speed of the intracellular conversion of CO_2 to HCO_3^-, that is on intracellular carbonic anhydrase activity. The rate of disappearance of $C^{18}O^{16}O$ from the extracellular fluid is followed by a mass spectrometer equipped with a special inlet system for fluids as first described by Itada and Forster.[68] From the time course of this first phase of disappearance of $C^{18}O^{16}O$ (as seen in Fig. 1c, first phase after addition of cells), the membrane permeability for CO_2 can be calculated, if the intracellular carbonic anhydrase activity has been determined independently. After this first rapid phase of the mass spectrometric record, a slower phase follows (also seen in Fig. 1c), which reflects reactions

and transport processes of $HC^{18}O^{16}O_2$, $C^{18}O^{16}O$ and $H_2{}^{18}O$. Thus, this second phase allows one to determine membrane HCO_3^- permeability (complete method reviewed in Endeward *et al.*,[6]).

To perform mass spectrometric measurements, a chamber with a volume of 2.2 mL was used that was attached to the high vacuum of the mass spectrometer via the previously published inlet system.[1] This chamber had a water jacket that kept the solutions at 37 °C, and contained a magnetic stirrer that mixed the content continuously. The pH was adjusted to 7.4 and monitored during the entire measurement with a pH electrode. Fifty microlitre of cardiomyocyte suspension was used in each experiment.

All experiments were performed using a buffer that contained 92 mM NaCl, 5.7 mM KCl, 1.2 mM NaH$_2$PO$_4$, 0.66 mM MgSO$_4$*7H$_2$O, 10 mM glucose, 5 mM Na-pyruvate, 10 mM creatine, 20 mM Hepes and 1.25 mM CaCl$_2$*H$_2$O, called CM solution. 1.93 mL of CM solution was added to the measuring chamber together with 220 μL of 250 mM ^{18}O-labelled bicarbonate solution (degree of labelling 1%). Then, 50 μL of the final cell suspension was added. After the characteristic biphasic time course of $C^{18}O^{16}O$ had been recorded, the experiments were terminated by the addition of excess carbonic anhydrase in order to reach final isotopic equilibrium in the suspension within the reaction chamber.

In several experiments, the extracellular carbonic anhydrase inhibitor 2,4,6-trimethyl-1-(4-sulfamoylphenyl)-pyridinium perchlorate salt (FC5-208A[69]) was used in a final concentration of 2.5×10^{-5} M and/or the inhibitor of the aquaporin-1 gas channel 4.4′-diisothiocyanato-2.2′-stilbenedisulfonate (DIDS; Sigma-Aldrich, Taufkirchen, Germany) in a final concentration of 1×10^{-4} M.[8] Ethoxzolamide (Sigma-Aldrich) was used in some other experiments as a highly membrane-permeable carbonic anhydrase inhibitor.

Carbonic anhydrase activity of cardiomyocytes

Activities were determined in the following way. After first performing a normal mass spectrometric measurement with control cells, 22 μL 10% Triton was added to the chamber to lyse all cells. Cell lysis led to a straight line in the semilogarithmic plot of $C^{18}O^{16}O$ vs. time, whose slope was used to calculate the carbonic anhydrase activity (for example, see Fig. 1b). CA activity +1 is obtained as the ratio of the slope after cell lysis over the slope before the addition of cells as indicated by the arrow. Dividing the activity of the lysate by the total volume of all cells present, and multiplying it by the total chamber volume, gives the intracellular carbonic anhydrase activity. As explained above, we use for this calculation not the

total number of all cardiomyocytes but rather the total number of vital cardiomyocytes.

Experiments with non-vital cell suspensions were performed, when occasionally cell suspensions with 0% vitality were obtained (e.g. when the time interval between opening the thorax and starting coronary perfusion had been too long). We measured these non-vital cell suspensions under the following conditions: (i) the untreated cell suspension, (ii) the cell suspension with 0.1% Triton added to ensure that all cells were open, (iii) the cell suspension measured immediately after the addition of the extracellular CA inhibitor FC5-208A, which inhibits the extracellular CA activity only, and (iv) cells exposed to FC5-208A for an extended period of time of 5 min, (v) cells pre-incubated with ethoxzolamide, which is highly membrane permeable and inhibits intra- as well as extracellular CA activity completely.

Statistical analysis

Data are presented as means $\pm$ SD. Student's unpaired t-test was used for comparisons between two groups. For comparisons between more than two groups with one independent variable, we performed one-way ANOVA with Dunnett's *post hoc* test to allow multiple comparisons with the control group.

Conflict of interest

The authors declare no conflict of interest.

References

1. Endeward V, Gros G: Low carbon dioxide permeability of the apical epithelial membrane of guinea-pig colon. *J Physiol* 567: 253–265, 2005.
2. Arias-Hidalgo M, Hegermann J, Tsiavaliaris G, Carta F, Supuran CT, Gros G, Endeward V: CO$_2$ and HCO$_3^-$ permeability of the rat liver mitochondrial membrane. *Cell Physiol Biochem* 39: 2014–2024, 2016.
3. Itel F, Al-Samir S, Öberg F, Chami M, Kumar M, Supuran CT, Deen PMT, Meier W, Hedfalk K, Gros G, Endeward V: CO$_2$ permeability of cell membranes is regulated by membrane cholesterol and protein gas channels. *FASEB J* 26: 5182–5191, 2012.
4. Hub JS, Winkler FK, Merrick M, De Groot BL: Potentials of mean force and permeabilities for carbon dioxide,

5. ammonia, and water flux across a Rhesus protein channel and lipid membranes. *J Am Chem Soc* 132: 13251–13263, 2010.
5. Kai L, Kaldenhoff R: A refined model of water and CO$_2$ membrane diffusion: effects and contribution of sterols and proteins. *Sci Rep* 4: 6665, 2014.
6. Endeward V, Al-Samir S, Itel F, Gros G: How does carbon dioxide permeate cell membranes? A discussion of concepts, results and methods. *Front Physiol* 4: 1–21, 2014.
7. Grote J: Gewebeatmung. In: *Physiologie des Menschen*, 23rd ed., edited by Schmidt RF, Thews G. Berlin, Heidelberg, Springer-Verlag, 1986, p 635.
8. Endeward V, Cartron JP, Ripoche P, Gros G: RhAG protein of the Rhesus complex is a CO$_2$ channel in the human red cell membrane. *FASEB J* 22: 64–73, 2008.
9. Endeward V, Musa-Aziz R, Cooper GJ, Chen L-M, Pelletier MF, Virkki LV, Supuran CT, King LS, Boron WF, Gros G: Evidence that aquaporin 1 is a major pathway for CO$_2$ transport across the human erythrocyte membrane. *FASEB J* 20: 1974–1981, 2006.
10. Dermietzel R, Leibstein A, Siffert W, Zamboglou N, Gros G: A fast screening method for histochemical localization of carbonic anhydrase. Application to kidney, skeletal muscle, and thrombocytes. *J Histochem Cytochem* 33: 93–98, 1985.
11. Park M, Ko SBH, Choi JY, Muallem G, Thomas PJ, Pushkin A, Lee MS, Kim JY, Lee MG, Muallem S, Kurtz I: The cystic fibrosis transmembrane conductance regulator interacts with and regulates the activity of the HCO$_3^-$ salvage transporter human Na$^+$-HCO$_3^-$ cotransport isoform 3. *J Biol Chem* 277: 50503–50509, 2002.
12. Romero MF, Chen A-P, Parker MD, Boron WF: The SLC4 family of bicarbonate (HCO$_3^-$) transporters. *Mol Aspects Med* 34: 159–182, 2013.
13. Piper HM, Probstt I, Schwartzs P, Hütter F, Spieckermannt PG: Culturing of calcium stable adult cardiac myocytes. *J Mol Cell Cardiol* 14: 397–412, 1982.
14. Piper H, Volz A, Schwartzs P: Adult ventricular rat heart muscle cells. In: *Cell Culture Techniques in Heart and Vessel Research*, edited by Piper H, Berlin, Heidelberg, Springer Verlag, 1990, pp 36–60.
15. Cheung J, Leaf A, Bonventre J: Determination of isolated myocyte viability: staining methods and functional criteria. *Basic Res Cardiol* 80: 23–29, 1985.
16. Claycomb W, Palazzo MC: Culture of the terminally differentiated adult cardiac muscle cell: a light and scanning electron microscope study. *Dev Biol* 80: 466–482, 1980.
17. Moses R, Claycomb W: Disorganization and reestablishment of cardiac muscle cell ultrastructure in cultured adult rat ventricular muscle cells. *J Ultrastruct Res* 81: 358–374, 1982.
18. Mutig N, Geers-Knoerr C, Piep B, Pahuja A, Vogt PM, Brenner B, Niederbichler AD, Kraft T: Lipoteichoic acid from *Staphylococcus aureus* directly affects cardiomyocyte contractility and calcium transients. *Mol Immunol* 56: 720–728, 2013.
19. Louch WE, Sheehan KA, Wolska BM: Methods in cardiomyocyte isolation, culture, and gene transfer. *J Mol Cell Cardiol* 51: 288–298, 2011.

20. Villafuerte FC, Swietach P, Youm J-B, Ford K, Cardenas R, Supuran CT, Cobden PM, Rohling M, Vaughan-Jones RD: Facilitation by intracellular carbonic anhydrase of Na⁺ –HCO₃⁻ co-transport but not Na⁺/H⁺ exchange activity in the mammalian ventricular myocyte. *J Physiol* 592: 991–1007, 2014.

21. Schroeder M, Ali M, Hulikova A, Supuran CT, Clarke K, Vaughan-Jones RD, Tyler DJ, Swietach P: Extramitochondrial domain rich in carbonic anhydrase activity improves myocardial energetics. *Proc Natl Acad Sci USA* 110: E958–E967, 2013.

22. Geers C, Krüger D, Siffert W, Schmid A, Bruns W, Gros G: Carbonic anhydrase in skeletal and cardiac muscle from rabbit and rat. *Biochem J* 282: 165–171, 1992.

23. Moyniham JB: Carbonic anhydrase activity in mammalian skeletal and cardiac muscle. *Biochem J* 168: 567–569, 1977.

24. Brown BF, Quon A, Dyck JRB, Casey JR: Carbonic anhydrase II promotes cardiomyocyte hypertrophy. *Can J Physiol Pharmacol* 90: 1599–1610, 2012.

25. Alvarez BV, Quon AL, Mullen J, Casey JR: Quantification of carbonic anhydrase gene expression in ventricle of hypertrophic and failing human heart. *BMC Cardiovasc Disord* 13: 2, 2013.

26. Torella D, Ellison GM, Torella M, Vicinanza C, Aquila I, Iaconetti C, Scalise M, Marino F, Henning BJ, Lewis FC, Gareri C, Lascar N, Cuda G, Salvatore T, Nappi G, Indolfi C, Torella R, Cozzolino D, Sasso FC: Carbonic anhydrase activation is associated with worsened pathological remodeling in human ischemic diabetic cardiomyopathy. *J Am Heart Assoc* 3: e000434, 2014.

27. Lehtonen J, Shen B, Vihinen M, Casini A, Scozzafava A, Supuran CT, Parkkila A-K, Saarnio J, Kivelä AJ, Waheed A, Sly WS, Parkkila S: Characterization of CA XIII, a novel member of the carbonic anhydrase isozyme family. *J Biol Chem* 279: 2719–2727, 2004.

28. Scheibe RJ, Gros G, Parkkila S, Waheed A, Grubb JH, Shah GN, Sly WS, Wetzel P: Expression of membrane-bound carbonic anhydrases IV, IX, and XIV in the mouse heart. *J Histochem Cytochem* 54: 1379–1391, 2006.

29. Sender S, Decker B, Fenske CD, Sly WS, Carter ND, Gros G: Localization of carbonic anhydrase IV in rat and human heart muscle. *J Histochem Cytochem* 46: 855–861, 1998.

30. Bruns W, Gros G: Membrane-bound carbonic anhydrase in the heart. *Am J Physiol* 262: 577–584, 1992.

31. Dodgson SJ, Forster RE II, Storey BT, Mela L: Mitochondrial carbonic anhydrase. *Proc Natl Acad Sci USA* 77: 5562–5566, 1980.

32. Ruiz-Meana M, Abellán A, Miró-Casas E, Agulló E, Garcia-Dorad D: Role of sarcoplasmic reticulum in mitochondrial permeability transition and cardiomyocyte death during reperfusion. *Am J Physiol Heart Circ Physiol* 207: H1281–H1289, 2009.

33. Zhao T, Huang X, Han L, Wang X, Cheng H, Zhao Y, Chen Q, Chen J, Cheng H, Xiao R, Zheng M: Central role of mitofusin 2 in autophagosome-lysosome fusion in cardiomyocytes. *J Biol Chem* 287: 23615–23625, 2012.

34. Pérez-Treviño P, Pérez-Treviño J, Borja-Villa C, García N, Altamirano J: Changes in t-tubules and sarcoplasmic reticulum in ventricular myocytes in early cardiac hypertrophy in a pressure overload model. *Cell Physiol Biochem* 37: 1329–1344, 2015.

35. Höfer M: *Transport durch Biologische Membranen.* Verlag Chemie, Weinheim and New York, NY, 1977, p 1.

36. Dupuy AD, Engelman DM: Protein area occupancy at the center of the red blood cell membrane. *Proc Natl Acad Sci USA* 105: 2848–2852, 2008.

37. D'Souza KM, Ashavaid TF: Caprine cardiac sarcoplasmic reticulum isolation and biochemical characterisation with emphasis on Ca(2+)-adenosine triphosphatase. *Indian J Clin Biochem* 22: 37–44, 2007.

38. Meissner G: Monovalent ion and calcium ion fluxes in sarcoplasmic reticulum. *Mol Cell Biochem* 55: 65–82, 1983.

39. Tanifuji M, Sokabe M, Kasai M: An anion channel of sarcoplasmic reticulum incorporated into planar lipid bilayers: Single-channel behavior and conductance properties. *J Membr Biol* 99: 103–111, 1987.

40. Schneider H-P, Alt MD, Klier M, Spiess A, Andes FT, Waheed A, Sly WS, Becker HM, Deitmer JW: GPI-anchored carbonic anhydrase IV displays both intra- and extracellular activity in cRNA-injected oocytes and in mouse neurons. *Proc Natl Acad Sci USA* 110: 1494–1499, 2013.

41. Romanowski F, Schierenbeck J, Gros G: Facilitated CO₂ diffusion in various striated muscles. In: *Quantitative Spectroscopy in Tissue*, edited by Frank K, Kessler M, Frankfurt/M, PMI-Verlag, 1992, pp 205–211.

42. Gros G, Moll W, Hoppe H, Gros H: Proton transport by phosphate diffusion - a mechanism of facilitated CO₂ transport. *J Gen Physiol* 67: 773–790, 1976.

43. Vengust M, Staempfli H, Viel L, Swenson ER, Heigenhauser G: Acetazolamide attenuates transvascular fluid flux in equine lungs during intense exercise. *J Physiol* 591: 4499–4513, 2013.

44. Swenson ER, Maren TH: A quantitative analysis of CO₂ transport at rest and during maximal exercise. *Respir Physiol* 35: 129–159, 1978.

45. Wetzel P, Hasse A, Papadopoulos S, Voipio J, Kaila K, Gros G: Extracellular carbonic anhydrase activity facilitates lactic acid transport in rat skeletal muscle fibres. *J Physiol* 531: 743–756, 2001.

46. Spitzer KW, Skolnick RL, Peercy BE, Keener JP: Facilitation of intracellular H + ion mobility by CO₂/HCO₃ in rabbit ventricular myocytes is regulated by carbonic anhydrase. *J Physiol* 541: 159–167, 2002.

47. Carter MJ, Parsons DS: The isoenzymes of carbonic anhydrase: tissue, subcellular distribution and functional significance, with particular reference to the intestinal tract. *J Physiol* 251: H705–H713, 1971.

48. Parsons DS: Role of anions and carbonic anhydrase in epithelia. *Philos Trans R Soc Lond B Biol Sci* 299: 369–381, 1982.

49. Stiel D, Murray DJ, Peters TJ: Activities and subcellular localization of enzymes implicated in gastroduodenal bicarbonate secretion. *Am J Physiol Gastrointest Liver Physiol* 247: G133–G139, 1984.

50. Butler TL, Au CG, Yang B, Egan JR, Tan YM, Hardeman EC, North KN, Verkman AS, Winlaw DS: Cardiac aquaporin expression in humans, rats, and mice. *Am J Physiol Heart Circ Physiol* 291: H705–H713, 2006.

51. Geyer RR, Musa-Aziz R, Qin X, Boron WF: Relative CO(2)/NH(3) selectivities of mammalian aquaporins 0-9. *Am J Physiol Cell Physiol* 304: C985–C994, 2013.

52. Nielsen S, Smith BL, Christensen EI, Agre P: Distribution of the aquaporin CHIP in secretory and resorptive epithelia and capillary endothelia. *Proc Natl Acad Sci USA* 90: 7275–7279, 1993.

53. Page E, Winterfield J, Goings G, Bastawrous A, Upshaw-Earley J: Water channel proteins in rat cardiac myocyte caveolae: osmolarity-dependent reversible internalization. *Am J Physiol* 274: H1988–H2000, 1998.

54. Netti VA, Vatrella MC, Chamorro MF, Rosón MI, Zotta E, Fellet AL, Balaszczuk AM: Comparison of cardiovascular aquaporin-1 changes during water restriction between 25- and 50-day-old rats. *Eur J Nutr* 53: 287–295, 2014.

55. de Jonge HW, Dekkers DH, Bastiaanse EM, Bezstarosti K, van der Laarse A, Lamers JM: Eicosapentaenoic acid incorporation in membrane phospholipids modulates receptor-mediated phospholipase C and membrane fluidity in rat ventricular myocytes in culture. *J Mol Cell Cardiol* 28: 1097–1108, 1996.

56. Bastiaanse EM, Atsma DE, Kuijpers MC, van der Laarse A: The effect of sarcolemmal cholesterol content on intracellular calcium ion concentration in cultured cardiomyocytes. *Arch Biochem Biophys* 313: 58–63, 1994.

57. Ma Z, Meddings JB, Lee SS: Cardiac plasma membrane physical properties and β-adrenergic receptor function are unaltered in portal-hypertensive rats. *Hepatology* 22: 188–193, 1995.

58. Weglicki WB, Owens K, Kennett FF, Kessner A, Harris L, Wise RM: Preparation and properties of highly enriched cardiac sarcolemma from isolated adult myocytes. *J Biol Chem* 255: 3605–3609, 1980.

59. Niederbichler AD, Westfall MV, Su GL, Donnerberg J, Usman A, Vogt PM, Ipaktchi KR, Arbabi S, Wang SC, Hemmila MR: Cardiomyocyte function after burn injury and lipopolysaccharide exposure: single cell contraction analysis and cytokine secretion profile. *Shock* 25: 176–183, 2006.

60. Failli P, Fazzini A, Franconi F, Stendardi I, Giotti A: Taurine antagonizes the increase in intracellular calcium concentration induced by alpha-adrenergic stimulation in freshly isolated guinea-pig cardiomyocytes. *J Mol Cell Cardiol* 24: 1253–1265, 1992.

61. Chung CS, Mechas C, Campbell KS: Myocyte contractility can be maintained by storing cells with the myosin ATPase inhibitor 2,3 butanedione monoxime. *Physiol Rep* 3: 1–9, 2015.

62. Sorenson AL, Tepper D, Sonnenblick EH, Robinson TF, Capasso JM: Size and shape of enzymatically isolated ventricular myocytes from rats and cardiomyopathic hamsters. *Cardiovasc Res* 19: 793–799, 1985.

63. Layland J, Grieve DJ, Cave AC, Sparks E, Solaro RJ, Shah AM: Essential role of troponin I in the positive inotropic response to isoprenaline in mouse hearts contracting auxotonically. *J Physiol* 556: 835–847, 2004.

64. Weber N, Schwanke K, Greten S, Wendland M, Iorga B, Fischer M, Geers-Knörr C, Hegermann J, Wrede C, Fiedler J, Kempf H, Franke A, Piep B, Pfanne A, Thum T, Martin U, Brenner B, Zweigerdt R, Kraft T: Stiff matrix induces switch to pure β-cardiac myosin heavy chain expression in human ESC-derived cardiomyocytes. *Basic Res Cardiol* 111: 68, 2016.

65. Chen RF, Kernohan JC: Combination of bovine carbonic anhydrase with a fluorescent sulfonamide. *J Biol Chem* 242: 5813–5823, 1967.

66. Wunder M, Böllert P, Gros G: Mathematical modelling of the role of intra- and extracellular carbonic anhydrase activity and membrane permeability. *Isotopes Environ Health Stud* 33: 197–205, 1997.

67. Wunder MA, Gros G: ^{18}O exchange in suspensions of red blood cells: determination of parameters of mass spectrometer inlet system. *Isotopes Environ Health Stud* 34: 303–310, 1998.

68. Itada N, Forster RE: Carbonic anhydrase activity in intact red blood cells measured with 18O exchange. *J Biol Chem* 252: 3881–3890, 1977.

69. Perut F, Carta F, Bonuccelli G, Grisendi G, Di Pompo G, Avnet S, Sbrana FV, Hosogi S, Dominici M, Kusuzaki K, Supuran CT, Baldini N: Carbonic anhydrase IX inhibition is an effective strategy for osteosarcoma treatment. *Expert Opin Ther Targets* 19: 1593–1605, 2015.

Curriculum Vitae

PERSONAL INFORMATION

Name: Mariela Eugenia Arias Hidalgo

Date and place of birth 28/10/1984, San Jose, Costa Rica

Nationality: Costarrican

E-mail: maribio2810@gmail.com, mariela.ariashidalgo@ucr.ac.cr

WORK EXPERIENCE

From March 2009 – July 2014: Junior Lecturer in Physiology, School of Medicine, Universidad de Costa Rica, San Jose, Costa Rica

First Trimester 2009: Junior Lecturer of Biology course for Nursing. Universidad Adventista de Centroamérica, Alajuela, Costa Rica

First semester 2008: Laboratory assistant, Course of General Genetics. School of Biology, Universidad de Costa Rica, San Jose, Costa Rica

EDUCATION

October 2013: M.Sc. in Biology, emphasis in genetics and molecular biology. Universidad de Costa Rica (Master Thesis in Human Genetics). San Jose, Costa Rica. Total Score: 8,92 from 10 possible points.

April 2013: License in Teaching. Universidad Estatal a Distancia. Teaching degree in Biology. San Jose, Costa Rica.

October 2007: Bachelor in Biology. Universidad de Costa Rica. San Jose, Costa Rica. Total Score: 8,12 from 10 possible points

From 1997– 2001: Bachelor in Middle Education. Saint John High School. Alajuela, Costa Rica. Total Score:

From 1991-1996: School. Saint John School. Alajuela, Costa Rica

PUBLICATIONS

Vega, A. **M. Arias**, A. Obando-Valverde and J. Chaverri. 2010. Clinical characterisctics of deaf children in Costa Rica. Otolaryngology- Head and Neck Surgery 143: 226.

Arias-Hidalgo M, Hegermann J, Tsiavaliaris G, Carta F, Supuran CT, Gros G & Endeward V (2016). CO_2 and HCO_3^- Permeability of the Rat Liver Mitochondrial Membrane. Cell Physiol Biochem 39, 2014–2024.

Arias-Hidalgo M, Al-Samir S, Weber N, Geers-Knörr C, Gros G, Endeward V. (2017) CO_2 Permeability and Carbonic Anhydrase Activity of Rat Cardiomyocytes. Acta Physiol (Oxf). Apr 20. doi: 10.1111/apha.12887. [Epub ahead of print].